Journal Pre-proof

Modes of climate variability: Synthesis and review of proxy-based reconstructions through the Holocene

Armand Hernández, Celia Martin-Puertas, Paola Moffa-Sánchez, Eduardo Moreno-Chamarro, Pablo Ortega, Simon Blockley, Kim M. Cobb, Laia Comas-Bru, Santiago Giralt, Hugues Goosse, Jürg Luterbacher, Belen Martrat, Raimund Muscheler, Andrew Parnell, Sergi Pla-Rabes, Jesper Sjolte, Adam A. Scaife, Didier Swingedouw, Erika Wise, Guobao Xu

PII: S0012-8252(20)30332-9

DOI: https://doi.org/10.1016/j.earscirev.2020.103286

Reference: EARTH 103286

To appear in: *Earth-Science Reviews*

Received date: 15 December 2019

Revised date: 30 June 2020

Accepted date: 8 July 2020

Please cite this article as: A. Hernández, C. Martin-Puertas, P. Moffa-Sánchez, et al., Modes of climate variability: Synthesis and review of proxy-based reconstructions through the Holocene, *Earth-Science Reviews* (2020), https://doi.org/10.1016/j.earscirev.2020.103286

Modes of climate variability: Synthesis and review of proxy-based reconstructions through the Holocene

Armand Hernández[1*], Celia Martin-Puertas[2], Paola Moffa-Sánchez[3], Eduardo Moreno-Chamarro[4], Pablo Ortega[4], Simon Blockley[2], Kim M. Cobb[5], Laia Comas-Bru[6], Santiago Giralt[1], Hugues Goosse[7], Jürg Luterbacher[8,9], Belen Martrat[10], Raimund Muscheler[11], Andrew Parnell[12], Sergi Pla-Rabes[13,14], Jesper Sjolte[11], Adam A. Scaife[15,16], Didier Swingedouw[17], Erika Wise[18], Guobao Xu[19,20]

[1] Institute of Earth Sciences Jaume Almera, ICTJA, CSIC, 08028 Barcelona, Spain
[2] Department of Geography. Royal Holloway University of London. TW20 0EX Egham, UK
[3] Department of Geography, Durham University, Durham, UK, DH1 3LE
[4] Barcelona Supercomputing Center (BSC), Barcelona, Spain.
[5] School of Earth and Atmospheric Sciences, Georgia Institute of Technology, Atlanta, GA, USA
[6] School of Archaeology, Geography & Environmental Sciences, University of Reading, RG6 6AH Reading, Berkshire, United Kingdom
[7] Earth and Life Institute, Université catholique de Louvain, Belgium.
[8] World Meteorological Organization (WMO), Department for Science and Innovation, 7bis Avenue de la Paix, 1211 Geneva, Switzerland
[9] Department of Geography, Climatology, Climate Dynamic and Climate Change, And Center of International Development and Environmental Research, Justus Liebig University of Giessen, Germany
[10] Institute of Environmental Assessment and Water Research (IDAEA-CSIC), Barcelona, Spain
[11] Department of Geology – Quaternary Science, Lund University, Sölvegatan 12, 223 62, Lund, Sweden
[12] Hamilton Institute, Insight Centre for Data Analytics, Maynooth University, Kildare, Ireland
[13] CREAF,08193, Bellaterra (Cerdanyola del Vallès), Spain.
[14] Universitat Autònoma de Barcelona (UAB), Bellaterra (Cerdanyola del Vallès), 08193, Spain.
[15] Met Office Hadley Centre. Exeter, UK
[16] College of Engineering, Mathematics and Physical Sciences, Exeter University, Exeter, UK
[17] Environnements et Paléoenvironnements Océaniques et Continentaux (EPOC), UMR CNRS 5805, EPOC-OASU Université de Bordeaux, Allée Geoffroy Saint-Hilaire, 33615 Pessac, France
[18] Department of Geography, University of North Carolina at Chapel Hill, Chapel Hill, North Carolina 27599, USA
[19] State Key Laboratory of Cryospheric Science, Northwest Institute of Eco-Environment and Resources, Chinese Academy of Sciences, Lanzhou 730000, China
[20] Laboratory of Tree-Ring Research, University of Arizona, Tucson, 85721, USA

*Corresponding author: armandhernandezh@gmail.com

Abstract

Modes of climate variability affect global and regional climates on different spatio-temporal scales, and they have important impacts on human activities and ecosystems. As these modes are a useful tool for simplifying the understanding of the climate system, it is crucial that we gain improved knowledge of their long-term past evolution and interactions over time to contextualise their present and future behaviour. We review the literature focused on proxy-based reconstructions of modes of climate variability during the Holocene (i.e., the last 11.7 thousand years) with a special emphasis on i) proxy-based reconstruction methods; ii) available proxy-based reconstructions of the main modes of variability, i.e., El Niño Southern Oscillation, Pacific Decadal Variability, Atlantic Multidecadal Variability, the North Atlantic Oscillation, the Southern Annular Mode and the Indian Ocean Dipole; iii) major interactions between these modes; and iv) external forcing mechanisms related to the evolution of these modes. This review shows that modes of variability can be reconstructed using proxy-based records from a wide range of natural archives, but these reconstructions are scarce beyond the last millennium, partly due to the lack of robust chronologies with reduced dating uncertainties, technical issues related to proxy calibration, and difficulty elucidating their stationary impact (or not) on regional climates over time. While for each mode the available reconstructions tend to agree at mutidecadal timescales, they show notable disagreement on shorter timescales beyond the instrumental period. The reviewed evidence suggests that the intrinsic variability of modes can be modulated by external forcing, such as orbital, solar, volcanic, and anthropogenic forcing. The review also highlights some modes experience higher variability over the instrumental period, which is partly ascribed to anthropogenic forcing. These features stress the paramount importance of further studying their past variations using long climate-proxy records for the progress of climate science.

1.- Introduction

The Earth is a complex system in which climate variability, i.e., variations in the mean state of the climate system, results from intricate interactions between its components (atmosphere, hydrosphere, geosphere, cryosphere, and biosphere). Different geophysical processes are, therefore, capable of contributing to climatic variability on different timescales (Mitchell, 1976). The potential sources of climatic variability are mainly the result of: i) internal processes involving interactions between the different parts of the system; and/or ii) external forcing mechanisms from independent environmental changes. A large proportion of the spatial structure of climate variability follows recurrent patterns, often referred to as modes of climate variability (Stephenson et al., 2004). The term modes of climate variability is, however, ambiguously employed in the climate community, with a range of uses that make its definition difficult (IPCC, 2013). Here, we define modes of climate variability as preferred spatial patterns and their fluctuations across different timescales, which represent a simplification of the complex spatial and temporal evolution of the climate system.

Modes of variability have typically been identified through statistical analysis of observational and model data and are generally described by a characteristic spatial pattern and its associated timeseries (Christensen et al., 2013). While these modes of variability are at most quasiperiodic, they are oscillatory in character, and their state is monitored using so-called climate indices. Empirical orthogonal function analysis is among the most widely and extensively used methods to calculate climate indices (Hannachi et al., 2007). This methodology allows a display of the space-time field that is useful for dimensionality reduction and pattern extraction, although it is not exempt from problems (i.e., bias in the variance) (Beguería et al., 2016). Alternatively, simple indices based on data from fixed meteorological stations have been traditionally used as they can provide continuous timeseries that extend further back in time, in some cases beyond the 20th century (Comas-Bru and Hernández, 2018; Cropper et al., 2015; Hurrell, 1995; Jones et al., 1997; Vinther et al., 2003a; Visbeck, 2009). The main disadvantage of station-based indices is that they are anchored to their locations, and they might not effectively represent the centres of action of some modes. Consequently, modes of variability are usually defined from gridded data (Folland et al., 2009; Moore et al., 2013; Roundy, 2014). The correlation between a given index of a mode of climate variability and a large-scale climate field are often named teleconnections. This concept refers to the ability of modes of climate variability to explain the connections between climate in remote regions through associated atmospheric or oceanic pathways (Barnston and Livezey, 1987; Shaman, 2014).

The impact of some of the best-known modes of variability, i.e., the El Niño–Southern Oscillation (ENSO), the North Atlantic Oscillation (NAO), the Pacific Decadal Variability (PDV), Atlantic Multidecadal Variability (AMV), the Northern and Southern Annular Modes (NAM and SAM) and the Indian Ocean Dipole (IOD), extend over large areas and/or ocean basins. These modes of variability are often associated with severe climate events such as droughts, floods, heat waves and cold spells (e.g., Benito et al., 2015; Cook et al., 2015; Ionita et al., 2012) affecting agriculture, water resources and blue economies, which, in turn, modulate air quality, fire risk, energy availability and human health (Bastos et al., 2016; Jerez et al., 2013; Zubiate et al., 2017). In this context, understanding the evolution of modes of variability and associated teleconnections on a global scale during the last few millennia is essential to i) attribute climate changes to internal variability versus external forcing factors, ii) evaluate the ability of different climate models to reproduce them robustly, and iii) constrain uncertainties in future climate projections and associated hazards.

Instrumental measurements of the climatic variables used to characterise these modes have been available for a couple of centuries in the best case (e.g., Jones, 2001; Luterbacher et al., 2002; Parker et al., 2007, 1992; Prohom et al., 2016). A better understanding of these modes, many of which operate from submonthly to multidecadal timescales, requires longer climate records beyond the limited temporal and spatial coverage of instrumental measurements. Consequently, the use of indirect climate indicators from natural archives (proxy-based records) becomes of paramount importance (Gornitz, 2009; Marcott et al., 2013; Neukom et al., 2019). These indirect climate indicators generally respond to environmental parameters such as temperature and precipitation, and, in turn, may be indirectly linked to certain modes of variability, through, for example, their response to the atmospheric circulation (e.g., Bradley, 2015; Jones et al., 2009; Jones and Mann, 2004). Over the last decades, several studies have attempted to reconstruct a number of modes of climate variability at different timescales using historical documents and natural archives. Major findings show evidence of the spatio-temporal variability of these modes and their impacts, interactions and possible links to external forcings for the Holocene in general (e.g., Chen et al., 2016; Ivanochko et al., 2008; Koutavas and Joanides, 2012) and the last millennium in particular (e.g., Dätwyler et al., 2018; Mann et al., 2009; Ortega et al., 2015; Wang et al., 2017). Nevertheless, they are not exempt from limitations, such as chronological uncertainties, an oversimplification or misinterpretation of stationarity, and limited capability to attribute observed climate changes to internal variability and/or external forcing factors (e.g. solar and volcanic activity) (e.g., Evans et al., 2013; Raible et al., 2014). These limitations may partly be overcome using climate models. There is a number of approaches based on palaeoclimatic simulations, such as large-multimodel ensembles (e.g., Lee et al., 2019; Phillips et al., 2014; Terray, 2012) and proxy system modeling (e.g., Dee et al., 2017; Evans et al., 2013), that have already shown their ability to reproduce and differentiate external and internal processes affecting the climate system. However, the obtained results are disparate (Haywood et al., 2019) and their potential to simulate some aspects (e.g., extreme changes) related to modes of variability is still poor (e.g., Zhang and Sun, 2014).

Despite the dramatic increase in the number of proxy-based reconstructions over the past decades, a synthesis of the main modes of variability and teleconnections in a palaeoclimatic context is lacking. This paper focuses on reviewing the literature centred on proxy-based reconstructions of modes of climate variability during our current interglacial, the Holocene (i.e., the last 11.7 ka). The article is organised as follows: Section 2 introduces the different reconstruction methods that are frequently employed and evaluates ongoing work and future developments. Section 3 provides an account of the proxy-based reconstructions available for the main modes of climate variability (Fig. 1). Section 4 describes major interactions between modes of variability, while section 5 focuses on mechanisms driven by external forcing, which have been related to the changes in modes of variability through the Holocene. Finally, section 6 synthesises the main review outputs and includes future perspectives.

2.- Reconstruction methods

2.1.- Archives, spatial distributions and sensitivities

Information on past climatic and environmental conditions (i.e., proxy data) is commonly preserved in natural and documentary archives across the globe. To yield reliable reconstructions of a mode of variability, proxy-based records should i) be sensitive to climatic variables (e.g., temperature, precipitation, wind); ii) be continuous and highly-resolved (monthly to decadal), at least, for several hundreds of years to detect decadal-scale variability beyond the instrumental period; iii) mantain a stationary modern proxy-climate relationship over time (the principle of uniformitarianism); and iv) cover a large and homogeneous spatial region that includes the areas influencing the targeted mode of variability (Table 1).

It is important to highlight that high-quality proxy-based climatic records do not reconstruct the temporal evolution of modes of climate variability by themselves but their impacts and interactions on the physical and biogeochemical dynamics of the proxy-based record. The common approach to establish a reliable proxy-climate relationship is to calibrate the proxy signal using modern data (see Section 2.3). However, this can introduce large uncertainties and is not possible when the record does not cover the instrumental period. In addition, some other overarching challenges remain when working with proxy data, presented as follows in approximate order of decreasing importance:

1. The relationship between climate and a given proxy-based record may vary over time. This variation may occur because either the proxy reacts to climate differently under different non-climate related conditions, or because the sensitivity of the proxy to a given set of climate drivers may vary with changes in the mean climate state. This phenomenon may be solved by using mechanistic modelling of the proxy-climate relationship by accounting for these important non-climate variables in the calibration model if available. The climate-proxy linkage may also vary as a function of timescale. For example corals might have a different relationship with climate on annual, interannual and decadal timescales (Gagan et al., 2012).

2. The calibration data do not fully explore the range of proxy/climate behaviours (with few exceptions such as coral archives). This is the so-called ‘no modern analogue’ problem and can be reduced by increasing the calibration dataset size, or by using mechanistic models of proxy/climate behaviour.

3. A weak relationship between proxies and climate, which may occur where proxies or climate variables are poorly chosen and can be accounted for using a probabilistic modelling approach (such as the Bayesian inverse approach) where the models are sufficiently flexible so that weak relationships yield large uncertainties in reconstructed climates. Employing a multi-proxy approach can identify common climate signals of interest amongst individual proxies that may be only correlated to local climate variables.

4. Poor chronological control may occur even if the proxy climate relationship is strong but the dating methods (or extraction/counting methods for the proxy) are not able to accurately quantify the information in the archive. This phenomenon can be accounted for by modelling the uncertainty in the process so that poor data yield large climate uncertainty estimates (e.g., Parnell et al., 2015).

Table 1.- Examples of the most commonly used archives to carry out high-resolution proxy-based reconstruction of modes of climate variability.

Archive	Advantages	Limitations	Proxies used for reconstructions	Mode	Nominal Temporal Resolution	Interpretable Temporal Resolution	Reference
Tree rings	- Absolute chronologies (precise calendar year dates) - High-resolution proxy records (sub-annual to annual) - Widespread distribution in both Hemispheres - Strong climate signal - Continuous records	- Climate sensitivity typically reflects a particular season - Concentrated in the mid-latitudes; many trees in tropical regions do not have annual rings - Most records < 1000 years in length.	Total tree-ring widths, earlywood widths, latewood widths, maximum latewood density, $\delta^{18}O$	PDO, ENSO, NAO, SAM, AMV	Annual	Sub-annual/Annual/ and above	e.g., Abram et al., 2014; Cook et al., 2019; D'Arrigo and Wilson, 2006; Dätwyler et al., 2019; Gray et al., 2004; Li et al., 2013; MacDonald and Case, 2005; Verdon and Franks, 2006
Ice cores	- Absolute chronologies (annual-layer counts). - Age uncertainty < ± 50 years - High-resolution proxy records (annual) - Continuous record > 1000 years in length	-Limited to polar and high-elevation regions	Network of $\delta^{18}O$; $\delta^{18}O$	NAO	Annual	Annual/Multiannual and above	e.g., Jones et al., 2009; Ortega et al., 2014; Sjolte et al., 2018; Vinther et al., 2010, 2003b
Speleothems	- Absolute chronologies (radiometric methods and annual layer counts) - Age uncertainty < ± 50 years - High-resolution proxy records (sub-annual) - Most continuous records > 1000 years in	- Possible presence of growth hiatuses - Variable water transit time: difficult to quantify. - Potential non-equilibrium isotopic deposition (kinetic effects)	Sr/Ca; $\delta^{18}O$; $\delta^{13}C$; growth rate of laminae	NAO, ENSO	Sub-Annual to multi-centennial	Sub-Annual to multi-centennial	e.g., Chen et al., 2016; Frappier et al., 2002; Lachniet et al., 2004; Smith et al., 2016a; Trouet et al., 2009; Wassenburg et al., 2016

		length - Distribution in a large range of hydroclimatic conditions						
Corals		- Absolute chronologies (radiometric methods and annual layer counts) - Age uncertainty < 1 year - High-resolution proxy records (sub-annual)	- Limited to tropical regions - Record < 1000 years in length	$\delta^{18}O$; Sr/Ca	ENSO, PDO, IOD, AMV	Monthly to seasonal	Seasonal and above	e.g., Abram et al., 2020; Cobb et al., 2013; Gong and Luterbacher, 2008; McGregor et al., 2010; Verdon and Franks, 2006; Wilson et al., 2010
Marine sediments		- Continuous record > 1000 years in length - Widespread distribution	- Age uncertainty > ± 50 years - Low-resolution proxy records (sub-decadal at best)	Sediment and foraminifera geochemistry	ENSO, PDO, NAO	Sub-decadal and above	Decadal and above	e.g., Dean and Kemp, 2004; Faust et al., 2016; Goslin et al., 2018; White et al., 2018
Lake sediments	Non-varved	- Continuous record > 1000 years in length - Widespread distribution	- Age uncertainty > ±50 years - Low-resolution proxy records (sub-decadal at best) - Human impact	Mn/Fe ratio; Grain size; Laminae colour scale	NAO, ENSO, PDO	Sub-decadal and above	Decadal and above	e.g., Kirby et al., 2010; Moy et al., 2002; Olsen et al., 2012
	Varved	- Independent varve chronologies - High-resolution proxy records (sub-annual) - Most continuous records	- Human impact - Most varve chronologies are floating and need to be anchored to a calendar timescale using other independent dating methods, e.g. ^{14}C			Annual	Annual/Multiannual and above	

	> 1000 years in length. - Widespread distribution	dating and tephrochronology					
Historical documents	- High variety of resources - Good age control - High temporal resolution (sub-annual)	- Short continuous record length (the last few hundred years) - Most reporting on the North Atlantic and the Pacific	Ice-Snow observations; Phenological and biological observations, historical written evidence; Ships' logbooks	NAO	Monthly to Seasonal	Seasonal and above	e.g., Küttel et al., 2010; Luterbacher et al., 2001, 1999; Mellado-Cano et al., 2019

2.2.- Timescales and chronologies

Understanding the temporal and spatial expression of modes of variability over the Holocene requires precise chronological resolution covering a wide geographical range. This is a challenge for climate science that seeks to address the entire Holocene, as there are inherent dating uncertainties in most contexts and the most precise approaches are spatially and temporally constrained (Table 1).

There exists for the Holocene there exists a dendrochronological timescale that is considered to be accurate with virtually no uncertainties. This timescale underlies the ^{14}C calibration curve (IntCal curve; Reimer et al., 2020), as tree rings record the atmospheric 14C concentrations during the period of their growth. Sampling of the Holocene IntCal curve is decadal, typically 10 rings per radiocarbon sample (Reimer et al., 2020, 2013), and the structure of the curve has implications for dating. Radiocarbon ages are commonly determined in the Holocene with 1 sigma counting errors of ca. ± 20 – 50 years; and the shape of the calibration curve, which can mean single age estimates will have 2 sigma calibrated ranges of 100 to, in some cases, 300 years. The sampling density of radiocarbon ages available at individual sites, as well as the shape of the radiocarbon calibration curve at different points, can influence the precision at which an event can be dated. This phenomenon can be overcome with the so-called wiggle match dating approach, i.e., the matching of a series of ^{14}C determinations to the calibration curve (Pearson, 1986). However, this approach is expensive, and may pose potential issues of sample contamination and reworking that can influence the chronological accuracy (e.g., Blockley et al., 2007). Another approach to deal with the challenges of radiocarbon dating of individual sites is to calculate average dates by combining low-resolution radiocarbon dating in multiple records, which are correlated by biostratrigraphy, to establish a robust regional chronology (e.g. Wanner et al., 2011). This approach has its own limitations. For example, Blaauw et al. (2007) tested proposed periods of regional wet conditions reported from biostratigraphically-correlated European raised bogs. Tests were based on improving the dating of the individual sites, using very high-resolution ^{14}C sampling, and integrating formal Bayesian interrogation of the statistical likelihood synchronicity between sites. This study failed to reproduce many of the previously proposed synchronous wet shifts because of either the full chronological uncertainties of comparing climate events is not incorporated into the assessment of the timing of an event or, even if an event exists, that might not be synchronous between regions. Nevertheless, two periods of low solar activity, the Maunder and Spörer solar minima were statistically correlated with wetter conditions across multiple sites (Blaauw et al., 2007). In the marine realm, in addition, radiocarbon-based dating has an added source of uncertainty mostly deriving from regional differences in the radiocarbon ages of specific water masses that may have been isolated since they were in contact with the atmosphere (Stuiver et al., 1986; Stuiver and Braziunas, 1993). This is often referred as the marine reservoir effect and has been studied globally and regionally (Reimer and Reimer, 2001). There has been, however, notable success in improving the precision of radiocarbon-based chronologies using a high density of radiocarbon dates and Bayesian modelling techniques (e.g., Crann et al., 2015), although these have not as yet been applied to a sufficient number of Holocene sediment chronologies, in part due to the number of dates required to achieve the best improvements in model precision (Blaauw et al., 2018).

Another important dating method relies on the radioactive decay of uranium and the ingrowth of thorium with age. The $^{234}U/^{230}Th$ dating method has been particularly successful for speleothem records leading to absolute dating uncertainties on the order of 50-100 years for Holocene records (Wang et al., 2005). Such dating precision allows the linking of speleothem-based monsoon records to ice core-based climate records and/or comparisons to solar forcing records, although some timescale adjustments within uncertainties may still generate misleading results (Muscheler et al., 2004). When applied to dating fossil corals, U/Th dating uncertainties approach 0.1% for Holocene samples (Cobb et al., 2003b, 2013; Grothe et al., 2019) and near-absolute age (less than ± 1 year) for overlapping fossil coral ensembles during the last millennium (Dee et al., 2020) (Table 1).

Counting of annual layers of deposition in ice cores and lake sediments (varves) relies on the preservation of the annual layers. The Greenland ice core timescale, for example, accumulates approximately 100 years (2 sigma) of uncertainty years over the Holocene (Rasmussen et al., 2006), although this is of considerably greater precision than usual with ^{14}C dating of single samples in the same period, and uncertainties are significantly smaller for the majority of the Holocene ice core (Table 1). One issue with comparing dating approaches is the different notations used in various chronologies, with the Greenland ice core record using “years b2k” (before 2000 CE), differing by 50 years from the commonly used “years BP” notation, where BP refers to before 1950 CE / AD 1950. This should, however, not be an issue if the reference used for a given chronology is clearly reported in the paper.

Varved lake sediments are more geographically dispersed than polar ice cores, with data reported from every continent and not necessarily at high-altitude sites. However, published records are dominantly from North America and Europe, with little coverage in the Southern Hemisphere (SH; Zolitschka et al., 2015). Varve chronologies accumulate a counting error ranging from approximately 1 - 10% (Ojala et al., 2015). The most common problem with varved sediments is that they are often not continuously layered across the whole of the Holocene and need to be anchored to calendar time by some other method (e.g., Snowball et al., 2010). For instance, radiocarbon dated records from parts of the NH suggest a short-lived climatic oscillation of ca. 2.8 ka BP, which may be correlated to a period of low solar activity (Wanner et al., 2011). This event has now been precisely constrained to a solar minimum at 2759 (±39) years BP by combining sediment climate proxies and cosmogenic radionuclide tracers for solar activity from a varved lake record (Martin-Puertas et al., 2012).

Variations in cosmic rays that are modulated by the solar and geomagnetic shielding leave a globally synchronous signal in cosmogenic radionuclide records as these particles are produced by the interaction of high-energy cosmic rays with the constituents of the atmosphere. This signal has been used to tie together ice core and absolutely dated tree ring records during the Holocene (Adolphi and Muscheler, 2016; Muscheler et al., 2014) and to U/Th-dated speleothems during the past 50 ka (Adolphi et al., 2018). This method also underlies the above-mentioned ^{14}C wiggle-match dating technique and the synchronisation of ^{10}Be records from

Greenland ice cores and lake sediments (Czymzik et al., 2018; Martin-Puertas et al., 2012). Recently, the signature of solar storms has been found in tree rings and ice core records (Mekhaldi et al., 2015; Miyake et al., 2012). Synchronising these sharp radionuclide peaks allows the synchronisation of timescales with uncertainties of 1 year or less. These signatures have helped to resolve long-standing differences between tree ring and ice core timescales (Sigl et al., 2015).

Finally, apart from absolute dating methods, there are correlation methods that have significant potential for aligning records on the same timescale. The most prominent method aims to recognise tephra horizons from the same eruption in different sites (Lane et al., 2013; Wulf et al., 2013). Especially promising for correlating records is the application of cryptotephra to lake, bog and ice core archives. For example, the event at ~2.8 ka BP highlighted above from a varve chronology is also recognised as a change in the precipitation signal in Irish bogs and is associated with several cryptotephra horizons in that region (e.g., Plunkett and Swindles, 2008). The technique has the greatest potential where multiple tephra horizons can anchor different varved lake sequences (e.g., Wulf et al., 2016), or where ice core and varved records can be anchored using widespread tephra (e.g., Lane et al., 2013).

2.3.- Statistical approaches

As mentioned in Section 2.1, the calibration of the proxy data is crucial for the reconstruction of modes of variability. From a statistical standpoint, the problem can be stated as follows: given a calibration set which contains both proxy data and climate variables, produce a reconstruction back in time that estimates the climate variables from ancient proxy data.

To evaluate the robustness of the reconstruction approach, it is necessary to perform a calibration, or learning period, over only a fraction of the available time frame where both the proxy record and the mode of variability timeseries are overlapping, keeping part of it to test whether the proxy-based reconstruction is robust over this testing time period. Many issues can cause this idealised relationship to break down and yield incorrect reconstructions (see Section 2.1).

Given the above statistical definition there are two proposed approaches (Table 2) to estimate past changes in modes of variability:

a. A regression approach where the climate variables are treated as the response and the proxies as covariates in a regression model. These approaches may range from simple linear regression up to complex machine learning (see below). The fitted model is then used to predict the modes of variability for the ancient proxy data. We term this the ‘forward regression’ approach (though other names are sometimes used), which is very common in climate science (e.g., Cook et al., 2019; Juggins and Birks, 2012; Luterbacher et al., 2002; Mann et al., 1998; Michel et al., 2020; Xoplaki et al., 2005). Popular methods such as the Composite Plus Scale and Modern Analogue techniques fall under this banner.

b. An inverse approach by which a regression model is built that describes how the proxy reacts to changes in modes of variability. Inverse regression is then used to predict the climate variable from the proxy data via this fitted model. Sometimes this inverse regression is performed *ad hoc* (Huntley et al., 1993), though more recent approaches have used Bayes' theorem, which performs the inverse regression in a probabilistic manner (e.g., Cahill et al., 2015; Haslett et al., 2006; Luterbacher et al., 2016; Parnell et al., 2015; Tingley and Huybers, 2009). We term this the 'inverse regression' approach.

The key difference between the two approaches is that in forward regression the climate variables are treated as the response variables, whereas in inverse regression the proxies are treated as response variables. In situations where normal distributions are assumed throughout, both can produce identical reconstructions. Some advantages and disadvantages of the approaches are shown in Table 2, although they have been discussed at length in other papers (Sweeney et al., 2018). In either case, the model should be thoroughly checked using the calibration period, and the use out-of-sample approaches is strongly recommended, such as cross-validation to check the fit of the model. Such an approach has been demonstrated by Cahill et al., (2016) . Once checked, estimates of climate variables must include uncertainties that are quantified via, e.g., 50% and 95% uncertainty intervals, at the very least. Both methods can be applied to the reconstruction of modes of variability. To our knowledge, regression methods have been mostly used until now, including principal component regression approaches (Cook et al., 2002; Ortega et al., 2015), partial least squares, elastic net and random forest (Breiman, 2001; Zou and Hastie, 2005). Michel et al. (2020) evaluated the strengths of these different methods to reconstruct the NAO over the last millennium using the PAGES 2K database. They showed that the random forest provides the best scores, which may be related to the capability of this method to account for non-linear linkages between the mode and proxy records, although we must be careful of overfitting with non-linear methods. Additionally, recent initiatives applying the inverse regression approach to reconstruct modes of variability are appearing (Hernández et al., In Review; Sánchez-López, 2016).

The use of pseudo-proxy approaches within climate modelling can then further help to evaluate the capability of these approaches to appropriately reconstruct the variability modes. In such a pseudo-proxy experiment, simulated data are modified to mimic real-world proxies and instrumental observations (called pseudo-proxy and pseudo instrumental datasets). The reconstruction results are then compared with the available simulated target field, providing an estimation of the skill of the method in real-world applications (Lehner et al., 2012; Ortega et al., 2015; Smerdon, 2012).

Table 2: Advantages and disadvantages of the forward and inverse regression approaches

Forward regression advantages	**Forward regression disadvantages**

·Fits into most standard regression modelling approaches so can be easily used with existing software packages (Ilvonen et al., 2016) ·Simple regression models can be replaced with more complex models, e.g., machine learning approaches	·Does not model the causal link between the proxy and the climate variable ·Can struggle to incorporate issues with the data such as measurement error (e.g., chronological error) ·No simple way to include climate model information (e.g., to constrain the reconstructed climate variables)
Inverse regression advantages	**Inverse regression disadvantages**
·Directly models the causal relationship between the proxy and the climate variables ·Allows for the easier inclusion of prior information (if the model is Bayesian) on climate changes over time ·Easier to incorporate mechanistic models into the approach	·Very little software currently available (though see Parnell et al. (2016a)). ·Requires considerable expertise to build suitable models, e.g. with high-dimensional proxy data ·Model running is considerably slower and often requires high-dimensional numerical integration

The recent rise in machine learning approaches may allow for far richer reconstructions, especially in situations where large data sets area available and where proxy data and/or climate variables are high dimensional (i.e., multiple measurements from each sample). Indeed, there is now a suite of probabilistic machine learning approaches (Chipman et al., 2010) that may fit more neatly into the current paradigm.

The introduction of mechanistic models is also a challenging target. These may occur in two different parts of the above-described approaches: the first part includes guiding the behaviour of the climate variables over time, and the second focuses on the inverse approach to create richer models of the proxy response to climate change, e.g., under non-stationary climate/proxy relationships. Whilst it has been possible for some time to use a few ensemble members of, e.g., a GCM to guide the climate reconstruction (Ilvonen et al., 2016), one can now attempt to calibrate such a mechanistic model via the proxy data. This possibility has been proposed in several recent papers under the (Bayesian) inverse regression approach (e.g., Carson et al., 2018; Parnell et al., 2015, 2016b). The introduction of such mechanistic models promises a superior understanding of climate dynamics.

Last but not least is the development of data assimilation techniques for proxy data over the last millennium (e.g., Hakim et al., 2016; Singh et al., 2018) within a climate model, some of which include modules that directly simulate the proxies to better reflect the observations - offering a new route for reconstructed modes of climate variability. Nevertheless, such methods are not dedicated to the reconstruction of the modes, which might hamper their results, since other aspects of the climate representation might interfere (model biases, absence of calibration over present-day, proxy records that are poorly sensitive to a given mode) with the target of producing a robust reconstruction with a good confidence level.

3.- Modes of climate variability

3.1.- El Niño-Southern Oscillation

El Niño-Southern Oscillation (ENSO) is the largest source of interannual climate variability on a global scale, and arises from ocean-atmosphere interactions in the tropical Pacific (Fig. 1) (Diaz and Markgraf, 2000; McPhaden et al., 2006; Philander, 1989; Rasmusson and Wallace, 1983). During El Niño warm extremes, a weakening of the easterly trade winds leads to a reduction in upwelling of cooler subsurface waters, driving anomalous surface warming in the eastern and central equatorial Pacific Ocean and a slight cooling in the far western equatorial Pacific. The spatial pattern of El Niño events varies markedly, with some characterised by maximum warming in the eastern equatorial Pacific region – so-called "Eastern Pacific" events – while others exhibit maximum warming in the central Pacific region, often referred to as "Central Pacific" or El Niño Modoki events (Ashok et al., 2007; Capotondi et al., 2014). In both cases, the redistribution of surface ocean temperatures is associated with a large eastward shift in the Walker Cell, bringing enhanced atmospheric convection and increased precipitation to the central Pacific Ocean. This reorganization of large-scale atmospheric circulation further enhances central and eastern Pacific warming and leads to profound shifts in temperature and precipitation patterns across many regions of the world via atmospheric teleconnections (Halpert and Ropelewski, 1992; Ropelewski and Halpert, 1989). El Niño impacts include drought across the Maritime Continent and in parts of India, southwestern North America, and west Africa, while flooding occurs in Central and South America and East Africa (Ropelewski and Halpert, 1987). During a La Niña events, a strengthening of the Pacific trade winds drives increased upwelling resulting in cooler ocean surface temperatures, with a set of global climate impacts that are largely opposite to those of El Niño events (Horel and Wallace, 1981).

Proxy-based reconstructions of ENSO rely on high-resolution archives (Fig. 2) such as corals, tree rings, ice cores, molluscs, speleothems and select lake and marine sediments collected from ENSO-sensitive regions (see review by Emile-Geay et al., (2020) and references therein). Individual ENSO reconstructions capture local changes in temperature and/or precipitation related to ENSO variability with varying fidelity, whereby calibration against instrumental climate records can reveal important information about proxy-specific and/or site-specific biases. Towards this goal, proxy system models, which link process models to observations to explain how archives are imprinted with environmental signals, leverage such calibration studies to inform the transformation of instrumental and/or model-derived variables of the physical climate system into plausible proxy-based records that can facilitate data-model intercomparison studies (Dee et al., 2015; Evans et al., 2013). Multiproxy syntheses of ENSO use networks of individual ENSO-sensitive records to increase signal-to-noise ratios (Braganza et al., 2009; Evans et al., 2002; Mann et al., 2000; Stahle et al., 1998; Wilson et al., 2010), with the most recent such reconstructions extending back several centuries (Dätwyler et al., 2019; Freund et al., 2019; McGregor et al., 2013).

Models and theory provide a compelling case for weakened ENSO variability during the mid-Holocene (commonly defined as 6-7 ka BP), but ENSO proxy-based reconstructions spanning the Holocene provide mixed support for this scenario (Fig. 2). Early proxy-based reconstructions from the far eastern (Moy et al., 2002; Rodbell et al., 1999) and western tropical Pacific (Tudhope et al., 2001) have lent support to this framework showing some decreased ENSO variability over the early and mid-Holocene. However, subsequent work from a diverse array of proxy-based records spanning the central to eastern tropical Pacific document a prolonged reduction in ENSO variability at some point during the 3-6 ka BP period (Carré et al., 2014; Chen et al., 2016; Cobb et al., 2013; Emile-Geay et al., 2016; Grothe et al., 2019; Koutavas and Joanides, 2012). In contrast, a newly available reconstruction based on single foraminifera chemistry analyses on a marine sediment core has revealed relatively low amplitude ENSO variability between 5.5-10 ka BP (White et al., 2018), in contrast to those derived from a coral-based reconstruction several hundred kilometres away (Cobb et al., 2013), which only show it for the mid-Holocene. This discrepancy between records (Table 3) has been suggested to result from the combination of centennial variability juxtaposed on the millennial scale changes over the Holocene (White et al., 2018), as also found in the modeled Holocene ENSO (Liu et al., 2014a). The proposed mechanism to explain the dampened ENSO in the early to mid-Holocene involves warming of the tropical Pacific thermocline due to insolation response of the south Pacific Sea Surface Temperature (SST) and/or changes in the strength of trade or westerly winds (see White et al., (2018) and references therein). As highlighted in these discrepancies, the high degree of internal variability in ENSO characteristics (amplitude, frequency, spatial footprint, and teleconnections) presents a significant barrier to the detection of forced responses in proxy-based records spanning the Holocene to present (see section 5).

Existing proxy-based ENSO reconstructions spanning the last millennium rely largely on coral records that extend back several centuries (Fig. 2), in the case of coral records recovered from living coral colonies (Freund et al., 2019; Urban et al., 2000), and/or fossil coral records dated using 234U/230Th (Chen et al., 2018; Cobb et al., 2003a). Other ENSO reconstructions include single foraminifera (Rustic et al., 2015) and tree ring-based records (Cook et al., 2008; D'Arrigo et al., 2005; Li et al., 2013, 2011; Liu et al., 2017). Against a backdrop of high variability in ENSO properties over the last millennium (Fig. 2), several studies have provided evidence for an intensification of ENSO during the Little Ice Age (LIA), approximately 400-500 years ago (Cobb et al., 2003a; Gergis and Fowler, 2009; Rustic et al., 2015). The larger availability of high-quality and resolution proxy-based ENSO records and the significant correlation between most of them during the last millennium (Table 3) provide a unique opportunity to constrain the relative roles of external forcing versus internal variability in shaping the decadal- to centennial-scale evolution of ENSO over recent centuries (see section 5).

In recent years, a number of new proxy-based records of ENSO variability spanning the last centuries to millennia resolve a significant increase in the amplitude of ENSO in recent decades (Cobb et al., 2013; Grothe et al., 2019; Li et al., 2013; Liu et al., 2017; McGregor et al., 2013). This phenomenon is in agreement with analyses of 21st century projections of ENSO properties, which reveal evidence for an intensification of ENSO's hydrological response under anthropogenic forcing (Cai et al., 2015a, 2015b, 2014; Power et al., 2013), and/or an increase in the variability of ENSO SST anomalies (Cai et al., 2018). A new reconstruction of ENSO variations using a large network of published coral records reveals an intensification of central Pacific El Niño events in the last century (Freund et al., 2019), consistent with a shift towards stronger central Pacific El Niño events derived from an analysis of the instrumental record of climate (Wang et al., 2019a). Furthermore, the longest single high-resolution reconstruction of ENSO, derived from central Pacific corals, also supports an intensification of central Pacific ENSO impacts in the last 50 years relative to the previous millennia (Grothe et al., 2019). The addition of more multicentury proxy-based ENSO reconstructions would provide more context regarding the natural variability of ENSO, allowing a more robust assessment of the hypothesised anthropogenic shifts in ENSO's spatial footprint, which remains difficult to constrain with available records. At present, all available lines of evidence point to an intensification of ENSO's impacts in the coming decades, providing stakeholders with useful information to guide climate adaptation plans. With millions of people and many valuable ecosystems severely impacted by ENSO extremes, there is a pressing need to increase the number of centuries-long, high-resolution proxy-based reconstructions of ENSO variability from a gradient of sites spanning the tropical Pacific.

Table 3.- Summary of Spearman´s rank correlation coefficients computed among the different reconstructions available for each mode of variability presented in this work. For each mode, the following information is included: the number of timeseries incorporated in the analysis, the total number of pairwise correlations computed, the amount (and percentage from the total in brackets) of pairwise correlations that are positive and significant at the 95 and 90% confidence levels, the lowest, highest and mean of all significant values at 90% correlation values. For each pairwise correlation the degrees of freedom were corrected to account for the timeseries autocorrelation. All pairwise correlations were performed between 1000 CE and 1850 or in the period of overlap between the two reconstructions if some of them were shorter. The industrial era (1850 onwards) was excluded to ensure that the calibration period of both timeseries was not included. All timeseries were interpolated to decadal resolution prior to the computation of the correlations. All Spearman´s rank pairwise correlation coefficients for each mode and their associated p-values as well as links to original dataset sources are included in the supplementary material.

Mode	N° Timeseries	N° correlations	Significant at 95%	Significant at 90%	Lowest	Highest	Mean
PDV	8	28	3 (11%)	4 (14%)	-0.66	0.53	**0.08**
ENSO	11	55	19 (35%)	20 (36%)	-0.83	0.84	**0.20**
AMV	4	6	1 (17%)	1 (17%)	0.30	0.30	**0.30**
NAO	11	55	7 (13%)	10 (18%)	-0.27	0.52	**0.26**
IOD	-	-	-	-	-	-	**-**
SAM	3	3	2 (67%)	2 (67%)	0.18	0.47	**0.32**

3.2.- Pacific Decadal Variability

Pacific Decadal Variability (PDV), which characterises low-frequency variability in the Pacific Ocean (Fig. 1), is measured by a variety of statistical patterns in Pacific SSTs or sea surface heights, most commonly the Pacific Decadal Oscillation –PDO– (Mantua et al., 1997) and the Interdecadal Pacific Oscillation –IPO– (Power et al., 1999). The PDO is based on the leading component of SSTs in the Pacific Ocean north of 20°N; when PDO is negative, there are anomalously cool SSTs along the west coast of North America and warm SSTs in the central and western North Pacific (Mantua and Hare, 2002). The IPO is defined based on the second principal component of low-frequency global SSTs (Henley et al., 2015), which allows a better definition of the IPO than using the tropical SST-based indices, since the latter includes many other variations, such as the global warming signal (Dai, 2013). During negative IPO phases, North Pacific SSTs are above average, while tropical Pacific SSTs are below average (Peng et al., 2015). Over the instrumental period, PDV has been marked by a combination of bidecadal and pentadecadal periodicities (i.e., 20 and 50 year cycles) thought to cause regime shifts when synchronised (Minobe, 1999). These shifts in PDV have been linked to global temperature trends (Kosaka and Xie, 2013; Meehl et al., 2016), as well as regional impacts on hydrology, ecological systems, and climate in North America (Dai, 2013; Kitzberger et al., 2007; Mantua et al., 1997; Trenberth et al., 2014), South America (Andreoli and Kayano, 2005; Boisier et al., 2016), East Asia (Hsu and Chen, 2011; Wang et al., 2008; Yao et al., 2018), and Australasia (Power et al., 1999; Rodriguez-Ramirez et al., 2014; Vance et al., 2015). The underlying dynamics of PDV, which may represent the superposition of multiple physical processes (Liu and Di Lorenzo, 2018; Newman et al., 2016; Schneider and Cornuelle, 2005), are not well understood. It is likely that at least some of the Pacific low-frequency variance originates from the ENSO system (Di Lorenzo et al., 2015; Newman et al., 2003) (see section 5).

Reconstructions of PDV extending to the early- or mid-Holocene are derived from bidecadal or longer periodicities found in lacustrine and marine sediments. In a 13-ka lacustrine sediment record from Montana, USA (Stone and Fritz, 2006), it was suggested that the PDO may have experienced characteristic periodicities with fundamental state changes over time, with the strongest periodicity during the mid- Holocene and a complete breakdown of multidecadal frequencies from approximately 4.5 to 3.5 ka BP (Fig. 3). This shift in periodicity over the Holocene was also noted in a 10-ka reconstruction of PDV based on marine sediments near British Columbia, Canada, which revealed a change from bidecadal and pentadecadal variability in the early Holocene to only pentadecadal periodicities in the late Holocene (Ivanochko et al., 2008). Similarly, a 9.7 ka lacustrine record of PDO from California, USA, indicated the PDO regimes may have had variable length intervals over time, lasting from 150-550 years, with extended positive PDO phases recorded in the early-Holocene (9.7–8.85 cal ka BP), mid-to-late Holocene (4.8–3.2 cal ka BP) and late Holocene (1.5–0.15 cal ka BP) (Fig. 3; Kirby et al., 2010). Lacustrine and marine sediment records covering just the late Holocene also indicate that the prominent PDV periodicities may have varied over time (Beaufort and Grelaud, 2017; Lapointe et al., 2017).

Records of PDV covering the Medieval Climate Anomaly (MCA) are available from ice cores, tree rings, and speleothems (Fig. 3). A reconstruction based on an Antarctic ice core showed that the IPO was in a persistently positive state from 1000-1212 CE, and this period was associated with extended Australian megadrought conditions (Vance et al., 2015). A lack of variance in North Pacific SSTs was also detected in a speleothem-based reconstruction during the MCA from California, USA (850-1100 CE; (McCabe-Glynn et al., 2013)). A millennial-length North American tree ring reconstruction substantiated the breakdown of pentadecadal variability from 1000-1200 CE and likewise found that the MCA was characterised by an extremely persistent negative PDO state from 992-1300 CE, contemporaneous with severe drought in North America (MacDonald and Case, 2005). Unlike the persistent positive conditions identified by Vance et al. (2015), MacDonald and Case, (2005) identified persistently negative PDO conditions during the MCA (Fig. 3).

Reconstructions of PDV from tree rings, coral, and historical records also extend through the LIA. By integrating a network of coral records from the South Pacific and tree rings from diverse locations around the Pacific Basin, Evans et al. (2001) showed that PDV was synchronised across the NH and SH over the past 200-years. A range of proxy-based records from both hemispheres indicate a muted PDV signal in the LIA and an increase in pentadecadal variability concurrent with the end of the LIA in the mid-1800s (Fig. 3). Shen et al. (2006), reconstructing PDO to the mid-1400s from Chinese historical documents, found inconsistent periodicities over the 530-year record: although the decadal and bidecadal signals were relatively consistent, the pentadecadal signal only existed after the end of the LIA around 1850. A lack of pentadecadal variability in the LIA was also reported in multiple NH tree ring-based PDO reconstructions (Biondi et al., 2001; MacDonald and Case, 2005); the bidecadal component may also have been weaker in the late-1700s and early-1800s (Biondi et al., 2001; Gedalof et al., 2002). This signal dampening extended to the SH, where a coral-based IPO reconstruction showed muted PDV in the 1700s (Linsley et al., 2008).

Much of what we know about PDV is based on the 20th century, which was characterised by quasiregular regime shifts in the 1920s, 1940s, and 1970s (Mantua et al., 1997; Minobe, 2000). Proxy-based reconstructions of PDV often diverge on pre-instrumental regime phases and timing (McAfee, 2014; Wise, 2015), which is reflected in the low correlations shown in Table 3. However, these reconstructions consistently report that the 20th century is not characteristic of the pre-instrumental past. Reconstructions show that PDV, particularly the pentadecadal component, has been highly variable over time (Ivanochko et al., 2008; Kirby et al., 2010; MacDonald and Case, 2005), with a shift in the mid-1800s (D'Arrigo et al., 2001; Gedalof and Smith, 2001) leading to a notable increase in low-frequency (pentadecadal) variability over the past century (Biondi et al., 2001; Felis et al., 2010; McCabe-Glynn et al., 2013; Shen et al., 2006). These 20th century changes indicate that there may be different drivers of PDV in the instrumental period than in the palaeoclimate past. The increase in low-frequency variability after 1850 corresponds to an increase in greenhouse gas forcing (Shen et al., 2006), and in modelling simulations, PDV continues to show significant power at longer timescales while the bidecadal signal is overwhelmed by the warming forcing (d'Orgeville and Peltier, 2009). Other potential drivers of PDV change include an increasing influence of the tropical Pacific on PDV over the past century, as indicated by proxy records (D'Arrigo et al., 2015; Wise, 2015), and decadal warming trends in the Atlantic that may be affecting PDV through changes in Walker circulation (Cai et al., 2019).

3.3.- Atlantic Multidecadal Variability

The Atlantic Multidecadal Variability (AMV) - also referred to as the Atlantic Multidecadal Oscillation (AMO) - is a coherent pattern of multidecadal variability in the North Atlantic SSTs with an estimated period ranguing from approximately 50-80 years (Schlesinger and Ramankutty, 1994). The AMV is defined as an area average of detrended low-pass filtered North Atlantic (0-65°N, 80-0°W; Fig. 1) SST anomalies (Enfield et al., 2001; Trenberth and

Shea, 2006). The AMV has wide-ranging climatic impacts on the circum-North Atlantic climate (Knight et al., 2006; Sutton and Hodson, 2005) and hurricane activity (Goldenberg et al., 2001) and farther afield including precipitation in Sahel, India and Brazil (Feng and Hu, 2008; Folland et al., 2001, 1986; Rowell et al., 1995).

The origin of the AMV remains debated in the observational and modelling community. Several hypotheses include the response of the North Atlantic SSTs to external radiative forcing, specifically by either anthropogenic or volcanic aerosols (e.g., Booth et al., 2012; Otterå et al., 2010), atmospheric-induced surface heat flux (Clement et al., 2015) and changes in the Atlantic Meridional Overturning Circulation (see Zhang et al., (2019) for a comprehensive review on this). Uncertainty not only surrounds the origin of the AMV but also its long-term periodicity. This phenomenon is largely because the length of instrumental records (~150 years) is too short to study the multidecadal nature of this mode of climate variability, which is also complicated by the underlying anthropogenically forced warming. Similarly, reconstructing this mode in the past is also challenging as the temporal resolution of most marine proxy archives is often not sufficient to study this multidecadal timescale. Only a few long oceanic records from tropical Atlantic corals exist (Black et al., 2007; Haase- Schramm et al., 2003; Kilbourne et al., 2008; Vásquez- Bedoya et al., 2012), which were initially compiled together to study their multidecadal variability (Kilbourne et al., 2014) and further updated with shorter marine records by Svendsen et al. (2014). Past reconstructions of this mode of variability (Fig. 4) are heavily reliant on high-resolution terrestrial archives, including ice cores, lake varves, historical records and tree rings (Gray et al., 2004; Mann et al., 2009; Wang et al., 2017). These AMV reconstructions either exploit the hydro and temperature climate spatial patterns associated with this mode of climate variability in the modern and assume stationarity of these in the past or rely on the spectral properties in these archives. Other studies, however, have found similar AMV patterns (Mjell et al., 2016) and spectral peaks (50-80 years) (Moffa-Sanchez et al., 2015) in past flow reconstructions in deep components of the AMOC, hence hinting at past AMV-AMOC linkage over the recent millennia as suggested in the last millennium models (Lohmann et al., 2015). However, coeval changes in SST and in other reconstructions of deep flow strength in the North Atlantic are not always found (e.g. Mjell et al., 2015).

Continuous reconstructions of the AMV over the entire Holocene are sparse due to the limited availability of subdecadally resolved climate reconstructions to study a multidecadal mode (Fig. 4). Spectral analysis of seven palaeoclimatic datasets from around the North Atlantic exhibit similar quasi-periodic oscillations to the AMV (55-70 year) with latitudinal variability in the timing of the stronger peaks across the last 8 ka (Knudsen et al., 2011). In contrast, the comparison between drought indices and SST suggested a stronger centennial AMV-like spatial pattern during the late Holocene compared with the early-Holocene (Feng et al., 2011).

Studies focused on the Common Era suggest a fairly positive AMV over the first millennium (0-1000 CE; Fig. 4) (Mann et al., 2009; Singh et al., 2018). Over the last millennium (or part of), reconstructions predominantly show a negative AMV during the LIA and a positive AMV during the MCA (Gray et al., 2004; Mann et al., 2009; Singh et al., 2018; Wang et al., 2017) (Fig. 4). These findings are in line with the warmer surface temperatures from the tropical Atlantic records (Kilbourne et al., 2014). Analysis of the available reconstructions, however, present varied degrees of correlation amongst the available records (Table 3). Spectral analysis over the last millennia show varied results. Greenland ice cores reveal different periodicities between the LIA (~20 years) and the MCA (11 and 45 years), which are noticeably different from the modern (45-65 years) (Chylek et al., 2012), whereas SSTs from the Caribbean have revealed consistent multidecadal variability since 1350 CE. In contrast, data assimilation studies show a lack of distinct multidecadal/centennial variability over the last 2 ka with the strongest multidecadal peaks found after 1900 CE (Singh et al., 2018). From 1850 CE, AMV reconstructions consistently reveal multidecadal cycles underlain by the warming signal as seen in the observational timeseries (Alexander et al., 2014; Hetzinger et al., 2008; Singh et al., 2018).

3.4.- North Atlantic Oscillation

The North Atlantic Oscillation (NAO), a mode of variability closely related to the Northern Annular Mode (NAM) / Arctic Oscillation (AO) (Thompson and Wallace, 2001, 2000), is the most prominent boreal winter (December to March) atmospheric mode of climate variability in the North Atlantic extra-tropics (Glueck and Stockton, 2001; Hurrell, 1995; Hurrell et al., 2003; Jones et al., 1997; Kodera, 2002; Wanner et al., 2001). The pattern consists of two opposite-sign centres of action over the Icelandic low and Azores high (Fig. 1), with an equivalent barotropic structure explaining up to 50% of the winter variability of the troposphere pressure fields (Hurrell et al., 2003; Wanner et al., 2001). Changes in the mean circulation patterns over the North Atlantic associated with the NAO are accompanied by changes in the mean wind direction over the Atlantic, in the heat and moisture transport between the Atlantic and the surrounding areas, and in the intensity and number of storms and their paths (Hurrell, 1995). For a comprehensive review of the wide range of responses of marine, terrestrial and freshwater ecosystems to NAO variability, see Wanner et al., (2001).

The NAO is typically defined through the leading Principal Component of gridded winter monthly Sea Level Pressure (SLP) (Portis et al., 2001; Stephenson et al., 2003), which leads to limits in its time extension since a sufficiently wide dataset on SLP mainly covers the last century. Over the past decades, there has been interest in documenting and understanding the NAO variability on annual to multidecadal timescales, by extending estimates of the NAO index as far back in time as possible (Fig. 5). The NAO variability within the instrumental period has been examined in the form of normalised pressure differences that reflect changes in the atmospheric pressure gradient between the so-called Icelandic Low and the subtropical northern Atlantic with suitably located instrumental SLP records (Stykkisholmur, Akureyri, Reykjavik; Gibraltar, Lisbon, Ponta Delgada). Recent efforts have also used other measures of the westerly strength including information from London and Paris (Cornes et al., 2013), ship logbook information from the Channel and the North Atlantic (Barriopedro et al., 2014; Mellado-Cano et al., 2019), and a combination of instrumental and ship log book data (Küttel et al., 2010). The timescales of the NAO range from days to centuries (Cook et al., 2019; Feldstein, 2000; Luterbacher et al., 2001, 1999; Ortega et al., 2015). Periods when the same state of the main NAO characteristics persist over several consecutive winters are observed within the instrumental record (e.g., the 1960s were characterised by an unusually negative NAO index and the 1990s by unusually positive values (Osborn, 2004; Scaife et al., 2005).

The NAO accounts for 35 to 50% of the variance in the winter SLP field over the North Atlantic region (Cassou and Terray, 2001; Hurrell et al., 2003; Osborn et al., 1999), and other atmospheric circulation patterns are, therefore, important to fully characterise the winter climate in the region (Cassou and Terray, 2001; Trigo et al., 2008). In particular, studies suggest that non-linear relationships between atmospheric modes and winter precipitation in the Euro-Atlantic region, modulate the climatic imprint of the NAO (Álvarez-García et al., 2019; Comas-Bru et al., 2016; Moore et al., 2013; Pinto and Raible, 2012). This phenomenon may, in turn, affect the robustness of reconstructions of past NAO states if calibrated with a short period in the recent past. In particular, the East Atlantic (EA) pattern plays an important role in positioning the primary North Atlantic storm track (Moore et al., 2011; Woollings and Blackburn, 2011), likely affecting precipitation patterns over Europe and the Mediterranean (Comas-Bru and Hernández, 2018; Comas- Bru and McDermott, 2014; Trigo et al., 2008; Xoplaki et al., 2004).

A few NAO reconstructions for the last centuries have been published and/or compared with each other(Baker et al., 2015; Cook et al., 2019; Faust et al., 2016; Hernández et al., In Review; Luterbacher et al., 2001; Olsen et al., 2012; Ortega et al., 2015; Schmutz et al., 2000; Sjolte et al., 2018; Timm et al., 2004; Trouet et al., 2009). Taking into consideration the associated reconstruction uncertainties and disparate correlations between them (Table 3), they demonstrate with high confidence that the strong positive NAO phases of the 1990s and early 20th century are not unusual in the context of the past centuries (Fig. 5). The NAO reconstruction by Trouet et al. (2009) yielded a persistent positive phase throughout most of the medieval era from the 11th to the 14th centuries, which is not, however, consistent with a strong NAO imprint in the Greenland ice core data (Sjolte et al., 2018; Vinther et al., 2010). Recent independent NAO reconstructions (Cook et al., 2019; Ortega et al., 2015) and transient model simulations neither support a persistent positive NAO during the MCA, nor a strong NAO phase shift during the LIA (Lehner et al., 2012; Masson-Delmotte et al., 2013; Moreno-Chamarro et al., 2017b; Yiou et al., 2012). Less is known about the NAO variability before medieval times (Hernández et al., In Review; Olsen et al., 2012).

A 5.2-ka lake sediment record from southwestern Greenland suggests that, approximately 4.5 and 0.65 ka ago, variability associated with the NAO changed from generally positive to variable, with intermittently negative conditions (Olsen et al., 2012). Recently, a long marine reconstruction from the Irish Shelf suggested an easterly shift of the Icelandic Low at 4.2 ka, resulting in a transition from a zonal to more meridional flow of the westerly winds over the East North Atlantic (Curran et al., 2019). However, a negative NAO-type pattern is suggested for the early- and late-Holocene, proposed to be associated with periods of higher flux of ice rafting debris (IRD) recorded in North Atlantic sediments (Bond et al., 2001, 1997) as a result of an enhanced transport of sea ice (Blindheim and Østerhus, 2013; Brahim et al., 2019). A multiproxy lake record from the Middle Atlas in Morocco, also revealed that a multi-centennial-scale NAO-type pattern, potentially related to solar variability, modulates the Western Mediterranean climate (Zielhofer et al., 2017). Another study based on two speleothem records from NW Morocco and Germany suggested that during the early-Holocene, the NAO centres were shifted in response to the deglaciation of the Laurentide ice sheet, which affected the position of the southern rainfall correlation belt (Wassenburg et al., 2016). For the mid-

Holocene, Mauri et al. (2014), using a reconstruction of temperature over Europe mainly based on pollen data, suggested that the mean state atmospheric circulation may have been shifted into a positive NAO-like configuration, although this possibility remains debated due to model simulations do not reproduce such a signal (Găinuşă-Bogdan et al., 2020).

4.5.- Indian Ocean Dipole

The Indian Ocean Dipole (IOD) is an irregular oscillation of SSTs (Fig. 1) in which the western Indian Ocean becomes alternately warmer and colder than its eastern counterpart (Abram et al., 2015). By definition, the positive IOD phases correspond to a weakening in the zonal SST gradient, and vice versa. The IOD can be classified into different types (e.g., canonical IOD and IOD Modoki) according to the location and occurrence time (Endo and Tozuka, 2016; Guo et al., 2018). IOD affects precipitation and temperature across the regions around the Indian Ocean (Abram et al., 2015), such as Africa, Australia, southern China, and southern Asia. During positive IOD phases, abnormally warm SSTs in the western Indian Ocean cause a westward shift in the convection cell that is usually situated over the eastern Indian Ocean warm pool, bringing heavy rainfall over East Africa and severe droughts over the Indonesian region and southeastern Australia (Ummenhofer et al., 2016).

Direct instrumental SST records are the most reliable source of IOD variability, but they only extend back to 1958 CE. Longer estimates are derived via interpolation or assimilation of distant observations (e.g., HadSST4; Kennedy et al., (2019)). Long-term IOD reconstructions (Fig. 6) have been developed from proxy-base climate records, such as coral, marine sediments and tree rings (Abram et al., 2020, 2015, 2007; D'Arrigo et al., 2008; Kwiatkowski et al., 2015; Watanabe et al., 2019). For example, coral δ^{18}O records are sensitive to the balance between evaporation and precipitation in the surface ocean, which is strongly related to SST, therefore allowing for monthly reconstructions that go back to 1846 CE (Abram et al., 2015). Coral Sr/Ca ratios also record SST variability and can reconstruct past IOD variations. Likewise, the Mg/Ca ratio and δ^{18}O of foraminiferal records from sediments of the Indian Ocean reflect the thermocline and temperature variability and thus capture the IOD variability (D'Arrigo et al., 2008; Kuhnert et al., 2014; Kwiatkowski et al., 2015). Annual tree ring width measurements from Java (Indonesia) reflect local changes in the Palmer Drought Severity Index and thus describe IOD variability through one of its well-established climate impacts (D'Arrigo et al., 2008).

Coral-based IOD reconstructions show consistent variability on yearly scales (Fig. 6) and support that during the 20th century, the IOD experienced an increase in frequency and intensity of its positive phases (from every 20 years at the beginning to every 4 years at the end, with a mean every 17.3 years; Abram et al. (2020, 2008)). The increase in positive IOD phases may be caused by an enhanced warming of the western Indian Ocean and by strengthened IOD-monsoon interactions, as well as by increasing greenhouse gas concentrations (Cai et al., 2014; Nakamura et al., 2009). Extreme positive IOD values were rare before 1960 (Abram et al., 2020); however, three exceptionally strong positive IOD signals in 1961, 1994, and 1997 CE were detected in several coral records (Abram et al., 2015). Also noteworthy are the recorded low events in recent years, some of which have been linked to a strong sea-ice decline in Antarctica since 2016 (Meehl et al., 2019; Wang et al., 2019b). Comparisons of highly resolved last millennium IOD reconstructions with observations suggest that the latter tend to underestimate the recurrence interval of positive IOD events during the pre-industrial period (i.e., before 1850 CE), especially in smaller reconstruction windows (Abram et al., 2015). This phenomenon might explain why positive IOD events are less frequent during the pre-industrial period compared with the 20th century.

Early- and mid-Holocene IOD records are scarcer, especially for the western Indian Ocean, thus limiting the characterization of the west-east SST gradient. IOD Holocene reconstructions based on SST-sensitive records from the eastern Indian basin (Abram et al., 2009, 2007) and precipitation pattern changes between Sumatra and East Africa and Southeast India (Niedermeyer et al., 2014) suggest a tendency towards more negative phases (i.e., a strengthened zonal SST gradient) from the mid- to the late-Holocene. In particular, SST reconstructions from fossil corals covering approximately the past 6.5 ka revealed that IOD events were probably characterised by a more persistent and stronger positive IOD during the mid-Holocene, associated with a stronger Asian monsoon driving strengthened cross-equatorial winds that enhanced the cooling conditions in the East Indian ocean (Abram et al., 2007). This positive IOD condition was further confirmed by concomitant precipitation patterns between Sumatra and East Africa and Southeast India (Niedermeyer et al., 2014). However, opposite results have also been reported. In particular, planktic foraminifera records and Mg/Ca ratios from western Sumatra suggest that the thermocline was deeper, indicative of more negative IOD conditions, in the early- and mid-Holocene compared with the late-Holocene (Kwiatkowski et al., 2015). This disagreement with previous reconstructions can be partly attributed to the different temporal resolutions and sensitivity to different climate variables of the proxies used in each study (see section 2.1). Concretely, corals well reflect the seasonal variability of the IOD while the marine sediment proxies have a lower resolution and may be more reflective of long-term changes. The characteristics of certain species (i.e., warm-water planktic foraminifera) may less accurately represent the generally cold ocean upwelling conditions, causing an overestimation of its strength (Kwiatkowski et al., 2015). In addition, the mid-Holocene climate experienced global-scale anomalies and temperature patterns in the Indian Ocean that possibly reflected remote forcing rather than the IOD, which might hamper direct comparisons in SST reconstructions between the west and east Indian Ocean (Kuhnert et al., 2014). New reconstructions including accurate dating and multiple proxies are thereby needed to better constrain the IOD variability during the Holocene.

3.6.- Southern Annular Mode

The Southern Annular Mode (SAM) is the strongest mode of atmospheric circulation variability in the extratropical regions of the SH (Gong and Wang, 1999; Marshall, 2003; Thompson and Wallace, 2000). A positive phase is associated with stronger and poleward shifted westerly winds in midlatitudes, while the negative phase is characterised by weaker and more equatorward westerlies. The SAM can be defined either as the normalised difference in pressure between 40°S and 65°S (Fig. 1) (Gong and Wang, 1999), or as the first principal component of the geopotential height, generally southward of 20°S at 850 hPa (Thompson and Wallace, 2000). The two definitions lead to similar patterns and conclusions over the instrumental era.

Changes in the SAM have been linked to widespread variations in the atmosphere, sea ice and the ocean (Gillett et al., 2006; Lefebvre et al., 2004; Sen Gupta and England, 2006; Thompson and Solomon, 2002; Thompson and Wallace, 2000). Corresponding shifts in westerlies induce anomalous temperature and precipitation patterns that include, for instance, dry conditions in Tasmania and warm anomalies over the Antarctic Peninsula during positive phases of the SAM (Gillett et al., 2006; Thompson and Solomon, 2002). The stronger winds enhance the transport of sea ice and surface oceanic waters that favour a decrease in sea-ice concentrations in the Weddell Sea and around the Antarctic Peninsula and an increase in the Ross Sea (Lefebvre et al., 2004; Oliva et al., 2017; Sen Gupta and England, 2006). Additionally, the stronger winds tend to increase upwelling in the Southern Ocean, causing a surface warming at high latitudes that may enhance the meridional overturning circulation in the Southern Ocean, although this effect could be partly counterbalanced by a concomitant increase in eddy activity (Gent, 2016; Meredith and Hogg, 2006; Sen Gupta and England, 2006). Furthermore, as the response of ocean surface currents, upwelling and eddies act at different timescales, the large-scale impacts of SAM variability may be different in interannual and longer periods (Ferreira et al., 2015).

Instrumental data allow a direct estimate of the SAM index since 1957 CE (Marshall, (2003) and update https://legacy.bas.ac.uk/met/gjma/sam.html). To extend back beyond the 1960s, SAM reconstructions (Fig. 7) have to rely on a few weather stations and indirect (proxy-based) records, mainly derived from tree rings in the mid-latitudes of the SH continents and Antarctic ice cores (Abram et al., 2014; Dätwyler et al., 2018; Fogt et al., 2009; Hessl et al., 2017; Villalba et al., 2012; Zhang et al., 2010). Reconstructions using only tree ring records are for the summer only (Villalba et al., 2012), while the annual reconstructions using a wider range of proxies may be biased towards summer as their main source of information at midlatitudes is also the tree rings (Abram et al., 2014; Dätwyler et al., 2018).

Those reconstructions indicate that the increase in the SAM index in summer observed recently and attributed to a response to anthropogenic forcing (greenhouse gas and ozone forcing; Arblaster and Meehl, 2006; Thompson et al., 2011) is likely unprecedented in the context of the past centuries (Abram et al., 2014; Dätwyler et al., 2018). Despite some inconsistencies before the 19th century (Hessl et al., 2017), long term reconstructions suggest a minimum occurred in the 15th century (Fig. 7), with a weak positive trend after that period and a relatively stable index oscillating around neutral conditions for the first centuries of the last millennium (Abram et al., 2014; Dätwyler et al., 2018; Villalba et al., 2012). This phenomenon leads to a relatively high and significant correlation between the available reconstructions (Table 3).

There is currently no formal reconstruction of the SAM covering more than 1 ka (Fig. 7). However, as the changes in the position and strength of the SH westerly winds are a major characteristic of the climate of the mid-to high latitudes of the SH, several studies have attempted to reconstruct their evolution (Fletcher and Moreno, 2012; Kilian and Lamy, 2012; Reynhout et al., 2019; Saunders et al., 2018). Unfortunately, a clear common consensus on the behaviour of the westerlies cannot be reached from those studies because of some inconsistencies between their conclusions, partly due to the proxies selected, which are influenced by precipitation or temperature and thus only indirectly related to the winds. The proxies may also reflect regional changes that would prevent a general and simple conclusion that is valid for all regions and longitudes.

Many studies suggest that the westerlies were strong during the early- to mid-Holocene (Fletcher and Moreno, 2012; Kilian and Lamy, 2012; Reynhout et al., 2019; Saunders et al., 2018), although there is also evidence for long periods of reduced winds (Anderson et al., 2018; Reynhout et al., 2019; Saunders et al., 2018). The situation appearsto be even more complex after 5 ka BP, with reconstructions showing significant centennial and millennial variability but no consistent trend among the available records, some of which suggest the development of a strong zonal regional asymmetry in the southern westerly winds (Anderson et al., 2018; Fletcher et al., 2018; Fletcher and Moreno, 2012; Reynhout et al., 2019; Saunders et al., 2018; Turney et al., 2017; Voigt et al., 2015).

4.- Mode interactions

This section summarises intra-basin and inter-basin interactions, interferences and interdependences between the modes previously described, starting with the modes in the Pacific basin (ENSO, PDV) followed by those in the Atlantic (AMV, NAO), the Indian basin (IOD) and Antarctica (SAM). For each case, we group such interactions over the observational period, the past two millennia, and the Holocene, and we summarise these in Figure 8. This Section also discusses climate signals, as recorded by proxies, that are simultaneously influenced by several modes, and that are thus sensitive to interplays between them, hampering their interpretation.

4.1. Pacific basin

Analysis based on observations suggests that atmospheric and oceanic teleconnections forced by ENSO can impact lower frequency variability, such as the PDV, through interactions of zonal and meridional modes in the Pacific (Di Lorenzo et al., 2015). However, this interaction might not be stationary in time, as found for the past millennium. While tree-ring records from California and Alberta consistently exhibit year-to-year ENSO variability across the past millennium, PDV-related multidecadal oscillations are not always present, in particular during the LIA (MacDonald and Case, 2005). In addition, two other independent multiproxy ENSO reconstructions based on precipitation- and temperature-sensitive records show no statistically significant correlation over the last millennium with PDV reconstructions based on North American and East Asian tree rings (Henke et al., 2017), yet this decoupling between ENSO/PDV is not supported by two other independent proxy-based records from Santa Barbara Basin laminated sediments covering the last 2.7 ka (Beaufort and Grelaud, 2017). In a longer context, the Santa Barbara Basin records suggest a dominant positive PDV and more intense warm ENSO events during the mid-Holocene (Friddell et al., 2003). Likewise, a record from Effingham Inlet shows evident bidecadal and pentadecadal variability in the early-Holocene but absent bidecadal variability during the late Holocene (Ivanochko et al., 2008). An opposite situation might have occurred for interannual ENSO variability, which banded corals from Papua New Guinea support, becoming stronger and more frequent over the course of the Holocene (Tudhope et al., 2001).

Regarding the link with other basins, both ENSO and NAO might have influenced the drought variability in Nicaragua over the past 1.4 ka (Stansell et al., 2013), and PDV variance has also been linked to the Atlantic Ocean (d'Orgeville and Peltier, 2007; Zhang and Delworth, 2006). The interplay between ENSO variability, Equatorial South Atlantic temperatures and the South American monsoon might have modulated mean moisture conditions in the high Ecuadorian Andes over the past a ka, with interdecadal Pacific and Atlantic variability providing the dominant forcing before and after 1500 CE, respectively (Ledru et al., 2013). ENSO may also have influenced Asian hydroclimate and monsoon variability in the MCA and LIA periods, with some possible contribution from the AMV and NAO as well (Chen et al., 2015). Medieval megadroughts over Europe have been connected with coinciding ENSO–NAO phases of the same sign during the MCA (Helama et al., 2009). A dynamic link is also suggested between the reconstructed ENSO variability and the NH climate in the past millennium, as a result of the interplay between ENSO, the Pacific Walker and monsoonal circulations, and NAO (Yan et al., 2011).

The review by Cai et al. (2019) summarises the state of knowledge regarding tropical climate variability and interactions between modes such as ENSO, PDV, AMV, and IOD both in the instrumental period and in climate models. The review details the strong and complex connections between the Atlantic, Pacific, and Indian tropical climate on interannual to multidecadal timescales; it further highlights the need for extended proxy-based records of such modes of variability in the past to provide a longer perspective for such interactions.

4.2. Atlantic, Arctic and Mediterranean basins

Multidecadal interactions between the NAO and the AMV were reviewed for the instrumental period by Grossmann and Klotzbach, (2009), interactions that were mediated via changes in the salt and heat ocean transport and the Atlantic meridional temperature gradient. More recently, Zhang et al., (2019) reviewed the impacts and teleconnections of the AMV, both from observations and model simulations, and the mechanisms by which the AMV could drive PDO phase changes or modulate ENSO and NAO variability. The review also summarises recent advances in the palaeoclimate to reconstruct AMV variability and its associated impacts.

Proxy-based studies suggest that during the MCA, hydroclimate changes over the Sahel and Mediterranean regions were caused by phase modulations in both the NAO and AMV (Lüning et al., 2019, 2018): aridity in Morocco typically coincides with a positive NAO, while increased rainfall in western Sahel occurs with a positive AMV. Likewise, rainfall on the African eastern coast has been linked to IOD phase changes (Lüning et al., 2018). Decadal and multidecadal periodicities in both NAO reconstructions and NAO-sensitive climate proxies have been extensively linked to the AMV in studies covering the entire Holocene and shorter periods within it (Fig. 8; Ait Brahim et al., 2018; Knight et al., 2006, 2005; Knudsen et al., 2011; Ojala et al., 2015; Ólafsdóttir et al., 2013; Olsen et al., 2012; Wassenburg et al., 2016). Further interactions between the NAO and other modes of variability in the NH have been proposed for the past millennia. A varve record from Lake Kalliojärvi (Central Finland) suggests alternating influences from the NAO and Siberian High over the past four millennia (Saarni et al., 2016). A compilation of Iberian marine and continental records suggests that local temperature and precipitation evolutions are explained by NAO interplays with the EA: the Roman Period (–200-500 CE) was dominated by persistent negative NAO and positive EA phases, the early Middle Ages (500-900 CE) by positive NAO and negative EA phases, the MCA (900-1300 CE) by positive NAO and EA phases, and the LIA (1300-1850 CE) by negative phases in both indices (Sánchez-López et al., 2016). In a shorter-time perspective, reconstructions since 1675 CE NAO suggest that the NAO covaried intermittently with other Eurasian circulation indices and that these interactions modulate the impact of the NAO on the European climate (Luterbacher et al., 1999; Mellado-Cano et al., 2019).

Finally, potential links between the NAO and ENSO modes (Fig. 8) have been documented in a proxy-based record from Central America, with prevailing Niña-like conditions coinciding with positive NAO phases over most of the early Middle Ages and MCA periods, and opposite situations in the most recent centuries (Stansell et al., 2013). More intricate interactions arise when considering together NAO, ENSO and AMV mode variability (Zhang et al., 2019), emphasizing the need to enhance temporal and spatial resolutions in reconstruction coverages.

4.3. Indian basin

Interactions between the IOD, monsoon, and ENSO remain poorly understood (Fig. 8) due to the short span of observations, and the presence of different types of IOD with different influences on regional precipitation (Endo and Tozuka, 2016). Studies based on observations have related decadal and interannual variability in IOD to PDV and ENSO variability, respectively (Krishnamurthy and Krishnamurthy, 2016).

A joint examination of IOD, ENSO and Asian monsoon reconstructions helps improve our understanding of precipitation and drought patterns in Africa, south-eastern Australia, and Asia (Abram et al., 2007; Endo and Tozuka, 2016; Fan et al., 2017). For example, the 1877 strong positive IOD event is widely revealed by coral-based SST reconstruction and tree ring PDSI records; this positive IOD event coincided with one of the strongest El Niño events in the last two centuries and with extreme Asian monsoon failure conditions (Abram et al., 2007; D’Arrigo et al., 2008), possibly leading to a major drought over Java (D’Arrigo et al., 2008). Other studies also support a relationship between IOD, ENSO and monsoon variability (Abram et al., 2008; D’Arrigo et al., 2008), a link that might also take place at decadal timescales between the PDV and the decadal modulations in the IOD (Krishnamurthy and Krishnamurthy, 2016). In the past millennium, a tight coupling has been detected between IOD and ENSO records, especially since 1590 CE (Abram et al., 2020). These interactions should be revisited with new proxy-based reconstructions incorporating state-of-the-art dating methods (e.g., $^{234}U/^{230}Th$ series) and archives (e.g., shells).

During the Holocene, interactions between IOD and ENSO might have modulated precipitation in Southeast Australia (Gouramanis et al., 2013) and Mauritian lowlands (de Boer et al., 2014), with quantifiable effects at Indian Ocean regional scales (Abram et al., 2008; Endo and Tozuka, 2016). Since the early-Holocene, SST variability from northwest Sumatra have experienced two dominant modes, one Indian-wide associated with ENSO impacting the tropical Pacific and

Indian oceans, and the other associated with the IOD, independent from ENSO and controlled by the equatorial monsoon system (Li et al., 2018).

4.4. Antarctica

In the instrumental record, SAM and ENSO interactions are thought to be phase-dependent (Fogt and Bromwich, 2006; Gong et al., 2010; Lim et al., 2013), with La Niña (El Niño) events being more likely during positive (negative) SAM phases (Fogt et al., 2011).

Similar interactions have also been revealed in reconstructions of the last millennium, suggesting a shift from a dominant central Pacific La Niña-like pattern concurrent with a positive SAM to a dominant El Niño-like pattern and a negative SAM phase at the onset of the LIA, i.e., approximately 1300 CE (Goodwin et al., 2014).

The linkage between the SAM and ENSO has likely fluctuated at millennial timescales over the Holocene due to its sensitivity to precession changes (Gomez et al., 2012). ENSO and SAM-like variability at centennial timescales were established after ~5.8 ka and reached peak development over the last 4600 years, according to a lake-sediment record from Chilean Patagonia (Moreno et al., 2018). Interestingly, multicentennial variability in the SAM might share a common structure and timing, within dating uncertainties, with palaeoclimate records from the NH over the last 3 ka, established through an interhemispheric coupling (Moreno et al., 2014).

5.- External natural forcing and feedback mechanisms

Climate variability during the Holocene was forced by a range of external natural forcings on different timescales. Orbital forcing varies on millennial timescales, solar forcing on decadal to centennial timescales and volcanic forcing on sub-decadal timescales (Figure 9). The timescales of the climate system response can, however, differ from the variability of the forcings, as the radiative imbalance imposed by changes in the forcings results in non-linear processes, i.e., feedbacks mechanisms, within the climate system (e.g., Hansen et al., 1997). For example, the climate system can respond fast when it is pushed past a threshold by a slow forcing (e.g., orbital forcing), or a response to a short term forcing (e.g. volcanic forcing) can be prolonged by ocean feedback. In the context of this review, variations in greenhouse gases prior to the industrial revolution are viewed as a feedback response of the climate system rather than a climate forcing itself, although some argue that the 20 ppm rise in CO_2 from -6000 CE to 1850 CE was anthropogenic (Ruddiman et al., 2011), while others argue that the ocean acted as a CO_2 source until the late Holocene (Brovkin et al., 2019).

5.1. Orbital forcing

The Earth's orbit is modulated by the gravitational pull of the major planets of the solar system. The eccentricity, obliquity and precession of the Earth's orbit vary with cycles of 100 ka, 41 ka and 25 ka, respectively, and have an effect on the distribution of seasonal insolation, and to a small extent, eccentricity affects total insolation. For example, at the end of the last ice age, the June insolation at 65°N was ~40 W/m² stronger than at present, while the autumn and winter insolation was weaker (Fig. 9a). In itself, this phenomenon provides a stronger seasonality in temperature during the early- and mid-Holocene, which are most pronounced at high latitudes (Fig. 9a). However, this phenomenon is also thought to cause a number of dynamic changes in climatic patterns.

Due to stronger modulation of insolation at high latitudes compared with low latitudes, the orbital forcing weakened the meridional temperature gradient during the early- to mid-Holocene. This phenomenon may, via different pathways, have weakened the AMOC (Fischer and Jungclaus, 2010), in turn related to North Atlantic modes of variability (Brahim et al., 2019). Nevertheless, such a response remains model dependent, as other processes, such as the reduction of sea ice export from the Arctic towards the North Atlantic, can lead to salinification of the convection sites and an increase in the AMOC (Born et al., 2010). When analysing the PMIP3 database for 6-ka BP, Găinuşă-Bogdan et al. (2020) found that the ensemble mean of models does show an intensification of the AMOC for that period compared to preindustrial simulations. Such an increase is also corroborated by deep water reconstruction (Thornalley et al., 2013) and AMOC reconstruction (Ayache et al., 2018). This increase in AMOC can also be related to the potential impact of Sapropel event in the Mediterranean, which might have enhanced the AMOC in the early-Holocene (Swingedouw et al., 2019). The orbital warming of the Arctic temperatures could have been further amplified in the mid-Holocene by ice-albedo feedbacks on sea-ice (Park et al., 2018) and northward migration of high vegetation (Renssen et al., 2005). Modelled anomalies in atmospheric circulation during the mid-Holocene have, on the one hand, shown tendencies toward a more positive mean state of the NAO (e.g., Fischer and Jungclaus, 2010) and, on the other hand, a more negative AO (Park et al., 2018), with the latter result observed in multiple models as being connected to sea-ice loss. Nevertheless, the whole PMIP3 database exhibits a very model-dependent result (Găinuşă-Bogdan et al., 2020), highlighting very poor agreement on this topic within models.

Additionally, a recent review paper examining Holocene variability in the ENSO concluded that a range of proxy-based records and model simulations all point to a weaker mid-Holocene ENSO variability (Lu et al., 2018a) (see section 3.1). Although the reason for the weaker ENSO is thought to originate from orbital forcing, the exact governing mechanisms remain unclear.

The enhanced mid-Holocene NH summer insolation also increased the low-latitude land-ocean temperature contrast driving the summer monsoons (Sjolte et al., 2014). In models, this phenomenon leads to a stronger Indian monsoon (Liu et al., 2014b) and West African monsoon (Claussen et al., 1999). The changes in the African monsoon are associated with a widespread vegetation covering what is now the Sahara Desert, known as “Green Sahara” – which in itself further amplified the monsoon flow (Lu et al., 2018b). Model results indicate that the post Green Sahara decline in vegetation could have increased the Arctic sea-ice and contributed to the negative trend of the Holocene high latitude NH temperature (Muschitiello et al., 2015).

5.2. Solar activity

Solar variability is driven by magnetic fields generated by the solar dynamo and leads to different effects, including non-stationary active processes that are visible on the solar surface such as sunspots and active regions. Solar activity can be quantified for the last 300 - 400 years using direct telescope-based solar observations, of which the most commonly used is the sunspot number (Clette et al., 2014; Svalgaard and Schatten, 2016) and, further back in time, indirect proxy data (Fig. 9b), i.e., cosmogenic radionuclides ^{14}C and ^{10}Be recorded in highly resolved natural archives such as tree rings and ice cores (Beer et al., 1990; Steinhilber et al., 2009; Stuiver and Braziunas, 1993). Cosmogenic radionuclides represent the incoming flux of galactic cosmic rays into the Earth's atmosphere, which is controlled by the heliomagnetic and geomagnetic field. Holocene solar activity reconstructions allow the identification of quasi-periodicities on different timescales such as the prominent 11-year sunspot cycle, Gleissberg (88 years), de-Vries (207 years) cycle and, more tentatively,2400-year Hallstatt cycle, as well as occasional multidecadal episodes of low / high activity known as grand solar minima/maxima (Gray et al., 2010).

Much of the evidence for solar-climate interactions relies on model simulations and statistical analyses showing 11-year sunspot cycle variations in atmospheric circulation patterns (Gray et al., 2010; Matthes et al., 2017). This evidence reveals that supposedly small solar variations (on the order of one per mil for total solar irradiance −TSI−) may cause significant climatic responses driven by feedback mechanisms and internal climate variability that are not yet fully understood (Gray et al., 2010; Haigh, 1996; Lean, 1997; Matthes et al., 2003; Swingedouw et al., 2011). Proposed sun-climate mechanisms include the following: i) changes in TSI affecting global mean surface temperature through direct heating and changes in Hadley and Walker circulation, which are sometimes expressed as the "bottom-up mechanisms" associated with ocean-atmosphere coupling (Gray et al., 2010; Haigh, 1996); ii) variations in the ultraviolet wavelength range, exceeding the range of relative TSI variability, triggering shifting stratospheric ozone concentrations and temperature gradients with an impact on the troposphere through effects on regional circulation patterns (Ineson et al., 2011; Thiéblemont et al., 2015), sometimes denoted the so-called "top-down mechanisms" (Haigh, 1994; Kodera, 2002; Matthes et al., 2006); and iii) the possible effect of charged particles generated by galactic cosmic rays with proposed impacts on cloud formation and ozone abundance (Marsh and Svensmark, 2003; Seppälä et al., 2014; Svensmark et al., 2009). Regional modes of variability might act as feedback mechanisms that amplify the solar signal as the observed climatic response to the 11-year sunspot cycle seems to have a similar spatial distribution to the main regional circulation patterns with a maximum lag of 2-4 years, e.g., AO/NAO and ENSO (Andrews et al., 2015; Gray et al., 2013; Ineson et al., 2015; Scaife et al., 2013; Seppälä and Clilverd, 2014; Tourpali et al., 2005). For instance, there is evidence for solar-induced changes in ENSO over the early-Holocene (Hernández et al., 2010; Marchitto et al., 2010), although there is also sparse evidence for this relationship during the last millennium in proxy data and models (Otto-Bliesner et al., 2016). Moreover, these solar-induced changes are also observed in PDV evolution (Beaufort and Grelaud, 2017; McCabe-Glynn et al., 2013). In turn, the linkages with the NAO over the instrumental era has remained debated both due to the short time frame and large intrinsic variability in chemistry-climate models (Chiodo et al., 2019; Gillett and Fyfe, 2013; Misios et al., 2016). On longer timescales, the number of studies reporting the interaction of solar forcing with modes of variability is still small. In the marine realm, episodes of low TSI over the last millennium could trigger persistent atmospheric blocking events associated with negative winter NAO conditions, affecting the strength of the North Atlantic subpolar gyre

(Moffa-Sánchez et al., 2014). Knudsen et al. (2014) and Menary and Scaife (2014) suggested that AMO variability might be paced by combined solar and volcanic forcings, but the impact of external forcings may have been modulated by the AMOC, resulting in a non-stationary relationship between AMO and these forcings. Reported evidence for the effects of solar forcing on atmospheric circulation is often focused on the NAO. Martin-Puertas et al. (2012) suggested the presence of a persistent reduced pressure gradient in the North Atlantic region resembling a negative NAO-like sea-level pressure pattern to explain a synchronous and in-phase response of early-spring wind strength to a grand solar minimum at 2.8 ka BP. A similar pattern could explain sun-climate linkages seen in Greenland ice cores for the last glacial maximum (Adolphi et al., 2014). Recent studies combining climate models with multiproxy reconstructions of atmospheric circulation for the North Atlantic region reveal a more complex picture as solar activity may have a major effect on the EA on decadal to centennial timescales, but no direct impact on the NAO over the last millennium (Michel et al., 2020; Sjolte et al., 2018).

5.3. Volcanism

Large explosive volcanic eruptions impact the radiative forcing of the Earth system, as these events can emit a large amount of sulphur into the stratosphere, where it is transformed through chemical reactions and microphysical processes into sulphate aerosols (Robock, 2000; Stoffel et al., 2015). These aerosols have residence times of a few months to years in the stratosphere, where they are rapidly transported everywhere through Brower-Dobson circulation. Their main radiative effect consists of reflecting shortwave radiation, the so-called parasol effect, leading to less shortwave radiation reaching the Earth's surface, thus tending to cool it. The direct radiative impact of a large tropical eruption, thus, lasts 2 to 3 years in total. If the eruption occurs at high latitudes, its transport within the stratosphere is not global, and the aerosols mainly remain at the high latitudes where the eruption occurs (Pausata et al., 2015; Toohey and Sigl, 2017). Nevertheless, a recent simulation of the relatively modest 1970 volcanic eruption that occurred in the Deception Volcano Island (Antarctica Peninsula) showed that ashes might have a larger distribution than previously thought (Geyer et al., 2017).

Over the last millennium, volcanic eruptions have been reconstructed using the deposition of sulphate aerosols within the ice cores from Greenland and Antarctica (Fig. 9c). The impacts of these eruptions are believed to have a major influence on the variability of the last millennium (Schurer et al., 2013). The cumulative effects of all the volcanic eruptions can explain the negative trend observed in the recent reconstructions from the PAGES2K database (PAGES2k Consortium et al., 2017). Volcanic eruptions can activate dynamic feedbacks within the climate system, making their impact last longer or differing only due to their radiative forcing. For instance, large volcanic eruptions lead to a positive NAO during the first few winters following the eruption (Fischer et al., 2007; Michel et al., 2020; Ortega et al., 2015; Sigl et al., 2015; Sjolte et al., 2018). Nevertheless, such an effect remains difficult to be reproduced by climate models (Driscoll et al., 2012; Swingedouw et al., 2017; Toohey et al., 2014) and may mainly concern only the largest eruptions of the last millennium. The impact of volcanic eruptions on the chance of having an "El Niño" event within the following years has also been highlighted (Adams et al., 2003; Emile-Geay et al., 2008; Khodri et al., 2017; Maher et al., 2015; Mann et al., 2005; McGregor and Timmermann, 2010; Stevenson et al., 2017), but without a systematic response of ENSO to strong volcanic eruptions (Otto-Bliesner et al., 2016). Some caveats concerning the detection of such signals in proxy-based ENSO reconstructions also exist. Modelling studies also support a causal relationship between a spate of frequent tropical eruptions during the 17th century and the relatively strong ENSO variability documented during this time (Cobb et al., 2003a). In contrast, a new 317-year-long, monthly-resolved reconstruction of ENSO spans the Samalas eruption but finds no evidence for a consistent impact on ENSO variability (Dee et al., 2020). Thus, while there may be a dynamic link between volcanic eruptions and ENSO, it may be masked by strong internal variability in ENSO (e.g., Cobb et al., 2003a; Wittenberg, 2009). Volcanic eruptions may also trigger large-scale variations in the ocean heat content and Atlantic circulation on longer timescales (Mignot et al., 2011; Otterå et al., 2010; Swingedouw et al., 2015; Zanchettin et al., 2013). Such an effect leads to a far longer climate impact of up to a few decades (Swingedouw et al., 2015), but it remains controversial within climate models in terms of the exact response (Swingedouw et al., 2017). Finally, large volcanic eruptions, such as Samalas in 1257, the largest volcanic eruption of the last millennium, or a cluster of volcanic eruptions, have been suggested to have led to a long-lasting shift of the Atlantic subpolar circulation system (Moreno-Chamarro et al., 2017a; Schleussner et al., 2015; Xoplaki et al., 2018). This circulation system has indeed been identified as a tipping element of the climate system (Born et al., 2013), which means that for a sufficiently large forcing, it can shift from one mode to another. The associated decrease in northward heat transport may then help to explain the onset and long-term duration of the LIA (Miller et al., 2012).

Volcanic activity could also have played a substantial role in climatic variability during the Holocene (Kobashi et al., 2017), but very little is known about this topic as well-dated and robust reconstructions of volcanic activity are scarce. Based on the GISP2 sulphate dataset, it has been suggested that there have been periods of more frequent explosive eruptions in the past (e.g. 9.5-11.5 ka cal BP; Zielinski et al. 1994), and based on ice core reconstruction from Antarctica, the last 2 ka may have been exceptional over the Holocene in terms of volcanic activity. Nevertheless, developments in volcanic activity reconstructions are starting to provide interesting benchmarks (e.g. Kobashi et al., (2017) for model simulations that merit further investigation to fully understand the potential role of volcanic eruptions over the Holocene.

6.- Summary and future perspectives

Global instrumental records now extend over a century into the past and provide some coverage in parts of the 19th century (Folland et al., 2002). Improvement of these datasets is on-going as data recovery efforts uncover new and forgotten sources of direct climate observations and integrate them into existing datasets to improve global reanalyses (Compo et al., 2011; Slivinski et al., 2019). These efforts are crucial for our understanding of climate variability and for testing dynamical climate predictions against observations. Indeed, recent progress indicates that large fluctuations in ENSO (Luo et al., 2008), the NAO (Smith et al., 2019) and the AMV (Hermanson et al., 2014) can now be skilfully predicted at multiyear timescales. However, questions persist regarding the robustness of these results, especially given that our direct observational data and climate prediction tests are limited to the century timescale at best (O'Reilly et al., 2017) and sample only a few phases of low frequency climate variability.

Multidecadal variations occur in all the modes of climate variability discussed in this review, and the lack of long-term instrumental data for these fluctuations present important challenges to climate science. First, we still do not fully understand the mechanisms of low frequency climate variability. As presented in this review, many studies have indentified large changes in the strength of reconstructed modes of variability. The debate still rages concerning whether observed variations in climate modes are predominantly due to internal variability or external forcing (e.g., Mann et al., 2020), and it is often unknown whether proxy measures represent changes in the modes themselves, longer timescale changes in the climate background state, non-linear interactions amongst modes or genuine non-stationarity. Fluctuations in ENSO, PDV, AMV, NAO, IOD and the SAM are all known to occur and appear to be modulated by natural forcing from solar and volcanic effects as well as anthropogenic forcing (greenhouse-gas) for the industrial period (Fig. 9; e.g., (Booth et al., 2012; Smith et al., 2016b; Wu et al., 2019). However, there are also outstanding questions about the magnitude of the response to these forcing mechanisms and their accumulated and delayed effects on the climate system (Section 5 of this review). Second, modes of variability induce changes in regional rainfall, storms and temperature that are comparable in magnitude to the effects of anthropogenic climate change (e.g., Deser et al., 2012). For example, northern European winter warming and wetting in the 1990s due to low-frequency variability in the NAO exceeded the multidecadal rate of regional climate change (Scaife et al., 2005), and extreme events worldwide are as susceptible to modes of variability as they are to decades of climate change (Fereday et al., 2018; Kenyon and Hegerl, 2008). Moreover, known interactions exist between at least some modes of variability (IOD, SAM) and anthropogenic climate change (Fig. 9d; Cai et al., 2014; Thompson et al., 2011), but they are not fully understood and require further to better comprehend their current links and perform future projections (Shepherd, 2014; Wei et al., 2019). Regardless, profound changes in regional climate are driven by climate modes and need to be carefully considered if the future bounds on regional climate change are to be understood and anticipated. Finally, some observed variability still appear to be poorly simulated in current climate models. Large synthetic samples from dynamical climate models suggest that more extreme fluctuations than are contained in the recent observations are quite plausible (Kent et al., 2017; Thompson et al., 2017), but even state-of-the-art climate models still do not appear to properly represent the amplitude of observed multidecadal variability (Kravtsov et al., 2018; Ljungqvist et al., 2019). The multidecadal variability of the NAO is difficult to reproduce in climate models and even ensembles of simulations with multiple models rarely produce trends as large as the observed change in the NAO between the 1960s and 1990s (Bracegirdle et al., 2018). There is now growing evidence that the modelled signals in climate simulations of the atmospheric circulation over the North Atlantic are simply too weak regardless of their origin (Scaife and Smith, 2018). Similarly, the most extreme El Niño events and their asymmetry with La Niña events is not well reproduced in comprehensive models (Zhang and Sun, 2014). These limitations challenge our ability to simulate the most severe and important fluctuations in regional climate and hence our ability to anticipate these climate impacts from modes of variability.

In addition to increasing information by obtaining new proxy-based reconstructions, a pressing issue is the lack of agreement between different proxy-based climate records, and continued efforts are needed to calibrate and combine multiple records to reduce reconstruction uncertainties. Such a synthesis of proxy-based data would have great utility for testing climate models. New efforts in the generation of proxy-based climate data on long timescales, with quantified errors (e.g., Dee et al., 2015; Steiger et al., 2017) and the development of free software (e.g., ClimoRec by Michel et al., 2020) using well dated and verified proxy databases, or of palaeoclimate data reanalysis techniques could yield such datasets (Amrhein et al., 2018; Tardif et al., 2019).

Hence, the presence of only a few cycles of low-frequency variability in our instrumental climate records, the importance of low-frequency variability for regional climate and the need for validation of climate models make modes of variability a high-priority topic for climate science. These points alone motivate the study of past variations in modes of climate variability using long climate-proxy records, and the extension of quantitative proxy-based records beyond the last millennium and their combination into improved reconstructions is needed to provide sufficiently long records with enough accuracy to understand low-frequency climate dynamics and draw robust conclusions from comparisons with climate models. This activity is all the more urgent given the current rapid rate of climate change.

Acknowledgements

A.H. is supported by a Beatriu de Pinós –Marie Curie Cofund programme fellowship (2016 BP 00023) and HOLMODRIVE - North Atlantic Atmospheric Patterns influence on Western Iberia Climate: From the Lateglacial to the Present (PTDC/CTA-GEO/29029/2017) project funded by the Fundação para a Ciência e a Tecnologia, Portugal (FCT). A.H., S.G., and S.P-R. thank the Spanish research project PaleoModes (CGL2016-75281-C2-1-R) which provided some of their financial support. E.M.-C. contribution was funded by the project PARAMOUR (30454083) from the EOS program by the FNR.SFNRS. CM-P is supported by the Royal Society (ref: DH150185). P.O. contribution has been supported by the Ramon y Cajal senior tenure programme from the Spanish Ministry of Economy and Competitiveness. The Spanish PTI PolarCSIC (https://www.polarcsic.es) is also acknowledged for providing partial financial support to S.G. A. P.'s work was supported by a Science Foundation Ireland Career Development Award (17/CDA/4695), a research centre award (12/RC/2289_P2), an investigator award (16/IA/4520), and a Marine Research Programme funded by the Irish Government, cofinanced by the European Regional Development Fund (Grant-Aid Agreement No. PBA/CC/18/01). J.S. is supported by the strategic research program of ModEling the Regional and Global Earth system (MERGE) hosted by the Faculty of Science at Lund University. D.S. is supported by Blue-Action (European Union's Horizon 2020 research and innovation program, Grant Number: 727852) and EUCP (European Union's Horizon 2020 research and innovation programme under grant agreement no 776613) projects as well as by the French national program LEFE/INSU with VADEMECUM project. G. X. thanks the funding from the Chinese Scholarship Council (201704910171). This study is partly based on discussions held during the joint workshop of the

CLIMOVAR group and IBCC-lo2k project, Barcelona, 25–27 September 2013. PAGES and IBCC-lo2k are thanked for supporting this workshop.

Figure Captions

Figure 1. Modes of climate variability presented in this review. Squares indicate the area where the mode is usually defined. Blue and grey colours indicate oceanic and atmospheric modes, respectively.

Figure 2. ENSO reconstructions for the past 8000 years (links to original sources are included in the Supplementary Material). a-c. Reconstructions between -6000 and 1000 CE (left panels): a. Koutavas and Joanides (2012): Zonal SST gradient anomaly (in K; blue) relative to the Late Holocene (-2000–2000 CE), calculated as the difference between the averages of seven western and two eastern Pacific sediment cores. Meridional gradient in $\delta^{18}O$ (in ‰ Vienna Pee-Dee Belemnite, VPDB; red) calculated as the difference between four northern and four southern sediment cores. Stronger gradients point to an increase in ENSO variability. Note the two series share the vertical axis. b. Chen et al. (2016). ENSO variability based on the standard deviation of the 2–7-year band in $\delta^{18}O$ of a speleothem with sub-annual resolution. c. Grothe et al. (2019). Relative ENSO variance changes in high-pass filtered fossil coral $\delta^{18}O$ relative to the 1987–2007 CE. Coral data include those from Cobb et al. (2003a), Cobb et al. (2013), and McGregor et al. (2010). d-k. ENSO reconstructions covering the past millennium (right panels): d. Stahle et al. (1998; blue) and Mann et al. (2000; red). e. D'Arrigo et al. (2005; red) and Cook et al. (2008; blue). f. Braganza et al. (2009)'s R5 (red) and R8 (blue) indices. g. Gergis and Fowler, (2009)'s magnitude of El Niño (red) and La Niña events (blue) ranging from weak (1) to extreme (5). h. Wilson et al. (2010)'s Pacific 'centre of action' (blue) and 'teleconnected' (red) indices. i. Li et al. (2011; blue) and Li et al. (2013; red). j. McGregor et al. (2010; red) and Dätwyler et al., (2019; blue), with 95% confidence intervals (shading). k. Freund et al. (2019)'s annual El Niño Cold Tongue (red) and El Niño Warm Pool (blue) indices. Indices in d, e, f, h, i, and k are normalised with respect to the common period 1940–1970 to facilitate comparison. Yearly indices (thin lines) are smoothed with an 11-year running mean (thick lines), but in i the thick blue is the 21-year running ENSO variance provided by Li et al. (2011). Note the time axis has a different scale before and after 1000 CE (indicated by the vertical dashed line).

Figure 3. PDV reconstructions for the past 2500 years (links to original sources are included in the Supplementary Material). a. D'Arrigo et al. (2001; blue) and Gedalof and Smith (2001; red). b. Biondi et al. (2001; blue), and MacDonald and Case (2005; red). c. D'Arrigo and Wilson (2006; red), Shen et al. (2006; gray), and Felis et al. (2010; blue) and d. Mann et al. (2009; red) with 95% confidence intervals (shading), and Linsley et al. (2008; blue) with 1 sigma error (shading). All indices are smoothed with an 11-year running mean.

Figure 4. AMV reconstructions for the past 1500 years (links to original sources are included in the Supplementary Material). a. Gray et al. (2004; blue), Mann et al. (2009; red), with 95% confidence intervals (shading); b. Kilbourne et al. (2014; red) with 1 sigma and 2 sigma (darker and lighter shading, respectively), and Wang et al. (2017; blue) with the root mean square error

(shading). For clarity, the indices by Gray et al., (2004) and Kilbourne et al., (2014) are scaled, and the one by Wang et al. (2017) is smoothed with an 11-year running mean.

Figure 5. NAO reconstructions for the past 5300 years (links to original sources are included in the Supplementary Material). a. Baker et al. (2015; red), and Faust et al. (2016; blue). b. Olsen et al. (2012; red) with estimated error (shading), and Timm et al. (2004; blue). c. Glueck and Stockton (2001; red) and December–February Luterbacher et al. (2001; blue). d. Trouet et al. (2009; blue) and Ortega et al. (2015; red), with the total ensemble spread and the regression uncertainty across the ensemble (lighter and darker shading respectively); e. Cook et al. (2019; red) with 90% quantile uncertainty (shading) and Mellado-Cano et al. (2019); f. Sjolte et al. (2018; red) and Michel et al. (2020; red). The indices with annual resolution from Glueck and Stockton (2001), Luterbacher et al. (2001), Timm et al. (2004), Ortega et al. (2015), Sjolte et al. (2018), Cook et al. (2019), Mellado-Cano et al. (2019), and Michel et al. (2020) are smoothed with an 11-year running mean. Note the time axis changes the scale before and after 1000 CE (indicated by the vertical dashed line).

Figure 6. IOD proxy-based reconstruction and instrumental data (links to original sources are included in the Supplementary Material). Annual-mean Abram et al. (2008; blue), with the unfiltered and filtered Dipole Mode Index in lighter and darker colour, and Abram et al. (2020; red).

Figure 7. SAM index reconstructions and instrumental data for the past 1000 years (links to original sources are included in the Supplementary Material). a. Fogt et al., (2009; blue), and Villalba et al., (2012; red), with the associated uncertainty bands (shading). b. Abram et al. (2014; red) with 95% confidence intervals (shading), and Dätwyler et al. (2018; blue) with 90% confidence intervals (shading). All indices are smoothed with an 11-year running mean.

Figure 8. Major modes of variability interactions. Arrows show connections between modes identified by the literature described in Section 7 for the instrumental (green), past millennium (blue) and Holocene (red) periods. Discontinuous lines indicate contradictory links or no link between PDV and ENSO according to different works (see Section 7 for details) and non-stationary links between the SAM and ENSO over time.

Figure 9. External forcing for the past 8000 years. a. Insolation at 65°N (in W/m²). b. Total solar irradiance (in W/m²) from Steinhilber et al. (2009; blue) and Sjolte et al. (2018; red). c. Global volcanic forcing (in W/m²) from Sigl et al. (2015; green) and Kobashi et al. (2017; gray). d. Concentration of well-mixed greenhouse gases: CO_2 (in ppm, orange) from Bereiter et al. (2015; solid line) and Rubino et al. (2019; dashed lines); N_20 (in ppb; gray) and CH_4 (in ppb; blue) from Spahni et al. (2005; solid lines) and Rubino et al. (2019; dashed lines). Note the different axis for CH_4.

Declaration of interests

☒ The authors declare that they have no known competing financial interests or personal relationships that could have appeared to influence the work reported in this paper.

REFERENCES

Abram, N.J., Dixon, B.C., Rosevear, M.G., Plunkett, B., Gagan, M.K., Hantoro, W.S., Phipps, S.J., 2015. Optimized coral reconstructions of the Indian Ocean Dipole: An assessment of location and length considerations. Paleoceanography 30, 1391–1405. https://doi.org/10.1002/2015PA002810

Abram, N.J., Gagan, M.K., Cole, J.E., Hantoro, W.S., Mudelsee, M., 2008. Recent intensification of tropical climate variability in the Indian Ocean. Nat. Geosci. 1, 849–853. https://doi.org/10.1038/ngeo357

Abram, N.J., Gagan, M.K., Liu, Z., Hantoro, W.S., McCulloch, M.T., Suwargadi, B.W., 2007. Seasonal characteristics of the Indian Ocean Dipole during the Holocene epoch. Nature 445, 299–302. https://doi.org/10.1038/nature05477

Abram, N.J., McGregor, H.V., Gagan, M.K., Hantoro, W.S., Suwargadi, B.W., 2009. Oscillations in the southern extent of the Indo-Pacific Warm Pool during the mid-Holocene. Quat. Sci. Rev. 28, 2794–2803. https://doi.org/10.1016/j.quascirev.2009.07.006

Abram, N.J., Mulvaney, R., Vimeux, F., Phipps, S.J., Turner, J., England, M.H., 2014. Evolution of the Southern Annular Mode during the past millennium. Nat. Clim. Change 4, 564–569. https://doi.org/10.1038/nclimate2235

Abram, N.J., Wright, N.M., Ellis, B., Dixon, B.C., Wurtzel, J.B., England, M.H., Ummenhofer, C.C., Philibosian, B., Cahyarini, S.Y., Yu, T.-L., Shen, C.-C., Cheng, H., Edwards, R.L., Heslop, D., 2020. Coupling of Indo-Pacific climate variability over the last millennium. Nature 579, 385–392. https://doi.org/10.1038/s41586-020-2084-4

Adams, J.B., Mann, M.E., Ammann, C.M., 2003. Proxy evidence for an El Niño-like response to volcanic forcing. Nature 426, 274–278. https://doi.org/10.1038/nature02101

Adolphi, F., Muscheler, R., 2016. Synchronizing the Greenland ice core and radiocarbon timescales over the Holocene – Bayesian wiggle-matching of cosmogenic radionuclide records. Clim. Past 12, 15–30. https://doi.org/10.5194/cp-12-15-2016

Adolphi, F., Muscheler, R., Svensson, A., Aldahan, A., Possnert, G., Beer, J., Sjolte, J., Björck, S., Matthes, K., Thiéblemont, R., 2014. Persistent link between solar activity and Greenland climate during the Last Glacial Maximum. Nat. Geosci. 7, 662–666. https://doi.org/10.1038/ngeo2225

Ait Brahim, Y., Wassenburg, J.A., Cruz, F.W., Sifeddine, A., Scholz, D., Bouchaou, L., Dassié, E.P., Jochum, K.P., Edwards, R.L., Cheng, H., 2018. Multi-decadal to centennial hydro-climate variability and linkage to solar forcing in the Western Mediterranean during the last 1000 years. Sci. Rep. 8, 1–8. https://doi.org/10.1038/s41598-018-35498-x

Alexander, M.A., Halimeda Kilbourne, K., Nye, J.A., 2014. Climate variability during warm and cold phases of the Atlantic Multidecadal Oscillation (AMO) 1871–2008. J. Mar. Syst., Atlantic Multidecadal Oscillation-mechanism and impact on marine ecosystems 133, 14–26. https://doi.org/10.1016/j.jmarsys.2013.07.017

Álvarez-García, F.J., OrtizBevia, M.J., Cabos, W., Tasambay-Salazar, M., RuizdeElvira, A., 2019. Linear and nonlinear links of winter European precipitation to Northern Hemisphere circulation patterns. Clim. Dyn. 52, 6533–6555. https://doi.org/10.1007/s00382-018-4531-6

Amrhein, D.E., Wunsch, C., Marchal, O., Forget, G., 2018. A Global Glacial Ocean State Estimate Constrained by Upper-Ocean Temperature Proxies. J. Clim. 31, 8059–8079. https://doi.org/10.1175/JCLI-D-17-0769.1

Anderson, H.J., Moy, C.M., Vandergoes, M.J., Nichols, J.E., Riesselman, C.R., Hale, R.V., 2018. Southern Hemisphere westerly wind influence on southern New Zealand hydrology during the Lateglacial and Holocene. J. Quat. Sci. 33, 689–701. https://doi.org/10.1002/jqs.3045

Andreoli, R.V., Kayano, M.T., 2005. ENSO-related rainfall anomalies in South America and associated circulation features during warm and cold Pacific decadal oscillation regimes. Int. J. Climatol. 25, 2017–2030. https://doi.org/10.1002/joc.1222

Andrews, M.B., Knight, J.R., Gray, L.J., 2015. A simulated lagged response of the North Atlantic Oscillation to the solar cycle over the period 1960–2009. Environ. Res. Lett. 10, 054022. https://doi.org/10.1088/1748-9326/10/5/054022

Arblaster, J.M., Meehl, G.A., 2006. Contributions of External Forcings to Southern Annular Mode Trends. J. Clim. 19, 2896–2905. https://doi.org/10.1175/JCLI3774.1

Ashok, K., Behera, S.K., Rao, S.A., Weng, H., Yamagata, T., 2007. El Niño Modoki and its possible teleconnection. J. Geophys. Res. Oceans 112. https://doi.org/10.1029/2006JC003798

Ayache, M., Swingedouw, D., Mary, Y., Eynaud, F., Colin, C., 2018. Multi-centennial variability of the AMOC over the Holocene: A new reconstruction based on multiple proxy-derived SST records. Glob. Planet. Change 170, 172–189. https://doi.org/10.1016/j.gloplacha.2018.08.016

Baker, A., Hellstrom, J.C., Kelly, B.F.J., Mariethoz, G., Trouet, V., 2015. A composite annual-resolution stalagmite record of North Atlantic climate over the last three millennia. Sci. Rep. 5, 1–8. https://doi.org/10.1038/srep10307

Barnston, A.G., Livezey, R.E., 1987. Classification, Seasonality and Persistence of Low-Frequency Atmospheric Circulation Patterns. Mon. Weather Rev. 115, 1083–1126. https://doi.org/10.1175/1520-0493(1987)115<1083:CSAPOL>2.0.CO;2

Barriopedro, D., Gallego, D., Alvarez-Castro, M.C., García-Herrera, R., Wheeler, D., Peña-Ortiz, C., Barbosa, S.M., 2014. Witnessing North Atlantic westerlies variability from ships' logbooks (1685–2008). Clim. Dyn. 43, 939–955. https://doi.org/10.1007/s00382-013-1957-8

Bastos, A., Janssens, I.A., Gouveia, C.M., Trigo, R.M., Ciais, P., Chevallier, F., Peñuelas, J., Rödenbeck, C., Piao, S., Friedlingstein, P., Running, S.W., 2016. European land CO 2 sink influenced by NAO and East-Atlantic Pattern coupling. Nat. Commun. 7, 1–9. https://doi.org/10.1038/ncomms10315

Beaufort, L., Grelaud, M., 2017. A 2700-year record of ENSO and PDO variability from the Californian margin based on coccolithophore assemblages and calcification. Prog. Earth Planet. Sci. 4, 5. https://doi.org/10.1186/s40645-017-0123-z

Beer, J., Blinov, A., Bonani, G., Finkel, R.C., Hofmann, H.J., Lehmann, B., Oeschger, H., Sigg, A., Schwander, J., Staffelbach, T., Stauffer, B., Suter, M., Wötfli, W., 1990. Use of 10 Be in polar ice to trace the 11-year cycle of solar activity. Nature 347, 164–166. https://doi.org/10.1038/347164a0

Beguería, S., Vicente-Serrano, S.M., Tomás-Burguera, M., Maneta, M., 2016. Bias in the variance of gridded data sets leads to misleading conclusions about changes in climate variability. Int. J. Climatol. 36, 3413–3422. https://doi.org/10.1002/joc.4561

Benito, G., Macklin, M.G., Panin, A., Rossato, S., Fontana, A., Jones, A.F., Machado, M.J., Matlakhova, E., Mozzi, P., Zielhofer, C., 2015. Recurring flood distribution patterns related to short-term Holocene climatic variability. Sci. Rep. 5, 16398. https://doi.org/10.1038/srep16398

Bereiter, B., Eggleston, S., Schmitt, J., Nehrbass-Ahles, C., Stocker, T.F., Fischer, H., Kipfstuhl, S., Chappellaz, J., 2015. Revision of the EPICA Dome C CO2 record from 800 to 600 kyr before present. Geophys. Res. Lett. 42, 542–549. https://doi.org/10.1002/2014GL061957

Biondi, F., Gershunov, A., Cayan, D.R., 2001. North Pacific Decadal Climate Variability since 1661. J. Clim. 14, 5–10. https://doi.org/10.1175/1520-0442(2001)014<0005:NPDCVS>2.0.CO;2

Blaauw, M., Christen, J.A., Bennett, K.D., Reimer, P.J., 2018. Double the dates and go for Bayes — Impacts of model choice, dating density and quality on chronologies. Quat. Sci. Rev. 188, 58–66. https://doi.org/10.1016/j.quascirev.2018.03.032

Blaauw, M., Christen, J.A., Mauquoy, D., van der Plicht, J., Bennett, K.D., 2007. Testing the timing of radiocarbon-dated events between proxy archives. The Holocene 17, 283–288. https://doi.org/10.1177/0959683607075857

Black, D.E., Abahazi, M.A., Thunell, R.C., Kaplan, A., Tappa, E.J., Peterson, L.C., 2007. An 8-century tropical Atlantic SST record from the Cariaco Basin: Baseline variability, twentieth-century warming, and Atlantic hurricane frequency. Paleoceanography 22. https://doi.org/10.1029/2007PA001427

Blindheim, J., Østerhus, S., 2013. The Nordic Seas, Main Oceanographic Features, in: The Nordic Seas: An Integrated Perspective. American Geophysical Union (AGU), pp. 11–37. https://doi.org/10.1029/158GM03

Blockley, S.P.E., Blaauw, M., Bronk Ramsey, C., van der Plicht, J., 2007. Building and testing age models for radiocarbon dates in Lateglacial and Early Holocene sediments. Quat. Sci. Rev., Early Holocene climate oscillations - causes and consequences 26, 1915–1926. https://doi.org/10.1016/j.quascirev.2007.06.007

Boisier, J.P., Rondanelli, R., Garreaud, R., Muñoz, F., 2016. Anthropogenic Contribution to the Southeast Pacific Precipitation Decline and Recent (2010-2015) Mega-Drought in Chile. Am. Geophys. Union Fall Meet. 2015 Abstr. Id H43E-1549 43, 1–9. https://doi.org/10.1002/2015GL067265.Abstract

Bond, G., Kromer, B., Beer, J., Muscheler, R., Evans, M.N., Showers, W., Hoffmann, S., Lotti-Bond, R., Hajdas, I., Bonani, G., 2001. Persistent Solar Influence on North Atlantic Climate During the Holocene. Science 294, 2130–2136. https://doi.org/10.1126/science.1065680

Bond, G., Showers, W., Cheseby, M., Lotti, R., Almasi, P., deMenocal, P., Priore, P., Cullen, H., Hajdas, I., Bonani, G., 1997. A Pervasive Millennial-Scale Cycle in North Atlantic Holocene and Glacial Climates. Science 278, 1257–1266. https://doi.org/10.1126/science.278.5341.1257

Booth, B.B.B., Dunstone, N.J., Halloran, P.R., Andrews, T., Bellouin, N., 2012. Aerosols implicated as a prime driver of twentieth-century North Atlantic climate variability. Nature 484, 228–232. https://doi.org/10.1038/nature10946

Born, A., Nisancioglu, K.H., Braconnot, P., 2010. Sea ice induced changes in ocean circulation during the Eemian. Clim. Dyn. 35, 1361–1371. https://doi.org/10.1007/s00382-009-0709-2

Born, A., Stocker, T.F., Raible, C.C., Levermann, A., 2013. Is the Atlantic subpolar gyre bistable in comprehensive coupled climate models? Clim. Dyn. 40, 2993–3007. https://doi.org/10.1007/s00382-012-1525-7

Bracegirdle, T.J., Lu, H., Eade, R., Woollings, T., 2018. Do CMIP5 Models Reproduce Observed Low-Frequency North Atlantic Jet Variability? Geophys. Res. Lett. 45, 7204–7212. https://doi.org/10.1029/2018GL078965

Bradley, R.S., 2015. Chapter 1 - Paleoclimatic Reconstruction, in: Bradley, R.S. (Ed.), Paleoclimatology (Third Edition). Academic Press, San Diego, pp. 1–11. https://doi.org/10.1016/B978-0-12-386913-5.00001-6

Braganza, K., Gergis, J.L., Power, S.B., Risbey, J.S., Fowler, A.M., 2009. A multiproxy index of the El Niño–Southern Oscillation, A.D. 1525–1982. J. Geophys. Res. Atmospheres 114. https://doi.org/10.1029/2008JD010896

Brahim, Y.A., Wassenburg, J.A., Sha, L., Cruz, F.W., Deininger, M., Sifeddine, A., Bouchaou, L., Spötl, C., Edwards, R.L., Cheng, H., 2019. North Atlantic Ice-Rafting, Ocean and Atmospheric Circulation During the Holocene: Insights From Western Mediterranean Speleothems. Geophys. Res. Lett. 46, 7614–7623. https://doi.org/10.1029/2019GL082405

Breiman, L., 2001. Random Forests. Mach. Learn. 45, 5–32. https://doi.org/10.1023/A:1010933404324

Brovkin, V., Lorenz, S., Raddatz, T., Ilyina, T., Stemmler, I., Toohey, M., Claussen, M., 2019. What was the source of the atmospheric CO_2 increase during the Holocene? Biogeosciences 16, 2543–2555. https://doi.org/10.5194/bg-16-2543-2019

Cahill, N., Kemp, A.C., Horton, B.P., Parnell, A.C., 2016. A Bayesian hierarchical model for reconstructing relative sea level: from raw data to rates of change. Clim. Past 12, 525–542. https://doi.org/10.5194/cp-12-525-2016

Cahill, N., Kemp, A.C., Horton, B.P., Parnell, A.C., 2015. MODELING SEA-LEVEL CHANGE USING ERRORS-IN-VARIABLES INTEGRATED GAUSSIAN PROCESSES. Ann. Appl. Stat. 9, 547–571.

Cai, W., Borlace, S., Lengaigne, M., van Rensch, P., Collins, M., Vecchi, G., Timmermann, A., Santoso, A., McPhaden, M.J., Wu, L., England, M.H., Wang, G., Guilyardi, E., Jin, F.-F., 2014. Increasing frequency of extreme El Niño events due to greenhouse warming. Nat. Clim. Change 4, 111–116. https://doi.org/10.1038/nclimate2100

Cai, W., Santoso, A., Wang, G., Yeh, S.-W., An, S.-I., Cobb, K.M., Collins, M., Guilyardi, E., Jin, F.-F., Kug, J.-S., Lengaigne, M., McPhaden, M.J., Takahashi, K., Timmermann, A., Vecchi, G., Watanabe, M., Wu, L., 2015a. ENSO and greenhouse warming. Nat. Clim. Change 5, 849–859. https://doi.org/10.1038/nclimate2743

Cai, W., Wang, G., Dewitte, B., Wu, L., Santoso, A., Takahashi, K., Yang, Y., Carréric, A., McPhaden, M.J., 2018. Increased variability of eastern Pacific El Niño under greenhouse warming. Nature 564, 201–206. https://doi.org/10.1038/s41586-018-0776-9

Cai, W., Wang, G., Santoso, A., McPhaden, M.J., Wu, L., Jin, F.-F., Timmermann, A., Collins, M., Vecchi, G., Lengaigne, M., England, M.H., Dommenget, D., Takahashi, K., Guilyardi, E., 2015b. Increased frequency of extreme La Niña events under greenhouse warming. Nat. Clim. Change 5, 132–137. https://doi.org/10.1038/nclimate2492

Cai, W., Wu, L., Lengaigne, M., Li, T., McGregor, S., Kug, J.-S., Yu, J.-Y., Stuecker, M.F., Santoso, A., Li, X., Ham, Y.-G., Chikamoto, Y., Ng, B., McPhaden, M.J., Du, Y., Dommenget, D., Jia, F., Kajtar, J.B., Keenlyside, N., Lin, X., Luo, J.-J., Martín-Rey, M., Ruprich-Robert, Y., Wang, G., Xie, S.-P., Yang, Y., Kang, S.M., Choi, J.-Y., Gan, B., Kim, G.-I., Kim, C.-E., Kim, S., Kim, J.-H., Chang, P., 2019. Pantropical climate interactions. Science 363. https://doi.org/10.1126/science.aav4236

Capotondi, A., Wittenberg, A.T., Newman, M., Di Lorenzo, E., Yu, J.-Y., Braconnot, P., Cole, J., Dewitte, B., Giese, B., Guilyardi, E., Jin, F.-F., Karnauskas, K., Kirtman, B., Lee, T., Schneider, N., Xue, Y., Yeh, S.-W., 2014. Understanding ENSO Diversity. Bull. Am. Meteorol. Soc. 96, 921–938. https://doi.org/10.1175/BAMS-D-13-00117.1

Carré, M., Sachs, J.P., Purca, S., Schauer, A.J., Braconnot, P., Falcón, R.A., Julien, M., Lavallée, D., 2014. Holocene history of ENSO variance and asymmetry in the eastern tropical Pacific. Science 345, 1045–1048. https://doi.org/10.1126/science.1252220

Carson, J., Crucifix, M., Preston, S., Wilkinson, R.D., 2018. Bayesian model selection for the glacial–interglacial cycle. J. R. Stat. Soc. Ser. C Appl. Stat. 67, 25–54. https://doi.org/10.1111/rssc.12222

Cassou, C., Terray, L., 2001. Dual influence of Atlantic and Pacific SST anomalies on the North Atlantic/Europe winter climate. Geophys. Res. Lett. 28, 3195–3198. https://doi.org/10.1029/2000GL012510

Chen, J., Chen, F., Feng, S., Huang, W., Liu, J., Zhou, A., 2015. Hydroclimatic changes in China and surroundings during the Medieval Climate Anomaly and Little Ice Age: spatial patterns and possible mechanisms. Quat. Sci. Rev. 107, 98–111. https://doi.org/10.1016/j.quascirev.2014.10.012

Chen, S., Hoffmann, S.S., Lund, D.C., Cobb, K.M., Emile-Geay, J., Adkins, J.F., 2016. A high-resolution speleothem record of western equatorial Pacific rainfall: Implications for Holocene ENSO evolution. Earth Planet. Sci. Lett. 442, 61–71. https://doi.org/10.1016/j.epsl.2016.02.050

Chen, T., Cobb, K.M., Roff, G., Zhao, J., Yang, H., Hu, M., Zhao, K., 2018. Coral-Derived Western Pacific Tropical Sea Surface Temperatures During the Last Millennium. Geophys. Res. Lett. 45, 3542–3549. https://doi.org/10.1002/2018GL077619

Chiodo, G., Oehrlein, J., Polvani, L.M., Fyfe, J.C., Smith, A.K., 2019. Insignificant influence of the 11-year solar cycle on the North Atlantic Oscillation. Nat. Geosci. 12, 94–99. https://doi.org/10.1038/s41561-018-0293-3

Chipman, H.A., George, E.I., McCulloch, R.E., 2010. BART: Bayesian additive regression trees. Ann. Appl. Stat. 4, 266–298. https://doi.org/10.1214/09-AOAS285

Christensen, J.H., Aldrian, E., Fonseca, I., Kanyanga, J., Kossin, J.P., Renwick, J., Stephenson, D.B., Zhou, T., 2013. Climate Phenomena and their Relevance for Future Regional Climate Change Supplementary Material. https://doi.org/10.1017/cbo9781107415324.028

Chylek, P., Folland, C., Frankcombe, L., Dijkstra, H., Lesins, G., Dubey, M., 2012. Greenland ice core evidence for spatial and temporal variability of the Atlantic Multidecadal Oscillation. Geophys. Res. Lett. 39. https://doi.org/10.1029/2012GL051241

Claussen, M., Kubatzki, C., Brovkin, V., Ganopolski, A., Hoelzmann, P., Pachur, H.-J., 1999. Simulation of an abrupt change in Saharan vegetation in the Mid-Holocene. Geophys. Res. Lett. 26, 2037–2040. https://doi.org/10.1029/1999GL900494

Clement, A., Bellomo, K., Murphy, L.N., Cane, M.A., Mauritsen, T., Rädel, G., Stevens, B., 2015. The Atlantic Multidecadal Oscillation without a role for ocean circulation. Science 350, 320–324. https://doi.org/10.1126/science.aab3980

Clette, F., Svalgaard, L., Vaquero, J.M., Cliver, E.W., 2014. Revisiting the Sunspot Number. Space Sci. Rev. 186, 35–103. https://doi.org/10.1007/s11214-014-0074-2

Cobb, K.M., Charles, C.D., Cheng, H., Edwards, R.L., 2003a. El Niño/Southern Oscillation and tropical Pacific climate during the last millennium. Nature 424, 271–276. https://doi.org/10.1038/nature01779

Cobb, K.M., Charles, C.D., Cheng, H., Kastner, M., Edwards, R.L., 2003b. U/Th-dating living and young fossil corals from the central tropical Pacific. Earth Planet. Sci. Lett. 210, 91–103. https://doi.org/10.1016/S0012-821X(03)00138-9

Cobb, K.M., Westphal, N., Sayani, H.R., Watson, J.T., Lorenzo, E.D., Cheng, H., Edwards, R.L., Charles, C.D., 2013. Highly Variable El Niño–Southern Oscillation Throughout the Holocene. Science 339, 67–70. https://doi.org/10.1126/science.1228246

Comas-Bru, L., Hernández, A., 2018. Reconciling North Atlantic climate modes: revised monthly indices for the East Atlantic and the Scandinavian patterns beyond the 20th century. Earth Syst. Sci. Data 10, 2329–2344. https://doi.org/10.5194/essd-10-2329-2018

Comas-Bru, L., McDermott, F., 2014. Impacts of the EA and SCA patterns on the European twentieth century NAO–winter climate relationship. Q. J. R. Meteorol. Soc. 140, 354–363. https://doi.org/10.1002/qj.2158

Comas-Bru, L., McDermott, F., Werner, M., 2016. The effect of the East Atlantic pattern on the precipitation δ 18 O-NAO relationship in Europe. Clim. Dyn. 47, 2059–2069.

Compo, G.P., Whitaker, J.S., Sardeshmukh, P.D., Matsui, N., Allan, R.J., Yin, X., Gleason, B.E., Vose, R.S., Rutledge, G., Bessemoulin, P., Brönnimann, S., Brunet, M., Crouthamel, R.I., Grant, A.N., Groisman, P.Y., Jones, P.D., Kruk, M.C., Kruger, A.C., Marshall, G.J., Maugeri, M., Mok, H.Y., Nordli, Ø., Ross, T.F., Trigo, R.M., Wang, X.L., Woodruff, S.D., Worley, S.J., 2011. The Twentieth Century Reanalysis Project. Q. J. R. Meteorol. Soc. 137, 1–28. https://doi.org/10.1002/qj.776

Cook, E.R., D'Arrigo, R.D., Anchukaitis, K.J., 2008. ENSO reconstructions from long tree-ring chronologies: Unifying the differences? Presented at the Reconciling ENSO Chronologies for the Past 500 Years, Moorea, French Polynesia.

Cook, E.R., D'Arrigo, R.D., Mann, M.E., 2002. A Well-Verified, Multiproxy Reconstruction of the Winter North Atlantic Oscillation Index since a.d. 1400. J. Clim. 15, 1754–1764. https://doi.org/10.1175/1520-0442(2002)015<1754:AWVMRO>2.0.CO;2

Cook, E.R., Kushnir, Y., Smerdon, J.E., Williams, A.P., Anchukaitis, K.J., Wahl, E.R., 2019. A Euro-Mediterranean tree-ring reconstruction of the winter NAO index since 910 C.E. Clim. Dyn. 53, 1567–1580. https://doi.org/10.1007/s00382-019-04696-2

Cook, E.R., Seager, R., Kushnir, Y., Briffa, K.R., Büntgen, U., Frank, D., Krusic, P.J., Tegel, W., Schrier, G. van der, Andreu-Hayles, L., Baillie, M., Baittinger, C., Bleicher, N., Bonde, N., Brown, D., Carrer, M., Cooper, R., Čufar, K., Dittmar, C., Esper, J., Griggs, C., Gunnarson, B., Günther, B., Gutierrez, E., Haneca, K., Helama, S., Herzig, F., Heussner, K.-U., Hofmann, J., Janda, P., Kontic, R., Köse, N., Kyncl, T., Levanič, T., Linderholm, H., Manning, S., Melvin, T.M., Miles, D., Neuwirth, B., Nicolussi, K., Nola, P., Panayotov, M., Popa, I., Rothe, A., Seftigen, K., Seim, A., Svarva, H., Svoboda, M., Thun, T., Timonen, M., Touchan, R., Trotsiuk, V., Trouet, V., Walder, F., Ważny, T., Wilson, R., Zang, C., 2015. Old World megadroughts and pluvials during the Common Era. Sci. Adv. 1, e1500561. https://doi.org/10.1126/sciadv.1500561

Cornes, R.C., Jones, P.D., Briffa, K.R., Osborn, T.J., 2013. Estimates of the North Atlantic Oscillation back to 1692 using a Paris–London westerly index. Int. J. Climatol. 33, 228–248. https://doi.org/10.1002/joc.3416

Crann, C.A., Patterson, R.T., Macumber, A.L., Galloway, J.M., Roe, H.M., Blaauw, M., Swindles, G.T., Falck, H., 2015. Sediment accumulation rates in subarctic lakes: Insights into age-depth modeling from 22 dated lake records from the Northwest Territories, Canada. Quat. Geochronol. 27, 131–144. https://doi.org/10.1016/j.quageo.2015.02.001

Cropper, T., Hanna, E., Valente, M.A., Jónsson, T., 2015. A daily Azores-Iceland North Atlantic Oscillation index back to 1850. Geosci. Data J. 2, 12–24. https://doi.org/10.1002/gdj3.23

Curran, M.J., Rosenthal, Y., Wright, J.D., Morley, A., 2019. Atmospheric response to mid-Holocene warming in the northeastern Atlantic: Implications for future storminess in the Ireland/UK region. Quat. Sci. Rev. 225, 106004. https://doi.org/10.1016/j.quascirev.2019.106004

Czymzik, M., Muscheler, R., Adolphi, F., Mekhaldi, F., Dräger, N., Ott, F., Słowinski, M., Błaszkiewicz, M., Aldahan, A., Possnert, G., Brauer, A., 2018. Synchronizing ^{10}Be in two varved lake sediment records to IntCal13 ^{14}C during three grand solar minima. Clim. Past 14, 687–696. https://doi.org/10.5194/cp-14-687-2018

d'Orgeville, M., Peltier, W.R., 2009. Implications of Both Statistical Equilibrium and Global Warming Simulations with CCSM3. Part I: On the Decadal Variability in the North Pacific Basin. J. Clim. 22, 5277–5297. https://doi.org/10.1175/2009JCLI2428.1

d'Orgeville, M., Peltier, W.R., 2007. On the Pacific Decadal Oscillation and the Atlantic Multidecadal Oscillation: Might they be related? Geophys. Res. Lett. 34. https://doi.org/10.1029/2007GL031584

Dai, A., 2013. The influence of the inter-decadal Pacific oscillation on US precipitation during 1923–2010. Clim. Dyn. 41, 633–646. https://doi.org/10.1007/s00382-012-1446-5

D'Arrigo, R., Allan, R., Wilson, R., Palmer, J., Sakulich, J., Smerdon, J.E., Bijaksana, S., Ngkoimani, L.O., 2008. Pacific and Indian Ocean climate signals in a tree-ring record of Java monsoon drought. Int. J. Climatol. 28, 1889–1901. https://doi.org/10.1002/joc.1679

D'Arrigo, R., Cook, E.R., Wilson, R.J., Allan, R., Mann, M.E., 2005. On the variability of ENSO over the past six centuries. Geophys. Res. Lett. 32. https://doi.org/10.1029/2004GL022055

D'Arrigo, R., Villalba, R., Wiles, G., 2001. Tree-ring estimates of Pacific decadal climate variability. Clim. Dyn. 18, 219–224. https://doi.org/10.1007/s003820100177

D'Arrigo, R., Wilson, R., 2006. On the Asian expression of the PDO. Int. J. Climatol. 26, 1607–1617. https://doi.org/10.1002/joc.1326

D'Arrigo, R., Wilson, R., Wiles, G., Anchukaitis, K., Solomina, O., Davi, N., Deser, C., Dolgova, E., 2015. Tree-ring reconstructed temperature index for coastal northern Japan: implications for western North Pacific variability. Int. J. Climatol. 35, 3713–3720. https://doi.org/10.1002/joc.4230

Dätwyler, C., Abram, N.J., Grosjean, M., Wahl, E.R., Neukom, R., 2019. El Niño–Southern Oscillation variability, teleconnection changes and responses to large volcanic eruptions since AD 1000. Int. J. Climatol. 39, 2711–2724. https://doi.org/10.1002/joc.5983

Dätwyler, C., Neukom, R., Abram, N.J., Gallant, A.J.E., Grosjean, M., Jacques-Coper, M., Karoly, D.J., Villalba, R., 2018. Teleconnection stationarity, variability and trends of the Southern Annular Mode (SAM) during the last millennium. Clim. Dyn. 51, 2321–2339. https://doi.org/10.1007/s00382-017-4015-0

de Boer, E.J., Tjallingii, R., Vélez, M.I., Rijsdijk, K.F., Vlug, A., Reichart, G.-J., Prendergast, A.L., de Louw, P.G.B., Florens, F.B.V., Baider, C., Hooghiemstra, H., 2014. Climate variability in the SW Indian Ocean from an 8000-yr long multi-proxy record in the Mauritian lowlands shows a middle to late Holocene shift from negative IOD-state to ENSO-state. Quat. Sci. Rev. 86, 175–189. https://doi.org/10.1016/j.quascirev.2013.12.026

Dean, J.M., Kemp, A.E.S., 2004. A 2100 year BP record of the Pacific Decadal Oscillation, El Niño Southern Oscillation and Quasi-Biennial Oscillation in marine production and fluvial input from Saanich Inlet, British Columbia. Palaeogeogr. Palaeoclimatol. Palaeoecol. 213, 207–229. https://doi.org/10.1016/j.palaeo.2004.05.001

Dee, S., Emile-Geay, J., Evans, M.N., Allam, A., Steig, E.J., Thompson, D.M., 2015. PRYSM: An open-source framework for PRoxY System Modeling, with applications to oxygen-isotope systems. J. Adv. Model. Earth Syst. 7, 1220–1247. https://doi.org/10.1002/2015MS000447

Dee, S.G., Cobb, K.M., Emile-Geay, J., Ault, T.R., Edwards, R.L., Cheng, H., Charles, C.D., 2020. No consistent ENSO response to volcanic forcing over the last millennium. Science 367, 1477–1481. https://doi.org/10.1126/science.aax2000

Dee, S.G., Parsons, L.A., Loope, G.R., Overpeck, J.T., Ault, T.R., Emile-Geay, J., 2017. Improved spectral comparisons of paleoclimate models and observations via proxy system modeling: Implications for multi-decadal variability. Earth Planet. Sci. Lett. 476, 34–46. https://doi.org/10.1016/j.epsl.2017.07.036

Deser, C., Phillips, A., Bourdette, V., Teng, H., 2012. Uncertainty in climate change projections: the role of internal variability. Clim. Dyn. 38, 527–546. https://doi.org/10.1007/s00382-010-0977-x

Di Lorenzo, E., Liguori, G., Schneider, N., Furtado, J.C., Anderson, B.T., Alexander, M.A., 2015. ENSO and meridional modes: A null hypothesis for Pacific climate variability. Geophys. Res. Lett. 42, 9440–9448. https://doi.org/10.1002/2015GL066281

Diaz, H.F., Markgraf, V. (Eds.), 2000. El Niño and the Southern Oscillation: Multiscale Variability and Global and Regional Impacts. Cambridge University Press, Cambridge. https://doi.org/10.1017/CBO9780511573125

Driscoll, S., Bozzo, A., Gray, L.J., Robock, A., Stenchikov, G., 2012. Coupled Model Intercomparison Project 5 (CMIP5) simulations of climate following volcanic eruptions. J. Geophys. Res. Atmospheres 117. https://doi.org/10.1029/2012JD017607

Emile-Geay, J., Cobb, K.M., Carré, M., Braconnot, P., Leloup, J., Zhou, Y., Harrison, S.P., Corrège, T., McGregor, H.V., Collins, M., Driscoll, R., Elliot, M., Schneider, B., Tudhope, A., 2016. Links between tropical Pacific seasonal, interannual and orbital variability during the Holocene. Nat. Geosci. 9, 168–173. https://doi.org/10.1038/ngeo2608

Emile-Geay, J., Cobb, K.M., Cole, J.E., Elliot, M., 2020. Past ENSO variability: reconstructions, models, and implication, in: El Niño Southern Oscillation in a Changing Climate, AGU Monograph. AGU.

Emile-Geay, J., Seager, R., Cane, M.A., Cook, E.R., Haug, G.H., 2008. Volcanoes and ENSO over the Past Millennium. J. Clim. 21, 3134–3148. https://doi.org/10.1175/2007JCLI1884.1

Endo, S., Tozuka, T., 2016. Two flavors of the Indian Ocean Dipole. Clim. Dyn. 46, 3371–3385. https://doi.org/10.1007/s00382-015-2773-0

Enfield, D.B., Mestas-Nuñez, A.M., Trimble, P.J., 2001. The Atlantic Multidecadal Oscillation and its relation to rainfall and river flows in the continental U.S. Geophys. Res. Lett. 28, 2077–2080. https://doi.org/10.1029/2000GL012745

Evans, M.N., Cane, M.A., Schrag, D.P., Kaplan, A., Linsley, B.K., Villalba, R., Wellington, G.M., 2001. Support for tropically-driven pacific decadal variability based on paleoproxy evidence. Geophys. Res. Lett. 28, 3689–3692. https://doi.org/10.1029/2001GL013223

Evans, M.N., Kaplan, A., Cane, M.A., 2002. Pacific sea surface temperature field reconstruction from coral δ18O data using reduced space objective analysis. Paleoceanography 17, 7-1-7–13. https://doi.org/10.1029/2000PA000590

Evans, M.N., Tolwinski-Ward, S.E., Thompson, D.M., Anchukaitis, K.J., 2013. Applications of proxy system modeling in high resolution paleoclimatology. Quat. Sci. Rev. 76, 16–28. https://doi.org/10.1016/j.quascirev.2013.05.024

Fan, F., Dong, X., Fang, X., Xue, F., Zheng, F., Zhu, J., 2017. Revisiting the relationship between the South Asian summer monsoon drought and El Niño warming pattern. Atmospheric Sci. Lett. 18, 175–182. https://doi.org/10.1002/asl.740

Faust, J.C., Fabian, K., Milzer, G., Giraudeau, J., Knies, J., 2016. Norwegian fjord sediments reveal NAO related winter temperature and precipitation changes of the past 2800 years. Earth Planet. Sci. Lett. 435, 84–93. https://doi.org/10.1016/j.epsl.2015.12.003

Feldstein, S.B., 2000. The Timescale, Power Spectra, and Climate Noise Properties of Teleconnection Patterns. J. Clim. 13, 4430–4440. https://doi.org/10.1175/1520-0442(2000)013<4430:TTPSAC>2.0.CO;2

Felis, T., Suzuki, A., Kuhnert, H., Rimbu, N., Kawahata, H., 2010. Pacific Decadal Oscillation documented in a coral record of North Pacific winter temperature since 1873. Geophys. Res. Lett. 37. https://doi.org/10.1029/2010GL043572

Feng, S., Hu, Q., 2008. How the North Atlantic Multidecadal Oscillation may have influenced the Indian summer monsoon during the past two millennia. Geophys. Res. Lett. 35. https://doi.org/10.1029/2007GL032484

Feng, S., Hu, Q., Oglesby, R.J., 2011. Influence of Atlantic sea surface temperatures on persistent drought in North America. Clim. Dyn. 37, 569–586. https://doi.org/10.1007/s00382-010-0835-x

Fereday, D., Chadwick, R., Knight, J., Scaife, A.A., 2018. Atmospheric Dynamics is the Largest Source of Uncertainty in Future Winter European Rainfall. J. Clim. 31, 963–977. https://doi.org/10.1175/JCLI-D-17-0048.1

Ferreira, D., Marshall, J., Bitz, C.M., Solomon, S., Plumb, A., 2015. Antarctic Ocean and Sea Ice Response to Ozone Depletion: A Two-Time-Scale Problem. J. Clim. 28, 1206–1226. https://doi.org/10.1175/JCLI-D-14-00313.1

Fischer, E.M., Luterbacher, J., Zorita, E., Tett, S.F.B., Casty, C., Wanner, H., 2007. European climate response to tropical volcanic eruptions over the last half millennium. Geophys. Res. Lett. 34. https://doi.org/10.1029/2006GL027992

Fischer, N., Jungclaus, J.H., 2010. Effects of orbital forcing on atmosphere and ocean heat transports in Holocene and Eemian climate simulations with a comprehensive Earth system model. Clim. Past 6, 155–168. https://doi.org/10.5194/cp-6-155-2010

Fletcher, M.-S., Benson, A., Bowman, D.M.J.S., Gadd, P.S., Heijnis, H., Mariani, M., Saunders, K.M., Wolfe, B.B., Zawadzki, A., 2018. Centennial-scale trends in the Southern Annular Mode revealed by hemisphere-wide fire and hydroclimatic trends over the past 2400 years. Geology 46, 363–366. https://doi.org/10.1130/G39661.1

Fletcher, M.-S., Moreno, P.I., 2012. Have the Southern Westerlies changed in a zonally symmetric manner over the last 14,000 years? A hemisphere-wide take on a controversial problem. Quat. Int., PASH-2: Controversies in the late Quaternary of the Southern Hemisphere 253, 32–46. https://doi.org/10.1016/j.quaint.2011.04.042

Fogt, R.L., Bromwich, D.H., 2006. Decadal Variability of the ENSO Teleconnection to the High-Latitude South Pacific Governed by Coupling with the Southern Annular Mode. J. Clim. 19, 979–997. https://doi.org/10.1175/JCLI3671.1

Fogt, R.L., Bromwich, D.H., Hines, K.M., 2011. Understanding the SAM influence on the South Pacific ENSO teleconnection. Clim. Dyn. 36, 1555–1576. https://doi.org/10.1007/s00382-010-0905-0

Fogt, R.L., Perlwitz, J., Monaghan, A.J., Bromwich, D.H., Jones, J.M., Marshall, G.J., 2009. Historical SAM Variability. Part II: Twentieth-Century Variability and Trends from Reconstructions, Observations, and the IPCC AR4 Models. J. Clim. 22, 5346–5365. https://doi.org/10.1175/2009JCLI2786.1

Folland, C.K., Colman, A.W., Rowell, D.P., Davey, M.K., 2001. Predictability of Northeast Brazil Rainfall and Real-Time Forecast Skill, 1987–98. J. Clim. 14, 1937–1958. https://doi.org/10.1175/1520-0442(2001)014<1937:PONBRA>2.0.CO;2

Folland, C.K., Karl, T.R., Salinger, M.J., 2002. Observed climate variability and change. Weather 57, 269–278. https://doi.org/10.1256/004316502320517353

Folland, C.K., Knight, J., Linderholm, H.W., Fereday, D., Ineson, S., Hurrell, J.W., 2009. The Summer North Atlantic Oscillation: Past, Present, and Future. J. Clim. 22, 1082–1103. https://doi.org/10.1175/2008JCLI2459.1

Folland, C.K., Palmer, T.N., Parker, D.E., 1986. Sahel rainfall and worldwide sea temperatures, 1901–85. Nature 320, 602–607. https://doi.org/10.1038/320602a0

Frappier, A., Sahagian, D., González, L.A., Carpenter, S.J., 2002. El Niño Events Recorded by Stalagmite Carbon Isotopes. Science 298, 565–565. https://doi.org/10.1126/science.1076446

Freund, M.B., Henley, B.J., Karoly, D.J., McGregor, H.V., Abram, N.J., Dommenget, D., 2019. Higher frequency of Central Pacific El Niño events in recent decades relative to past centuries. Nat. Geosci. 12, 450–455. https://doi.org/10.1038/s41561-019-0353-3

Friddell, J.E., Thunell, R.C., Guilderson, T.P., Kashgarian, M., 2003. Increased northeast Pacific climatic variability during the warm middle Holocene. Geophys. Res. Lett. 30. https://doi.org/10.1029/2002GL016834

Gagan, M.K., Dunbar, G.B., Suzuki, A., 2012. The effect of skeletal mass accumulation in Porites on coral Sr/Ca and δ18O paleothermometry. Paleoceanography 27. https://doi.org/10.1029/2011PA002215

Găinuşă-Bogdan, A., Swingedouw, D., Yiou, P., Cattiaux, J., Codron, F., Michel, S., 2020. AMOC and summer sea ice as key drivers of the spread in mid-holocene winter temperature patterns over Europe in PMIP3 models. Glob. Planet. Change 184, 103055. https://doi.org/10.1016/j.gloplacha.2019.103055

Gedalof, Z., Mantua, N.J., Peterson, D.L., 2002. A multi-century perspective of variability in the Pacific Decadal Oscillation: new insights from tree rings and coral. Geophys. Res. Lett. 29, 2204–2204. https://doi.org/10.1029/2002GL015824

Gedalof, Z., Smith, D.J., 2001. Interdecadal climate variability and regime-scale shifts in Pacific North America. Geophys. Res. Lett. 28, 1515–1518.

Gent, P.R., 2016. Effects of Southern Hemisphere Wind Changes on the Meridional Overturning Circulation in Ocean Models. Annu. Rev. Mar. Sci. 8, 79–94. https://doi.org/10.1146/annurev-marine-122414-033929

Gergis, J.L., Fowler, A.M., 2009. A history of ENSO events since A.D. 1525: implications for future climate change. Clim. Change 92, 343–387. https://doi.org/10.1007/s10584-008-9476-z

Geyer, A., Marti, A., Giralt, S., Folch, A., 2017. Potential ash impact from Antarctic volcanoes: Insights from Deception Island’s most recent eruption. Sci. Rep. 7, 1–10. https://doi.org/10.1038/s41598-017-16630-9

Gillett, N.P., Fyfe, J.C., 2013. Annular mode changes in the CMIP5 simulations. Geophys. Res. Lett. 40, 1189–1193. https://doi.org/10.1002/grl.50249

Gillett, N.P., Kell, T.D., Jones, P.D., 2006. Regional climate impacts of the Southern Annular Mode. Geophys. Res. Lett. 33. https://doi.org/10.1029/2006GL027721

Glueck, M.F., Stockton, C.W., 2001. Reconstruction of the North Atlantic Oscillation, 1429-1983. Int. J. Climatol. 21, 1453–1465. https://doi.org/10.1002/joc.684

Goldenberg, S.B., Landsea, C.W., Mestas-Nuñez, A.M., Gray, W.M., 2001. The Recent Increase in Atlantic Hurricane Activity: Causes and Implications. Science 293, 474–479. https://doi.org/10.1126/science.1060040

Gomez, B., Carter, L., Orpin, A.R., Cobb, K.M., Page, M.J., Trustrum, N.A., Palmer, A.S., 2012. ENSO/SAM interactions during the middle and late Holocene. The Holocene 22, 23–30. https://doi.org/10.1177/0959683611405241

Gong, D., Wang, S., 1999. Definition of Antarctic Oscillation index. Geophys. Res. Lett. 26, 459–462. https://doi.org/10.1029/1999GL900003

Gong, D.-Y., Luterbacher, J., 2008. Variability of the low-level cross-equatorial jet of the western Indian Ocean since 1660 as derived from coral proxies. Geophys. Res. Lett. 35. https://doi.org/10.1029/2007GL032409

Gong, T., Feldstein, S.B., Luo, D., 2010. The Impact of ENSO on Wave Breaking and Southern Annular Mode Events. J. Atmospheric Sci. 67, 2854–2870. https://doi.org/10.1175/2010JAS3311.1

Goodwin, I.D., Browning, S., Lorrey, A.M., Mayewski, P.A., Phipps, S.J., Bertler, N.A.N., Edwards, R.P., Cohen, T.J., van Ommen, T., Curran, M., Barr, C., Stager, J.C., 2014. A reconstruction of extratropical Indo-Pacific sea-level pressure patterns during the Medieval Climate Anomaly. Clim. Dyn. 43, 1197–1219. https://doi.org/10.1007/s00382-013-1899-1

Gornitz, V., 2009. Paleoclimate Proxies, An Introduction, in: Gornitz, V. (Ed.), Encyclopedia of Paleoclimatology and Ancient Environments. Springer Netherlands, Dordrecht, pp. 716–721. https://doi.org/10.1007/978-1-4020-4411-3_171

Goslin, J., Fruergaard, M., Sander, L., Gałka, M., Menviel, L., Monkenbusch, J., Thibault, N., Clemmensen, L.B., 2018. Holocene centennial to millennial shifts in North-Atlantic storminess and ocean dynamics. Sci. Rep. 8, 1–12. https://doi.org/10.1038/s41598-018-29949-8

Gouramanis, C., De Deckker, P., Switzer, A.D., Wilkins, D., 2013. Cross-continent comparison of high-resolution Holocene climate records from southern Australia — Deciphering the impacts of far-field teleconnections. Earth-Sci. Rev. 121, 55–72. https://doi.org/10.1016/j.earscirev.2013.02.006

Gray, L.J., Beer, J., Geller, M., Haigh, J.D., Lockwood, M., Matthes, K., Cubasch, U., Fleitmann, D., Harrison, G., Hood, L., Luterbacher, J., Meehl, G.A., Shindell, D., Geel, B. van, White, W., 2010. Solar Influences on Climate. Rev. Geophys. 48. https://doi.org/10.1029/2009RG000282

Gray, L.J., Scaife, A.A., Mitchell, D.M., Osprey, S., Ineson, S., Hardiman, S., Butchart, N., Knight, J., Sutton, R., Kodera, K., 2013. A lagged response to the 11 year solar cycle in observed winter Atlantic/European weather patterns. J. Geophys. Res. Atmospheres 118, 13,405-13,420. https://doi.org/10.1002/2013JD020062

Gray, S.T., Graumlich, L.J., Betancourt, J.L., Pederson, G.T., 2004. A tree-ring based reconstruction of the Atlantic Multidecadal Oscillation since 1567 A.D. Geophys. Res. Lett. 31. https://doi.org/10.1029/2004GL019932

Grossmann, I., Klotzbach, P.J., 2009. A review of North Atlantic modes of natural variability and their driving mechanisms. J. Geophys. Res. Atmospheres 114. https://doi.org/10.1029/2009JD012728

Grothe, P.R., Cobb, K.M., Liguori, G., Lorenzo, E.D., Capotondi, A., Lu, Y., Cheng, H., Edwards, R.L., Southon, J.R., Santos, G.M., Deocampo, D.M., Lynch-Stieglitz, J., Chen, T., Sayani, H.R., Thompson, D.M., Conroy, J.L., Moore, A.L., Townsend, K., Hagos, M., O’Connor, G., Toth, L.T., 2019. Enhanced El Niño-Southern Oscillation variability in recent decades. Geophys. Res. Lett. n/a. https://doi.org/10.1029/2019GL083906

Guo, F., Liu, Q., Yang, J., Fan, L., 2018. Three types of Indian Ocean Basin modes. Clim. Dyn. 51, 4357–4370. https://doi.org/10.1007/s00382-017-3676-z

Haase-Schramm, A., Böhm, F., Eisenhauer, A., Dullo, W.-C., Joachimski, M.M., Hansen, B., Reitner, J., 2003. Sr/Ca ratios and oxygen isotopes from sclerosponges: Temperature history of the Caribbean mixed layer and thermocline during the Little Ice Age. Paleoceanography 18. https://doi.org/10.1029/2002PA000830

Haigh, J.D., 1996. The Impact of Solar Variability on Climate. Science 272, 981–984. https://doi.org/10.1126/science.272.5264.981

Haigh, J.D., 1994. The role of stratospheric ozone in modulating the solar radiative forcing of climate. Nature 370, 544–546. https://doi.org/10.1038/370544a0

Hakim, G.J., Emile-Geay, J., Steig, E.J., Noone, D., Anderson, D.M., Tardif, R., Steiger, N., Perkins, W.A., 2016. The last millennium climate reanalysis project: Framework and first results. J. Geophys. Res. Atmospheres 121, 6745–6764. https://doi.org/10.1002/2016JD024751

Halpert, M.S., Ropelewski, C.F., 1992. Surface Temperature Patterns Associated with the Southern Oscillation. J. Clim. 5, 577–593. https://doi.org/10.1175/1520-0442(1992)005<0577:STPAWT>2.0.CO;2

Hannachi, A., Jolliffe, I.T., Stephenson, D.B., 2007. Empirical orthogonal functions and related techniques in atmospheric science: A review. Int. J. Climatol. 27, 1119–1152. https://doi.org/10.1002/joc.1499

Hansen, J., Sato, M., Ruedy, R., 1997. Radiative forcing and climate response. J. Geophys. Res. Atmospheres 102, 6831–6864. https://doi.org/10.1029/96JD03436

Haslett, J., Whiley, M., Bhattacharya, S., Salter-Townshend, M., Wilson, S.P., Allen, J.R.M., Huntley, B., Mitchell, F.J.G., 2006. Bayesian palaeoclimate reconstruction. J. R. Stat. Soc. Ser. A Stat. Soc. 169, 395–438. https://doi.org/10.1111/j.1467-985X.2006.00429.x

Haywood, A.M., Valdes, P.J., Aze, T., Barlow, N., Burke, A., Dolan, A.M., von der Heydt, A.S., Hill, D.J., Jamieson, S.S.R., Otto-Bliesner, B.L., Salzmann, U., Saupe, E., Voss, J., 2019. What can Palaeoclimate Modelling do for you? Earth Syst. Environ. 3, 1–18. https://doi.org/10.1007/s41748-019-00093-1

Helama, S., Meriläinen, J., Tuomenvirta, H., 2009. Multicentennial megadrought in northern Europe coincided with a global El Niño–Southern Oscillation drought pattern during the Medieval Climate Anomaly. Geology 37, 175–178. https://doi.org/10.1130/G25329A.1

Henke, L.M.K., Lambert, F.H., Charman, D.J., 2017. Was the Little Ice Age more or less El Niño-like than the Medieval Climate Anomaly? Evidence from hydrological and temperature proxy data. Clim. Past 13, 267–301. https://doi.org/10.5194/cp-13-267-2017

Henley, B.J., Gergis, J., Karoly, D.J., Power, S., Kennedy, J., Folland, C.K., 2015. A Tripole Index for the Interdecadal Pacific Oscillation. Clim. Dyn. 45, 3077–3090. https://doi.org/10.1007/s00382-015-2525-1

Hermanson, L., Eade, R., Robinson, N.H., Dunstone, N.J., Andrews, M.B., Knight, J.R., Scaife, A.A., Smith, D.M., 2014. Forecast cooling of the Atlantic subpolar gyre and associated impacts. Geophys. Res. Lett. 41, 5167–5174. https://doi.org/10.1002/2014GL060420

Hernández, A., Giralt, S., Bao, R., Sáez, A., Leng, M.J., Barker, P.A., 2010. ENSO and solar activity signals from oxygen isotopes in diatom silica during late glacial-Holocene transition in Central Andes (18°S). J. Paleolimnol. 44, 413–429. https://doi.org/10.1007/s10933-010-9412-x

Hernández, A., Sánchez-López, G., Pla-Rabes, S., Comas-Bru, L., Parnell, A., Cahill, N., Geyer, A., Trigo, R.M., Giralt, S., In Review. Evaluating the decadal-to-centennial evolution of a new proxy-based NAO reconstruction during the Common Era. Sci. Rep. https://doi.org/10.31223/osf.io/p7ft6

Hessl, A., Allen, K.J., Vance, T., Abram, N.J., Saunders, K.M., 2017. Reconstructions of the southern annular mode (SAM) during the last millennium. Prog. Phys. Geogr. Earth Environ. 41, 834–849. https://doi.org/10.1177/0309133317743165

Hetzinger, S., Pfeiffer, M., Dullo, W.-C., Keenlyside, N., Latif, M., Zinke, J., 2008. Caribbean coral tracks Atlantic Multidecadal Oscillation and past hurricane activity. Geology 36, 11–14. https://doi.org/10.1130/G24321A.1

Horel, J.D., Wallace, J.M., 1981. Planetary-Scale Atmospheric Phenomena Associated with the Southern Oscillation. Mon. Weather Rev. 109, 813–829. https://doi.org/10.1175/1520-0493(1981)109<0813:PSAPAW>2.0.CO;2

Hsu, H.-H., Chen, Y.-L., 2011. Decadal to bi-decadal rainfall variation in the western Pacific: A footprint of South Pacific decadal variability? Geophys. Res. Lett. 38. https://doi.org/10.1029/2010GL046278

Huntley, B., Spicer, R.A., Chaloner, W.G., Jarzembowski, E.A., 1993. The Use of Climate Response Surfaces to Reconstruct Palaeoclimate from Quaternary Pollen and Plant Macrofossil Data [and Discussion]. Philos. Trans. Biol. Sci. 341, 215–224.

Hurrell, J.W., 1995. Decadal Trends in the North Atlantic Oscillation: Regional Temperatures and Precipitation. Science 269, 676–679. https://doi.org/10.1126/science.269.5224.676

Hurrell, J.W., Kushnir, Y., Ottersen, G., Visbeck, M., 2003. An Overview of the North Atlantic Oscillation, in: W, H.J., Y, K., G, O., M, V. (Eds.), The North Atlantic Oscillation: Climatic Significance and Environmental Impact. American Geophysical Union (AGU), Washington, US, pp. 1–35.

Ilvonen, L., Holmström, L., Seppä, H., Veski, S., 2016. A Bayesian multinomial regression model for palaeoclimate reconstruction with time uncertainty. Environmetrics 27, 409–422. https://doi.org/10.1002/env.2393

Ineson, S., Maycock, A.C., Gray, L.J., Scaife, A.A., Dunstone, N.J., Harder, J.W., Knight, J.R., Lockwood, M., Manners, J.C., Wood, R.A., 2015. Regional climate impacts of a possible future grand solar minimum. Nat. Commun. 6, 1–8. https://doi.org/10.1038/ncomms8535

Ineson, S., Scaife, A.A., Knight, J.R., Manners, J.C., Dunstone, N.J., Gray, L.J., Haigh, J.D., 2011. Solar forcing of winter climate variability in the Northern Hemisphere. Nat. Geosci. 4, 753–757. https://doi.org/10.1038/ngeo1282

Ionita, M., Lohmann, G., Rimbu, N., Chelcea, S., Dima, M., 2012. Interannual to decadal summer drought variability over Europe and its relationship to global sea surface temperature. Clim. Dyn. 38, 363–377. https://doi.org/10.1007/s00382-011-1028-y

Ivanochko, T.S., Calvert, S.E., Thomson, R.E., Pedersen, T.F., 2008. Geochemical reconstruction of Pacific decadal variability from the eastern North Pacific during the HoloceneThis article is one of a series of papers published in this Special Issue on the theme Polar Climate Stability Network. Can. J. Earth Sci. 45, 1317–1329. https://doi.org/10.1139/E08-037

Jerez, S., Trigo, R.M., Vicente-Serrano, S.M., Pozo-Vázquez, D., Lorente-Plazas, R., Lorenzo-Lacruz, J., Santos-Alamillos, F., Montávez, J.P., 2013. The Impact of the North Atlantic Oscillation on Renewable Energy Resources in Southwestern Europe. J. Appl. Meteorol. Climatol. 52, 2204–2225. https://doi.org/10.1175/JAMC-D-12-0257.1

Jones, P.D., Briffa, K.R., Osborn, T.J., Lough, J.M., van Ommen, T.D., Vinther, B.M., Luterbacher, J., Wahl, E.R., Zwiers, F.W., Mann, M.E., Schmidt, G.A., Ammann, C.M., Buckley, B.M., Cobb, K.M., Esper, J., Goosse, H., Graham, N., Jansen, E., Kiefer, T., Kull, C., Küttel, M., Mosley-Thompson, E., Overpeck, J.T., Riedwyl, N., Schulz, M., Tudhope, A.W., Villalba, R., Wanner, H., Wolff, E., Xoplaki, E., 2009. High-resolution palaeoclimatology of the last millennium: a review of current status and future prospects. The Holocene 19, 3–49. https://doi.org/10.1177/0959683608098952

Jones, P.D., Jonsson, T., Wheeler, D., 1997. Extension to the North Atlantic oscillation using early instrumental pressure observations from Gibraltar and south-west Iceland. Int. J. Climatol. 17, 1433–1450. https://doi.org/10.1002/(SICI)1097-0088(19971115)17:13<1433::AID-JOC203>3.0.CO;2-P

Jones, P.D., Mann, M.E., 2004. Climate over past millennia. Rev. Geophys. 42. https://doi.org/10.1029/2003RG000143

Jones, Philip D., 2001. Early European Instrumental Records, in: Jones, P. D., Ogilvie, A.E.J., Davies, T.D., Briffa, K.R. (Eds.), History and Climate: Memories of the Future? Springer US, Boston, MA, pp. 55–77. https://doi.org/10.1007/978-1-4757-3365-5_4

Juggins, S., Birks, H.J.B., 2012. Quantitative Environmental Reconstructions from Biological Data, in: Birks, H.J.B., Lotter, A.F., Juggins, S., Smol, J.P. (Eds.), Tracking Environmental Change Using Lake Sediments: Data Handling and Numerical Techniques, Developments in Paleoenvironmental Research. Springer Netherlands, Dordrecht, pp. 431–494. https://doi.org/10.1007/978-94-007-2745-8_14

Kennedy, J.J., Rayner, N.A., Atkinson, C.P., Killick, R.E., 2019. An Ensemble Data Set of Sea Surface Temperature Change From 1850: The Met Office Hadley Centre HadSST.4.0.0.0 Data Set. J. Geophys. Res. Atmospheres 124, 7719–7763. https://doi.org/10.1029/2018JD029867

Kent, C., Pope, E., Thompson, V., Lewis, K., Scaife, A.A., Dunstone, N., 2017. Using climate model simulations to assess the current climate risk to maize production. Environ. Res. Lett. 12, 054012. https://doi.org/10.1088/1748-9326/aa6cb9

Kenyon, J., Hegerl, G.C., 2008. Influence of Modes of Climate Variability on Global Temperature Extremes. J. Clim. 21, 3872–3889. https://doi.org/10.1175/2008JCLI2125.1

Khodri, M., Izumo, T., Vialard, J., Janicot, S., Cassou, C., Lengaigne, M., Mignot, J., Gastineau, G., Guilyardi, E., Lebas, N., Robock, A., McPhaden, M.J., 2017. Tropical explosive volcanic eruptions can trigger El Niño by cooling tropical Africa. Nat. Commun. 8, 1–13. https://doi.org/10.1038/s41467-017-00755-6

Kilbourne, K.H., Alexander, M.A., Nye, J.A., 2014. A low latitude paleoclimate perspective on Atlantic multidecadal variability. J. Mar. Syst., Atlantic Multidecadal Oscillation-mechanism and impact on marine ecosystems 133, 4–13. https://doi.org/10.1016/j.jmarsys.2013.09.004

Kilbourne, K.H., Quinn, T.M., Webb, R., Guilderson, T., Nyberg, J., Winter, A., 2008. Paleoclimate proxy perspective on Caribbean climate since the year 1751: Evidence of cooler temperatures and multidecadal variability. Paleoceanography 23. https://doi.org/10.1029/2008PA001598

Kilian, R., Lamy, F., 2012. A review of Glacial and Holocene paleoclimate records from southernmost Patagonia (49–55°S). Quat. Sci. Rev. 53, 1–23. https://doi.org/10.1016/j.quascirev.2012.07.017

Kirby, M.E., Lund, S.P., Patterson, W.P., Anderson, M.A., Bird, B.W., Ivanovici, L., Monarrez, P., Nielsen, S., 2010. A Holocene record of Pacific Decadal Oscillation (PDO)-related hydrologic variability in Southern California (Lake Elsinore, CA). J. Paleolimnol. 44, 819–839. https://doi.org/10.1007/s10933-010-9454-0

Kitzberger, T., Brown, P.M., Heyerdahl, E.K., Swetnam, T.W., Veblen, T.T., 2007. Contingent Pacific-Atlantic Ocean influence on multicentury wildfire synchrony over western North America. Proc. Natl. Acad. Sci. U. S. A. 104, 543–548. https://doi.org/10.1073/pnas.0606078104

Knight, J.R., Allan, R.J., Folland, C.K., Vellinga, M., Mann, M.E., 2005. A signature of persistent natural thermohaline circulation cycles in observed climate. Geophys. Res. Lett. 32, 1–4. https://doi.org/10.1029/2005GL024233

Knight, J.R., Folland, C.K., Scaife, A.A., 2006. Climate impacts of the Atlantic Multidecadal Oscillation. Geophys. Res. Lett. 33. https://doi.org/10.1029/2006GL026242

Knudsen, M.F., Jacobsen, B.H., Seidenkrantz, M.-S., Olsen, J., 2014. Evidence for external forcing of the Atlantic Multidecadal Oscillation since termination of the Little Ice Age. Nat. Commun. 5, 3323. https://doi.org/10.1038/ncomms4323

Knudsen, M.F., Seidenkrantz, M.-S., Jacobsen, B.H., Kuijpers, A., 2011. Tracking the Atlantic Multidecadal Oscillation through the last 8,000 years. Nat. Commun. 2, 1–8. https://doi.org/10.1038/ncomms1186

Kobashi, T., Menviel, L., Jeltsch-Thömmes, A., Vinther, B.M., Box, J.E., Muscheler, R., Nakaegawa, T., Pfister, P.L., Döring, M., Leuenberger, M., Wanner, H., Ohmura, A., 2017. Volcanic influence on centennial to millennial Holocene Greenland temperature change. Sci. Rep. 7, 1–10. https://doi.org/10.1038/s41598-017-01451-7

Kodera, K., 2002. Solar cycle modulation of the North Atlantic Oscillation: Implication in the spatial structure of the NAO. Geophys. Res. Lett. 29, 59-1-59–4. https://doi.org/10.1029/2001GL014557

Kosaka, Y., Xie, S.-P., 2013. Recent global-warming hiatus tied to equatorial Pacific surface cooling. Nature 501, 403–407. https://doi.org/10.1038/nature12534

Koutavas, A., Joanides, S., 2012. El Niño–Southern Oscillation extrema in the Holocene and Last Glacial Maximum. Paleoceanography 27. https://doi.org/10.1029/2012PA002378

Kravtsov, S., Grimm, C., Gu, S., 2018. Global-scale multidecadal variability missing in state-of-the-art climate models. Npj Clim. Atmospheric Sci. 1, 1–10. https://doi.org/10.1038/s41612-018-0044-6

Krishnamurthy, L., Krishnamurthy, V., 2016. Decadal and interannual variability of the Indian Ocean SST. Clim. Dyn. 46, 57–70. https://doi.org/10.1007/s00382-015-2568-3

Kuhnert, H., Kuhlmann, H., Mohtadi, M., Meggers, H., Baumann, K.-H., Pätzold, J., 2014. Holocene tropical western Indian Ocean sea surface temperatures in covariation with climatic changes in the Indonesian region. Paleoceanography 29, 423–437. https://doi.org/10.1002/2013PA002555

Küttel, M., Xoplaki, E., Gallego, D., Luterbacher, J., García-Herrera, R., Allan, R., Barriendos, M., Jones, P.D., Wheeler, D., Wanner, H., 2010. The importance of ship log data: reconstructing North Atlantic, European and Mediterranean sea level pressure fields back to 1750. Clim. Dyn. 34, 1115–1128. https://doi.org/10.1007/s00382-009-0577-9

Kwiatkowski, C., Prange, M., Varma, V., Steinke, S., Hebbeln, D., Mohtadi, M., 2015. Holocene variations of thermocline conditions in the eastern tropical Indian Ocean. Quat. Sci. Rev. 114, 33–42. https://doi.org/10.1016/j.quascirev.2015.01.028

Lachniet, M.S., Burns, S.J., Piperno, D.R., Asmerom, Y., Polyak, V.J., Moy, C.M., Christenson, K., 2004. A 1500-year El Niño/Southern Oscillation and rainfall history for the Isthmus of Panama from speleothem calcite. J. Geophys. Res. Atmospheres 109. https://doi.org/10.1029/2004JD004694

Lane, C.S., Brauer, A., Blockley, S.P.E., Dulski, P., 2013. Volcanic ash reveals time-transgressive abrupt climate change during the Younger Dryas. Geology 41, 1251–1254. https://doi.org/10.1130/G34867.1

Lapointe, F., Francus, P., Lamoureux, S.F., Vuille, M., Jenny, J.-P., Bradley, R.S., Massa, C., 2017. Influence of North Pacific decadal variability on the western Canadian Arctic over the past 700 years. Clim. Past 13, 411–420. https://doi.org/10.5194/cp-13-411-2017

Lean, J., 1997. The Sun's Variable Radiation and Its Relevance for Earth. Annu. Rev. Astron. Astrophys. 35, 33–67. https://doi.org/10.1146/annurev.astro.35.1.33

Ledru, M.-P., Jomelli, V., Samaniego, P., Vuille, M., Hidalgo, S., Herrera, M., Ceron, C., 2013. The Medieval Climate Anomaly and the Little Ice Age in the eastern Ecuadorian Andes. Clim. Past 9, 307–321. https://doi.org/10.5194/cp-9-307-2013

Lee, J., Sperber, K.R., Gleckler, P.J., Bonfils, C.J.W., Taylor, K.E., 2019. Quantifying the agreement between observed and simulated extratropical modes of interannual variability. Clim. Dyn. 52, 4057–4089. https://doi.org/10.1007/s00382-018-4355-4

Lefebvre, W., Goosse, H., Timmermann, R., Fichefet, T., 2004. Influence of the Southern Annular Mode on the sea ice–ocean system. J. Geophys. Res. Oceans 109. https://doi.org/10.1029/2004JC002403

Lehner, F., Raible, C.C., Stocker, T.F., 2012. Testing the robustness of a precipitation proxy-based North Atlantic Oscillation reconstruction. Quat. Sci. Rev. 45, 85–94. https://doi.org/10.1016/j.quascirev.2012.04.025

Li, J., Xie, S.-P., Cook, E.R., Huang, G., D'Arrigo, R., Liu, F., Ma, J., Zheng, X.-T., 2011. Interdecadal modulation of El Niño amplitude during the past millennium. Nat. Clim. Change 1, 114–118. https://doi.org/10.1038/nclimate1086

Li, J., Xie, S.-P., Cook, E.R., Morales, M.S., Christie, D.A., Johnson, N.C., Chen, F., D'Arrigo, R., Fowler, A.M., Gou, X., Fang, K., 2013. El Niño modulations over the past seven centuries. Nat. Clim. Change 3, 822–826. https://doi.org/10.1038/nclimate1936

Li, Z., Chen, M.-T., Lin, D.-C., Shi, X., Liu, S., Wang, H., Yokoyama, Y., Shen, C.-C., Mii, H.-S., Troa, R.A., Zuraida, R., Triarso, E., Hendrizan, M., 2018. Evidence of solar insolation and internal forcing of sea surface temperature changes in the eastern tropical Indian Ocean during the Holocene. Quat. Int. 490, 1–9. https://doi.org/10.1016/j.quaint.2018.04.001

Lim, E.-P., Hendon, H.H., Rashid, H., 2013. Seasonal Predictability of the Southern Annular Mode due to Its Association with ENSO. J. Clim. 26, 8037–8054. https://doi.org/10.1175/JCLI-D-13-00006.1

Linsley, B.K., Zhang, P., Kaplan, A., Howe, S.S., Wellington, G.M., 2008. Interdecadal-decadal climate variability from multicoral oxygen isotope records in the South Pacific Convergence Zone region since 1650 A.D. Paleoceanography 23. https://doi.org/10.1029/2007PA001539

Liu, Y., Cobb, K.M., Song, H., Li, Q., Li, C.-Y., Nakatsuka, T., An, Z., Zhou, W., Cai, Q., Li, J., Leavitt, S.W., Sun, C., Mei, R., Shen, C.-C., Chan, M.-H., Sun, J., Yan, L., Lei, Y., Ma, Y., Li, X., Chen, D., Linderholm, H.W., 2017. Recent enhancement of central Pacific El Niño variability relative to last eight centuries. Nat. Commun. 8, 1–8. https://doi.org/10.1038/ncomms15386

Liu, Z., Di Lorenzo, E., 2018. Mechanisms and Predictability of Pacific Decadal Variability. Curr. Clim. Change Rep. 4, 128–144. https://doi.org/10.1007/s40641-018-0090-5

Liu, Z., Lu, Z., Wen, X., Otto-Bliesner, B.L., Timmermann, A., Cobb, K.M., 2014a. Evolution and forcing mechanisms of El Niño over the past 21,000 years. Nature 515, 550–553. https://doi.org/10.1038/nature13963

Liu, Z., Wen, X., Brady, E.C., Otto-Bliesner, B., Yu, G., Lu, H., Cheng, H., Wang, Y., Zheng, W., Ding, Y., Edwards, R.L., Cheng, J., Liu, W., Yang, H., 2014b. Chinese cave records and the East Asia Summer Monsoon. Quat. Sci. Rev. 83, 115–128. https://doi.org/10.1016/j.quascirev.2013.10.021

Ljungqvist, F.C., Zhang, Qiong, Brattström, G., Krusic, P.J., Seim, A., Li, Q., Zhang, Qiang, Moberg, A., 2019. Centennial-Scale Temperature Change in Last Millennium Simulations and Proxy-Based Reconstructions. J. Clim. 32, 2441–2482. https://doi.org/10.1175/JCLI-D-18-0525.1

Lohmann, K., Mignot, J., Langehaug, H.R., Jungclaus, J.H., Matei, D., Otterå, O.H., Gao, Y.Q., Mjell, T.L., Ninnemann, U.S., Kleiven, H.F., 2015. Using simulations of the last millennium to understand climate variability seen in palaeo-observations: similar variation of Iceland–Scotland overflow strength and Atlantic Multidecadal Oscillation. Clim. Past 11, 203–216. https://doi.org/10.5194/cp-11-203-2015

Lu, Z., Liu, Z., Zhu, J., Cobb, K.M., 2018a. A Review of Paleo El Niño-Southern Oscillation. Atmosphere 9, 130. https://doi.org/10.3390/atmos9040130

Lu, Z., Miller, P.A., Zhang, Qiong, Zhang, Qiang, Wårlind, D., Nieradzik, L., Sjolte, J., Smith, B., 2018b. Dynamic Vegetation Simulations of the Mid-Holocene Green Sahara. Geophys. Res. Lett. 45, 8294–8303. https://doi.org/10.1029/2018GL079195

Lüning, S., Gałka, M., Danladi, I.B., Adagunodo, T.A., Vahrenholt, F., 2018. Hydroclimate in Africa during the Medieval Climate Anomaly. Palaeogeogr. Palaeoclimatol. Palaeoecol. 495, 309–322. https://doi.org/10.1016/j.palaeo.2018.01.025

Lüning, S., Schulte, L., Garcés-Pastor, S., Danladi, I.B., Gałka, M., 2019. The Medieval Climate Anomaly in the Mediterranean Region. Paleoceanogr. Paleoclimatology 34, 1625–1649. https://doi.org/10.1029/2019PA003734

Luo, J.-J., Masson, S., Behera, S.K., Yamagata, T., 2008. Extended ENSO Predictions Using a Fully Coupled Ocean–Atmosphere Model. J. Clim. 21, 84–93. https://doi.org/10.1175/2007JCLI1412.1

Luterbacher, J., Schmutz, C., Gyalistras, D., Xoplaki, E., Wanner, H., 1999. Reconstruction of monthly NAO and EU indices back to AD 1675. Geophys. Res. Lett. 26, 2745–2748. https://doi.org/10.1029/1999GL900576

Luterbacher, J., Werner, J.P., Smerdon, J.E., Fernández-Donado, L., González-Rouco, F.J., Barriopedro, D., Ljungqvist, F.C., Büntgen, U., Zorita, E., Wagner, S., Esper, J., McCarroll, D., Toreti, A., Frank, D., Jungclaus, J.H., Barriendos, M., Bertolin, C., Bothe, O., Brázdil, R., Camuffo, D., Dobrovolný, P., Gagen, M., García-

Bustamante, E., Ge, Q., Gómez-Navarro, J.J., Guiot, J., Hao, Z., Hegerl, G.C., Holmgren, K., Klimenko, V.V., Martín-Chivelet, J., Pfister, C., Roberts, N., Schindler, A., Schurer, A., Solomina, O., Gunten, L. von, Wahl, E., Wanner, H., Wetter, O., Xoplaki, E., Yuan, N., Zanchettin, D., Zhang, H., Zerefos, C., 2016. European summer temperatures since Roman times. Environ. Res. Lett. 11, 024001. https://doi.org/10.1088/1748-9326/11/2/024001

Luterbacher, J., Xoplaki, E., Dietrich, D., Jones, P.D., Davies, T.D., Portis, D., Gonzalez-Rouco, J.F., Storch, H. von, Gyalistras, D., Casty, C., Wanner, H., 2001. Extending North Atlantic oscillation reconstructions back to 1500. Atmospheric Sci. Lett. 2, 114–124. https://doi.org/10.1006/asle.2002.0047

Luterbacher, J., Xoplaki, E., Dietrich, D., Rickli, R., Jacobeit, J., Beck, C., Gyalistras, D., Schmutz, C., Wanner, H., 2002. Reconstruction of sea level pressure fields over the Eastern North Atlantic and Europe back to 1500. Clim. Dyn. 18, 545–561. https://doi.org/10.1007/s00382-001-0196-6

MacDonald, G.M., Case, R.A., 2005. Variations in the Pacific Decadal Oscillation over the past millennium. Geophys. Res. Lett. 32. https://doi.org/10.1029/2005GL022478

Maher, N., McGregor, S., England, M.H., Gupta, A.S., 2015. Effects of volcanism on tropical variability. Geophys. Res. Lett. 42, 6024–6033. https://doi.org/10.1002/2015GL064751

Mann, M.E., Bradley, R.S., Hughes, M.K., 1998. Global-scale temperature patterns and climate forcing over the past six centuries. Nature 392, 779–787. https://doi.org/10.1038/33859

Mann, M.E., Cane, M.A., Zebiak, S.E., Clement, A., 2005. Volcanic and Solar Forcing of the Tropical Pacific over the Past 1000 Years. J. Clim. 18, 447–456. https://doi.org/10.1175/JCLI-3276.1

Mann, M.E., Gille, E., Overpeck, J., Gross, W., Bradley, R.S., Keimig, F.T., Hughes, M.K., 2000. Global Temperature Patterns in Past Centuries: An Interactive Presentation. Earth Interact. 4, 1–1. https://doi.org/10.1175/1087-3562(2000)004<0001:GTPIPC>2.3.CO;2

Mann, M.E., Steinman, B.A., Miller, S.K., 2020. Absence of internal multidecadal and interdecadal oscillations in climate model simulations. Nat. Commun. 11, 49. https://doi.org/10.1038/s41467-019-13823-w

Mann, M.E., Zhang, Z., Rutherford, S., Bradley, R.S., Hughes, M.K., Shindell, D., Ammann, C., Faluvegi, G., Ni, F., 2009. Global signatures and dynamical origins of the Little Ice Age and Medieval Climate Anomaly. Science 326, 1256–1260. https://doi.org/10.1126/science.1177303

Mantua, N.J., Hare, S.R., 2002. The Pacific Decadal Oscillation. J. Oceanogr. 58, 35–44. https://doi.org/10.1023/A:1015820616384

Mantua, N.J., Hare, S.R., Zhang, Y., Wallace, J.M., Francis, R.C., 1997. A Pacific Interdecadal Climate Oscillation with Impacts on Salmon Production*. Bull. Am. Meteorol. Soc. 78, 1069–1080. https://doi.org/10.1175/1520-0477(1997)078<1069:APICOW>2.0.CO;2

Marchitto, T.M., Muscheler, R., Ortiz, J.D., Carriquiry, J.D., Geen, A. van, 2010. Dynamical Response of the Tropical Pacific Ocean to Solar Forcing During the Early Holocene. Science 330, 1378–1381. https://doi.org/10.1126/science.1194887

Marcott, S.A., Shakun, J.D., Clark, P.U., Mix, A.C., 2013. A Reconstruction of Regional and Global Temperature for the Past 11,300 Years. Science 339, 1198–1201. https://doi.org/10.1126/science.1228026

Marsh, N., Svensmark, H., 2003. Galactic cosmic ray and El Niño–Southern Oscillation trends in International Satellite Cloud Climatology Project D2 low-cloud properties. J. Geophys. Res. Atmospheres 108. https://doi.org/10.1029/2001JD001264

Marshall, G.J., 2003. Trends in the Southern Annular Mode from Observations and Reanalyses. J. Clim. 16, 4134–4143. https://doi.org/10.1175/1520-0442(2003)016<4134:TITSAM>2.0.CO;2

Martin-Puertas, C., Matthes, K., Brauer, A., Muscheler, R., Hansen, F., Petrick, C., Aldahan, A., Possnert, G., Geel, B. van, 2012. Regional atmospheric circulation shifts induced by a grand solar minimum. Nat. Geosci. 5, 397–401. https://doi.org/10.1038/ngeo1460

Masson-Delmotte, V., Schulz, M., Abe-Ouchi, A., Beer, J., Ganopolski, A., Gonzalez Rouco, J.F., Jansen, E., Lambeck, K., Luterbacher, J., Naish, T., Osborn, T., Otto-Bliesner, B., Quinn, T., Ramesh, R., Rojas, M., Shao, X., Timmermann, A., 2013. Information from paleoclimate archives, in: Stocker, T.F., Qin, D., Plattner, G.-K., Tignor, M.M.B., Allen, S.K., Boschung, J., Nauels, A., Xia, Y., Bex, V., Midgley, P.M. (Eds.), Climate Change 2013: The Physical Science Basis. Cambridge University Press, pp. 383–464. https://doi.org/10.1017/CBO9781107415324.013

Matthes, K., Funke, B., Andersson, M.E., Barnard, L., Beer, J., Charbonneau, P., Clilverd, M.A., Dudok de Wit, T., Haberreiter, M., Hendry, A., Jackman, C.H., Kretzschmar, M., Kruschke, T., Kunze, M., Langematz, U., Marsh, D.R., Maycock, A.C., Misios, S., Rodger, C.J., Scaife, A.A., Seppälä, A., Shangguan, M., Sinnhuber, M., Tourpali, K., Usoskin, I., Kamp, M. van de, Verronen, P.T., Versick, S., 2017. Solar forcing for CMIP6 (v3.2). Geosci. Model Dev. 10, 2247–2302. https://doi.org/10.5194/gmd-10-2247-2017

Matthes, K., Kodera, K., Haigh, J.D., Shindell, D.T., Shibata, K., Langematz, U., Rozanov, E., Kuroda, Y., 2003. GRIPS Solar Experiments Intercomparison Project: Initial Results. Pap. Meteorol. Geophys. 54, 71–90. https://doi.org/10.2467/mripapers.54.71

Matthes, K., Kuroda, Y., Kodera, K., Langematz, U., 2006. Transfer of the solar signal from the stratosphere to the troposphere: Northern winter. J. Geophys. Res. Atmospheres 111. https://doi.org/10.1029/2005JD006283

Mauri, A., Davis, B. a. S., Collins, P.M., Kaplan, J.O., 2014. The influence of atmospheric circulation on the mid-Holocene climate of Europe: a data–model comparison. Clim. Past 10, 1925–1938. https://doi.org/10.5194/cp-10-1925-2014

McAfee, S.A., 2014. Consistency and the Lack Thereof in Pacific Decadal Oscillation Impacts on North American Winter Climate. J. Clim. 27, 7410–7431. https://doi.org/10.1175/JCLI-D-14-00143.1

McCabe-Glynn, S., Johnson, K.R., Strong, C., Berkelhammer, M., Sinha, A., Cheng, H., Edwards, R.L., 2013. Variable North Pacific influence on drought in southwestern North America since AD 854. Nat. Geosci. 6, 617–621. https://doi.org/10.1038/ngeo1862

McGregor, S., Timmermann, A., 2010. The Effect of Explosive Tropical Volcanism on ENSO. J. Clim. 24, 2178–2191. https://doi.org/10.1175/2010JCLI3990.1

McGregor, S., Timmermann, A., England, M.H., Elison Timm, O., Wittenberg, A.T., 2013. Inferred changes in El Niño–Southern Oscillation variance over the past six centuries. Clim. Past 9, 2269–2284. https://doi.org/10.5194/cp-9-2269-2013

McGregor, S., Timmermann, A., Timm, O., 2010. A unified proxy for ENSO and PDO variability since 1650. Clim. Past 6, 1–17. https://doi.org/10.5194/cp-6-1-2010

McPhaden, M.J., Zebiak, S.E., Glantz, M.H., 2006. ENSO as an Integrating Concept in Earth Science. Science 314, 1740–1745. https://doi.org/10.1126/science.1132588

Meehl, G.A., Arblaster, J.M., Chung, C.T.Y., Holland, M.M., DuVivier, A., Thompson, L., Yang, D., Bitz, C.M., 2019. Sustained ocean changes contributed to sudden Antarctic sea ice retreat in late 2016. Nat. Commun. 10, 1–9. https://doi.org/10.1038/s41467-018-07865-9

Meehl, G.A., Hu, A., Santer, B.D., Xie, S.P., 2016. Contribution of the Interdecadal Pacific Oscillation to twentieth-century global surface temperature trends. Nat. Clim. Change 6, 1005–1008. https://doi.org/10.1038/nclimate3107

Mekhaldi, F., Muscheler, R., Adolphi, F., Aldahan, A., Beer, J., McConnell, J.R., Possnert, G., Sigl, M., Svensson, A., Synal, H.-A., Welten, K.C., Woodruff, T.E., 2015. Multiradionuclide evidence for the solar origin of the cosmic-ray events of AD 774/5 and 993/4. Nat. Commun. 6, 1–8. https://doi.org/10.1038/ncomms9611

Mellado-Cano, J., Barriopedro, D., García-Herrera, R., Trigo, R.M., Hernández, A., 2019. Examining the North Atlantic Oscillation, East Atlantic Pattern, and Jet Variability since 1685. J. Clim. 32, 6285–6298. https://doi.org/10.1175/JCLI-D-19-0135.1

Menary, M.B., Scaife, A.A., 2014. Naturally forced multidecadal variability of the Atlantic meridional overturning circulation. Clim. Dyn. 42, 1347–1362. https://doi.org/10.1007/s00382-013-2028-x

Meredith, M.P., Hogg, A.M., 2006. Circumpolar response of Southern Ocean eddy activity to a change in the Southern Annular Mode. Geophys. Res. Lett. 33. https://doi.org/10.1029/2006GL026499

Michel, S., Swingedouw, D., Chavent, M., Ortega, P., Mignot, J., Khodri, M., 2020. Reconstructing climatic modes of variability from proxy records using ClimIndRec version 1.0. Geosci. Model Dev. 13, 841–858. https://doi.org/10.5194/gmd-13-841-2020

Mignot, J., Khodri, M., Frankignoul, C., Servonnat, J., 2011. Volcanic impact on the Atlantic Ocean over the last millennium. Clim. Past 7, 1439–1455. https://doi.org/10.5194/cp-7-1439-2011

Miller, G.H., Geirsdóttir, Á., Zhong, Y., Larsen, D.J., Otto-Bliesner, B.L., Holland, M.M., Bailey, D.A., Refsnider, K.A., Lehman, S.J., Southon, J.R., Anderson, C., Björnsson, H., Thordarson, T., 2012. Abrupt onset of the Little Ice Age triggered by volcanism and sustained by sea-ice/ocean feedbacks. Geophys. Res. Lett. 39. https://doi.org/10.1029/2011GL050168

Minobe, S., 2000. Spatio-temporal structure of the pentadecadal variability over the North Pacific. Prog. Oceanogr. 47, 381–408. https://doi.org/10.1016/S0079-6611(00)00042-2

Minobe, S., 1999. Resonance in bidecadal and pentadecadal climate oscillations over the North Pacific: Role in climatic regime shifts. Geophys. Res. Lett. 26, 855–858. https://doi.org/1999GL900119

Misios, S., Mitchell, D.M., Gray, L.J., Tourpali, K., Matthes, K., Hood, L., Schmidt, H., Chiodo, G., Thiéblemont, R., Rozanov, E., Krivolutsky, A., 2016. Solar signals in CMIP-5 simulations: effects of atmosphere–ocean coupling. Q. J. R. Meteorol. Soc. 142, 928–941. https://doi.org/10.1002/qj.2695

Mitchell, J.M., 1976. An overview of climatic variability and its causal mechanisms. Quat. Res. 6, 481–493. https://doi.org/10.1016/0033-5894(76)90021-1

Miyake, F., Nagaya, K., Masuda, K., Nakamura, T., 2012. A signature of cosmic-ray increase in ad 774–775 from tree rings in Japan. Nature 486, 240–242. https://doi.org/10.1038/nature11123

Mjell, T.L., Ninnemann, U.S., Eldevik, T., Kleiven, H.K.F., 2015. Holocene multidecadal- to millennial-scale variations in Iceland-Scotland overflow and their relationship to climate. Paleoceanography 30, 558–569. https://doi.org/10.1002/2014PA002737

Mjell, T.L., Ninnemann, U.S., Kleiven, H.F., Hall, I.R., 2016. Multidecadal changes in Iceland Scotland Overflow Water vigor over the last 600 years and its relationship to climate. Geophys. Res. Lett. 43, 2111–2117. https://doi.org/10.1002/2016GL068227

Moffa-Sánchez, P., Born, A., Hall, I.R., Thornalley, D.J.R., Barker, S., 2014. Solar forcing of North Atlantic surface temperature and salinity over the past millennium. Nat. Geosci. 7, 275–278. https://doi.org/10.1038/ngeo2094

Moffa-Sanchez, P., Hall, I.R., Thornalley, D.J.R., Barker, S., Stewart, C., 2015. Changes in the strength of the Nordic Seas Overflows over the past 3000 years. Quat. Sci. Rev. 123, 134–143. https://doi.org/10.1016/j.quascirev.2015.06.007

Moore, G.W.K., Pickart, R.S., Renfrew, I.A., 2011. Complexities in the climate of the subpolar North Atlantic: a case study from the winter of 2007. Q. J. R. Meteorol. Soc. 137, 757–767. https://doi.org/10.1002/qj.778

Moore, G.W.K., Renfrew, I.A., Pickart, R.S., 2013. Multidecadal Mobility of the North Atlantic Oscillation. J. Clim. 26, 2453–2466. https://doi.org/10.1175/JCLI-D-12-00023.1

Moreno, P.I., Vilanova, I., Villa-Martínez, R., Dunbar, R.B., Mucciarone, D.A., Kaplan, M.R., Garreaud, R.D., Rojas, M., Moy, C.M., Pol-Holz, R.D., Lambert, F., 2018. Onset and Evolution of Southern Annular Mode-Like Changes at Centennial Timescale. Sci. Rep. 8, 1–9. https://doi.org/10.1038/s41598-018-21836-6

Moreno, P.I., Vilanova, I., Villa-Martínez, R., Garreaud, R.D., Rojas, M., Pol-Holz, R.D., 2014. Southern Annular Mode-like changes in southwestern Patagonia at centennial timescales over the last three millennia. Nat. Commun. 5, 1–7. https://doi.org/10.1038/ncomms5375

Moreno-Chamarro, E., Zanchettin, D., Lohmann, K., Jungclaus, J.H., 2017a. An abrupt weakening of the subpolar gyre as trigger of Little Ice Age-type episodes. Clim. Dyn. 48, 727–744. https://doi.org/10.1007/s00382-016-3106-7

Moreno-Chamarro, E., Zanchettin, D., Lohmann, K., Luterbacher, J., Jungclaus, J.H., 2017b. Winter amplification of the European Little Ice Age cooling by the subpolar gyre. Sci. Rep. 7, 1–8. https://doi.org/10.1038/s41598-017-07969-0

Moy, C.M., Seltzer, G.O., Rodbell, D.T., Anderson, D.M., 2002. Variability of El Niño/Southern Oscillation activity at millennial timescales during the Holocene epoch. Nature 420, 162–165. https://doi.org/10.1038/nature01194

Muscheler, R., Adolphi, F., Knudsen, M.F., 2014. Assessing the differences between the IntCal and Greenland ice-core time scales for the last 14,000 years via the common cosmogenic radionuclide variations. Quat. Sci. Rev., Dating, Synthesis, and Interpretation of Palaeoclimatic Records and Model-data Integration: Advances of the INTIMATE project(INTegration of Ice core, Marine and TErrestrial records, COST Action ES0907) 106, 81–87. https://doi.org/10.1016/j.quascirev.2014.08.017

Muscheler, R., Beer, J., Vonmoos, M., 2004. Causes and timing of the 8200yr BP event inferred from the comparison of the GRIP 10Be and the tree ring Δ14C record. Quat. Sci. Rev., Holocene climate variability - a marine perspective 23, 2101–2111. https://doi.org/10.1016/j.quascirev.2004.08.007

Muschitiello, F., Zhang, Q., Sundqvist, H.S., Davies, F.J., Renssen, H., 2015. Arctic climate response to the termination of the African Humid Period. Quat. Sci. Rev. 125, 91–97. https://doi.org/10.1016/j.quascirev.2015.08.012

Nakamura, N., Kayanne, H., Iijima, H., McClanahan, T.R., Behera, S.K., Yamagata, T., 2009. Mode shift in the Indian Ocean climate under global warming stress. Geophys. Res. Lett. 36. https://doi.org/10.1029/2009GL040590

Neukom, R., Barboza, L.A., Erb, M.P., Shi, F., Emile-Geay, J., Evans, M.N., Franke, J., Kaufman, D.S., Lücke, L., Rehfeld, K., Schurer, A., Zhu, F., Brönnimann, S., Hakim, G.J., Henley, B.J., Ljungqvist, F.C., McKay, N., Valler, V., von Gunten, L., PAGES 2k Consortium, 2019. Consistent multidecadal variability in global temperature reconstructions and simulations over the Common Era. Nat. Geosci. 12, 643–649. https://doi.org/10.1038/s41561-019-0400-0

Newman, M., Alexander, M.A., Ault, T.R., Cobb, K.M., Deser, C., Di Lorenzo, E., Mantua, N.J., Miller, A.J., Minobe, S., Nakamura, H., Schneider, N., Vimont, D.J., Phillips, A.S., Scott, J.D., Smith, C.A., 2016. The pacific decadal oscillation, revisited. J. Clim. 29, 4399–4427. https://doi.org/10.1175/JCLI-D-15-0508.1

Newman, M., Compo, G.P., Alexander, M.A., 2003. ENSO-Forced Variability of the Pacific Decadal Oscillation. J. Clim. 16, 3853–3857. https://doi.org/10.1175/1520-0442(2003)016<3853:EVOTPD>2.0.CO;2

Niedermeyer, E.M., Sessions, A.L., Feakins, S.J., Mohtadi, M., 2014. Hydroclimate of the western Indo-Pacific Warm Pool during the past 24,000 years. Proc. Natl. Acad. Sci. 111, 9402–9406. https://doi.org/10.1073/pnas.1323585111

Ojala, A.E.K., Launonen, I., Holmström, L., Tiljander, M., 2015. Effects of solar forcing and North Atlantic oscillation on the climate of continental Scandinavia during the Holocene. Quat. Sci. Rev. 112, 153–171. https://doi.org/10.1016/j.quascirev.2015.01.021

Ólafsdóttir, K.B., Geirsdóttir, Á., Miller, G.H., Larsen, D.J., 2013. Evolution of NAO and AMO strength and cyclicity derived from a 3-ka varve-thickness record from Iceland. Quat. Sci. Rev. 69, 142–154. https://doi.org/10.1016/j.quascirev.2013.03.009

Oliva, M., Navarro, F., Hrbáček, F., Hernández, A., Nývlt, D., Pereira, P., Ruiz-Fernández, J., Trigo, R., 2017. Recent regional climate cooling on the Antarctic Peninsula and associated impacts on the cryosphere. Sci. Total Environ. 580, 210–223. https://doi.org/10.1016/j.scitotenv.2016.12.030

Olsen, J., Anderson, N.J., Knudsen, M.F., 2012. Variability of the North Atlantic Oscillation over the past 5,200 years. Nat. Geosci. 5, 808–812. https://doi.org/10.1038/ngeo1589

O'Reilly, C.H., Woollings, T., Zanna, L., 2017. The Dynamical Influence of the Atlantic Multidecadal Oscillation on Continental Climate. J. Clim. 30, 7213–7230. https://doi.org/10.1175/JCLI-D-16-0345.1

Ortega, P., Lehner, F., Swingedouw, D., Masson-Delmotte, V., Raible, C.C., Casado, M., Yiou, P., 2015. A model-tested North Atlantic Oscillation reconstruction for the past millennium. Nature 523, 71–74. https://doi.org/10.1038/nature14518

Ortega, P., Swingedouw, D., Masson-Delmotte, V., Risi, C., Vinther, B., Yiou, P., Vautard, R., Yoshimura, K., 2014. Characterizing atmospheric circulation signals in Greenland ice cores: insights from a weather regime approach. Clim. Dyn. 43, 2585–2605. https://doi.org/10.1007/s00382-014-2074-z

Osborn, T.J., 2004. Simulating the winter North Atlantic Oscillation: the roles of internal variability and greenhouse gas forcing. Clim. Dyn. 22, 605–623. https://doi.org/10.1007/s00382-004-0405-1

Osborn, T.J., Briffa, K.R., Tett, S.F.B., Jones, P.D., Trigo, R.M., 1999. Evaluation of the North Atlantic Oscillation as simulated by a coupled climate model. Clim. Dyn. 15, 685–702. https://doi.org/10.1007/s003820050310

Otterå, O.H., Bentsen, M., Drange, H., Suo, L., 2010. External forcing as a metronome for Atlantic multidecadal variability. Nat. Geosci. 3, 688–694. https://doi.org/10.1038/ngeo955

Otto-Bliesner, B.L., Brady, E.C., Fasullo, J., Jahn, A., Landrum, L., Stevenson, S., Rosenbloom, N., Mai, A., Strand, G., 2016. Climate Variability and Change since 850 CE: An Ensemble Approach with the Community Earth System Model. Bull. Am. Meteorol. Soc. 97, 735–754. https://doi.org/10.1175/BAMS-D-14-00233.1

PAGES2k Consortium, Emile-Geay, J., McKay, N.P., Kaufman, D.S., von Gunten, L., Wang, J., Anchukaitis, K.J., Abram, N.J., Addison, J.A., Curran, M.A.J., Evans, M.N., Henley, B.J., Hao, Z., Martrat, B., McGregor, H.V., Neukom, R., Pederson, G.T., Stenni, B., Thirumalai, K., Werner, J.P., Xu, C., Divine, D.V., Dixon, B.C., Gergis, J., Mundo, I.A., Nakatsuka, T., Phipps, S.J., Routson, C.C., Steig, E.J., Tierney, J.E., Tyler, J.J., Allen, K.J., Bertler, N.A.N., Björklund, J., Chase, B.M., Chen, M.-T., Cook, E., de Jong, R., DeLong, K.L., Dixon, D.A., Ekaykin, A.A., Ersek, V., Filipsson, H.L., Francus, P., Freund, M.B., Frezzotti, M., Gaire, N.P., Gajewski, K., Ge, Q., Goosse, H., Gornostaeva, A., Grosjean, M., Horiuchi, K., Hormes, A., Husum, K., Isaksson, E., Kandasamy, S., Kawamura, K., Kilbourne, K.H., Koç, N., Leduc, G., Linderholm, H.W., Lorrey, A.M., Mikhalenko, V., Mortyn, P.G., Motoyama, H., Moy, A.D., Mulvaney, R., Munz, P.M., Nash, D.J., Oerter, H., Opel, T., Orsi, A.J., Ovchinnikov, D.V., Porter, T.J., Roop, H.A., Saenger, C., Sano, M., Sauchyn, D., Saunders, K.M., Seidenkrantz, M.-S., Severi, M., Shao, X., Sicre, M.-A., Sigl, M., Sinclair, K., George, S.S., Jacques, J.-M.S., Thamban, M., Kuwar Thapa, U., Thomas, E.R., Turney, C., Uemura, R., Viau, A.E., Vladimirova, D.O., Wahl, E.R., White, J.W.C., Yu, Z., Zinke, J., 2017. A global multiproxy database for temperature reconstructions of the Common Era. Sci. Data 4, 170088. https://doi.org/10.1038/sdata.2017.88

Park, H.-S., Kim, S.-J., Seo, K.-H., Stewart, A.L., Kim, S.-Y., Son, S.-W., 2018. The impact of Arctic sea ice loss on mid-Holocene climate. Nat. Commun. 9, 1–9. https://doi.org/10.1038/s41467-018-07068-2

Parker, D., Folland, C., Scaife, A., Knight, J., Colman, A., Baines, P., Dong, B., 2007. Decadal to multidecadal variability and the climate change background. J. Geophys. Res. Atmospheres 112. https://doi.org/10.1029/2007JD008411

Parker, D.E., Legg, T.P., Folland, C.K., 1992. A new daily central England temperature series, 1772–1991. Int. J. Climatol. 12, 317–342. https://doi.org/10.1002/joc.3370120402

Parnell, A., Sweeney, J., Doan, T., 2016. Bclim: Bayesian Palaeoclimate Reconstruction from Pollen Data.

Parnell, A.C., Haslett, J., Sweeney, J., Doan, T.K., Allen, J.R.M., Huntley, B., 2016. Joint palaeoclimate reconstruction from pollen data via forward models and climate histories. Quat. Sci. Rev. 151, 111–126. https://doi.org/10.1016/j.quascirev.2016.09.007

Parnell, A.C., Sweeney, J., Doan, T.K., Salter-Townshend, M., Allen, J.R.M., Huntley, B., Haslett, J., 2015. Bayesian inference for palaeoclimate with time uncertainty and stochastic volatility. J. R. Stat. Soc. Ser. C Appl. Stat. 64, 115–138. https://doi.org/10.1111/rssc.12065

Pausata, F.S.R., Chafik, L., Caballero, R., Battisti, D.S., 2015. Impacts of high-latitude volcanic eruptions on ENSO and AMOC. Proc. Natl. Acad. Sci. 112, 13784–13788. https://doi.org/10.1073/pnas.1509153112

Pearson, G.W., 1986. Precise Calendrical Dating of Known Growth-Period Samples Using a 'Curve Fitting' Technique. Radiocarbon 28, 292–299. https://doi.org/10.1017/S0033822200007396

Peng, Y., Shen, C., Cheng, H., Xu, Y., 2015. Simulation of the Interdecadal Pacific Oscillation and its impacts on the climate over eastern China during the last millennium. J. Geophys. Res. Atmospheres 120, 7573–7585. https://doi.org/10.1002/2015JD023104

Philander, G., 1989. El Nino, La Nina, and the Southern Oscillation, International Geophysics Series. Academic Press, San Diego.

Phillips, A.S., Deser, C., Fasullo, J., 2014. Evaluating Modes of Variability in Climate Models. Eos Trans. Am. Geophys. Union 95, 453–455. https://doi.org/10.1002/2014EO490002

Pinto, J.G., Raible, C.C., 2012. Past and recent changes in the North Atlantic oscillation. Wiley Interdiscip. Rev. Clim. Change 3, 79–90. https://doi.org/10.1002/wcc.150

Plunkett, G., Swindles, G.T., 2008. Determining the Sun's influence on Lateglacial and Holocene climates: a focus on climate response to centennial-scale solar forcing at 2800 cal.BP. Quat. Sci. Rev., INTegration of Ice-core, Marine and Terrestrial records (INTIMATE): Refining the record of the Last Glacial-Interglacial Transition 27, 175–184. https://doi.org/10.1016/j.quascirev.2007.01.015

Portis, D.H., Walsh, J.E., El Hamly, M., Lamb, P.J., 2001. Seasonality of the North Atlantic Oscillation. J. Clim. 14, 2069–2078. https://doi.org/10.1175/1520-0442(2001)014<2069:SOTNAO>2.0.CO;2

Power, S., Casey, T., Folland, C., Colman, A., Mehta, V., 1999. Inter-decadal modulation of the impact of ENSO on Australia. Clim. Dyn. 15, 319–324. https://doi.org/10.1007/s003820050284

Power, S., Delage, F., Chung, C., Kociuba, G., Keay, K., 2013. Robust twenty-first-century projections of El Niño and related precipitation variability. Nature 502, 541–545. https://doi.org/10.1038/nature12580

Prohom, M., Barriendos, M., Sanchez-Lorenzo, A., 2016. Reconstruction and homogenization of the longest instrumental precipitation series in the Iberian Peninsula (Barcelona, 1786–2014). Int. J. Climatol. 36, 3072–3087. https://doi.org/10.1002/joc.4537

Raible, C.C., Lehner, F., González-Rouco, J.F., Fernández-Donado, L., 2014. Changing correlation structures of the Northern Hemisphere atmospheric circulation from 1000 to 2100 AD. Clim. Past 10, 537–550. https://doi.org/10.5194/cp-10-537-2014

Rasmussen, S.O., Andersen, K.K., Svensson, A.M., Steffensen, J.P., Vinther, B.M., Clausen, H.B., Siggaard-Andersen, M.-L., Johnsen, S.J., Larsen, L.B., Dahl-Jensen, D., Bigler, M., Röthlisberger, R., Fischer, H., Goto-Azuma, K., Hansson, M.E., Ruth, U., 2006. A new Greenland ice core chronology for the last glacial termination. J. Geophys. Res. Atmospheres 111. https://doi.org/10.1029/2005JD006079

Rasmusson, E.M., Wallace, J.M., 1983. Meteorological Aspects of the El Niño/Southern Oscillation. Science 222, 1195–1202. https://doi.org/10.1126/science.222.4629.1195

Reimer, P., Austin, W.E.N., Bard, E., Bayliss, A., Blackwell, P.G., Bronk Ramsey, C., Butzin, M., Cheng, H., Edwards, R.L., Friedrich, M., Grootes, P.M., Guilderson, T.P., Hajdas, I., Heaton, T.J., Hogg, A.G., 2020. The IntCal20 Northern Hemisphere radiocarbon age calibration curve (0-55 kcal BP). Radiocarbon.

Reimer, P.J., Bard, E., Bayliss, A., Beck, J.W., Blackwell, P.G., Ramsey, C.B., Buck, C.E., Cheng, H., Edwards, R.L., Friedrich, M., Grootes, P.M., Guilderson, T.P., Haflidason, H., Hajdas, I., Hatté, C., Heaton, T.J., Hoffmann, D.L., Hogg, A.G., Hughen, K.A., Kaiser, K.F., Kromer, B., Manning, S.W., Niu, M., Reimer, R.W., Richards, D.A., Scott, E.M., Southon, J.R., Staff, R.A., Turney, C.S.M., Plicht, J. van der, 2013. IntCal13 and Marine13 Radiocarbon Age Calibration Curves 0–50,000 Years cal BP. Radiocarbon 55, 1869–1887.

Reimer, P.J., Reimer, R.W., 2001. A Marine Reservoir Correction Database and On-Line Interface. Radiocarbon 43, 461–463. https://doi.org/10.1017/S0033822200038339

Renssen, H., Goosse, H., Fichefet, T., Brovkin, V., Driesschaert, E., Wolk, F., 2005. Simulating the Holocene climate evolution at northern high latitudes using a coupled atmosphere-sea ice-ocean-vegetation model. Clim. Dyn. 24, 23–43. https://doi.org/10.1007/s00382-004-0485-y

Reynhout, S.A., Sagredo, E.A., Kaplan, M.R., Aravena, J.C., Martini, M.A., Moreno, P.I., Rojas, M., Schwartz, R., Schaefer, J.M., 2019. Holocene glacier fluctuations in Patagonia are modulated by summer insolation intensity and paced by Southern Annular Mode-like variability. Quat. Sci. Rev. 220, 178–187. https://doi.org/10.1016/j.quascirev.2019.05.029

Robock, A., 2000. Volcanic eruptions and climate. Rev. Geophys. 38, 191–219. https://doi.org/10.1029/1998RG000054

Rodbell, D.T., Seltzer, G.O., Anderson, D.M., Abbott, M.B., Enfield, D.B., Newman, J.H., 1999. An ~15,000-Year Record of El Niño-Driven Alluviation in Southwestern Ecuador. Science 283, 516–520. https://doi.org/10.1126/science.283.5401.516

Rodriguez-Ramirez, A., Grove, C.A., Zinke, J., Pandolfi, J.M., Zhao, J., 2014. Coral Luminescence Identifies the Pacific Decadal Oscillation as a Primary Driver of River Runoff Variability Impacting the Southern Great Barrier Reef. PLOS ONE 9, e84305. https://doi.org/10.1371/journal.pone.0084305

Ropelewski, C.F., Halpert, M.S., 1989. Precipitation Patterns Associated with the High Index Phase of the Southern Oscillation. J. Clim. 2, 268–284. https://doi.org/10.1175/1520-0442(1989)002<0268:PPAWTH>2.0.CO;2

Ropelewski, C.F., Halpert, M.S., 1987. Global and Regional Scale Precipitation Patterns Associated with the El Niño/Southern Oscillation. Mon. Weather Rev. 115, 1606–1626. https://doi.org/10.1175/1520-0493(1987)115<1606:GARSPP>2.0.CO;2

Roundy, P.E., 2014. On the Interpretation of EOF Analysis of ENSO, Atmospheric Kelvin Waves, and the MJO. J. Clim. 28, 1148–1165. https://doi.org/10.1175/JCLI-D-14-00398.1

Rowell, D.P., Folland, C.K., Maskell, K., Ward, M.N., 1995. Variability of summer rainfall over tropical north Africa (1906–92): Observations and modelling. Q. J. R. Meteorol. Soc. 121, 669–704. https://doi.org/10.1002/qj.49712152311

Rubino, M., Etheridge, D.M., Thornton, D.P., Howden, R., Allison, C.E., Francey, R.J., Langenfelds, R.L., Steele, L.P., Trudinger, C.M., Spencer, D.A., Curran, M.A.J., Ommen, T.D. van, Smith, A.M., 2019. Revised records of atmospheric trace gases CO_2, CH_4, N_2O, and $\delta^{13}C$-CO_2 over the last 2000 years from Law Dome, Antarctica. Earth Syst. Sci. Data 11, 473–492. https://doi.org/10.5194/essd-11-473-2019

Ruddiman, W.F., Kutzbach, J.E., Vavrus, S.J., 2011. Can natural or anthropogenic explanations of late-Holocene CO2 and CH4 increases be falsified?: The Holocene. https://doi.org/10.1177/0959683610387172

Rustic, G.T., Koutavas, A., Marchitto, T.M., Linsley, B.K., 2015. Dynamical excitation of the tropical Pacific Ocean and ENSO variability by Little Ice Age cooling. Science 350, 1537–1541. https://doi.org/10.1126/science.aac9937

Saarni, S., Saarinen, T., Dulski, P., 2016. Between the North Atlantic Oscillation and the Siberian High: A 4000-year snow accumulation history inferred from varved lake sediments in Finland. The Holocene 26, 423–431. https://doi.org/10.1177/0959683615609747

Sánchez-López, G., 2016. North Atlantic Oscillation imprints in the Central Iberian Peninsula for the last two millennia: from ordination analyses to the Bayesian approach. University of Barcelona, Barcelona.

Sánchez-López, G., Hernández, A., Pla-Rabes, S., Trigo, R.M., Toro, M., Granados, I., Sáez, A., Masqué, P., Pueyo, J.J., Rubio-Inglés, M.J., Giralt, S., 2016. Climate reconstruction for the last two millennia in central Iberia: The role of East Atlantic (EA), North Atlantic Oscillation (NAO) and their interplay over the Iberian Peninsula. Quat. Sci. Rev. 149, 135–150. https://doi.org/10.1016/j.quascirev.2016.07.021

Saunders, K.M., Roberts, S.J., Perren, B., Butz, C., Sime, L., Davies, S., Nieuwenhuyze, W.V., Grosjean, M., Hodgson, D.A., 2018. Holocene dynamics of the Southern Hemisphere westerly winds and possible links to CO 2 outgassing. Nat. Geosci. 11, 650–655. https://doi.org/10.1038/s41561-018-0186-5

Scaife, A.A., Ineson, S., Knight, J.R., Gray, L., Kodera, K., Smith, D.M., 2013. A mechanism for lagged North Atlantic climate response to solar variability. Geophys. Res. Lett. 40, 434–439. https://doi.org/10.1002/grl.50099

Scaife, A.A., Knight, J.R., Vallis, G.K., Folland, C.K., 2005. A stratospheric influence on the winter NAO and North Atlantic surface climate. Geophys. Res. Lett. 32. https://doi.org/10.1029/2005GL023226

Scaife, A.A., Smith, D., 2018. A signal-to-noise paradox in climate science. Npj Clim. Atmospheric Sci. 1, 1–8. https://doi.org/10.1038/s41612-018-0038-4

Schlesinger, M.E., Ramankutty, N., 1994. An oscillation in the global climate system of period 65–70 years. Nature 367, 723–726. https://doi.org/10.1038/367723a0

Schleussner, C.-F., Divine, D.V., Donges, J.F., Miettinen, A., Donner, R.V., 2015. Indications for a North Atlantic ocean circulation regime shift at the onset of the Little Ice Age. Clim. Dyn. 45, 3623–3633. https://doi.org/10.1007/s00382-015-2561-x

Schmutz, C., Luterbacher, J., Gyalistras, D., Xoplaki, E., Wanner, H., 2000. Can we trust proxy-based NAO index reconstructions? Geophys. Res. Lett. 27, 1135–1138. https://doi.org/10.1029/1999GL011045

Schneider, N., Cornuelle, B.D., 2005. The Forcing of the Pacific Decadal Oscillation. J. Clim. 18, 4355–4373. https://doi.org/10.1175/JCLI3527.1

Schurer, A.P., Hegerl, G.C., Mann, M.E., Tett, S.F.B., Phipps, S.J., 2013. Separating Forced from Chaotic Climate Variability over the Past Millennium. J. Clim. 26, 6954–6973. https://doi.org/10.1175/JCLI-D-12-00826.1

Sen Gupta, A., England, M.H., 2006. Coupled Ocean–Atmosphere–Ice Response to Variations in the Southern Annular Mode. J. Clim. 19, 4457–4486. https://doi.org/10.1175/JCLI3843.1

Seppälä, A., Clilverd, M.A., 2014. Energetic particle forcing of the Northern Hemisphere winter stratosphere: comparison to solar irradiance forcing. Front. Phys. 2. https://doi.org/10.3389/fphy.2014.00025

Seppälä, A., Matthes, K., Randall, C.E., Mironova, I.A., 2014. What is the solar influence on climate? Overview of activities during CAWSES-II. Prog. Earth Planet. Sci. 1, 24. https://doi.org/10.1186/s40645-014-0024-3

Shaman, J., 2014. The Seasonal Effects of ENSO on European Precipitation: Observational Analysis. J. Clim. 27, 6423–6438. https://doi.org/10.1175/JCLI-D-14-00008.1

Shen, C., Wang, W.-C., Gong, W., Hao, Z., 2006. A Pacific Decadal Oscillation record since 1470 AD reconstructed from proxy data of summer rainfall over eastern China. Geophys. Res. Lett. 33. https://doi.org/10.1029/2005GL024804

Shepherd, T.G., 2014. Atmospheric circulation as a source of uncertainty in climate change projections. Nat. Geosci. 7, 703–708. https://doi.org/10.1038/ngeo2253

Sigl, M., Winstrup, M., McConnell, J.R., Welten, K.C., Plunkett, G., Ludlow, F., Büntgen, U., Caffee, M., Chellman, N., Dahl-Jensen, D., Fischer, H., Kipfstuhl, S., Kostick, C., Maselli, O.J., Mekhaldi, F., Mulvaney, R., Muscheler, R., Pasteris, D.R., Pilcher, J.R., Salzer, M., Schüpbach, S., Steffensen, J.P., Vinther, B.M., Woodruff, T.E., 2015. Timing and climate forcing of volcanic eruptions for the past 2,500 years. Nature 523, 543–549. https://doi.org/10.1038/nature14565

Singh, H.K.A., Hakim, G.J., Tardif, R., Emile-Geay, J., Noone, D.C., 2018. Insights into Atlantic multidecadal variability using the Last Millennium Reanalysis framework. Clim. Past 14, 157–174. https://doi.org/10.5194/cp-14-157-2018

Sjolte, J., Hoffmann, G., Johnsen, S.J., 2014. Modelling the response of stable water isotopes in Greenland precipitation to orbital configurations of the previous interglacial. Tellus B Chem. Phys. Meteorol. 66, 22872. https://doi.org/10.3402/tellusb.v66.22872

Sjolte, J., Sturm, C., Adolphi, F., Vinther, B.M., Werner, M., Lohmann, G., Muscheler, R., 2018. Solar and volcanic forcing of North Atlantic climate inferred from a process-based reconstruction. Clim. Past 14, 1179–1194. https://doi.org/10.5194/cp-14-1179-2018

Slivinski, L.C., Compo, G.P., Whitaker, J.S., Sardeshmukh, P.D., Giese, B.S., McColl, C., Allan, R., Yin, X., Vose, R., Titchner, H., Kennedy, J., Spencer, L.J., Ashcroft, L., Brönnimann, S., Brunet, M., Camuffo, D., Cornes, R., Cram, T.A., Crouthamel, R., Domínguez-Castro, F., Freeman, J.E., Gergis, J., Hawkins, E., Jones, P.D., Jourdain, S., Kaplan, A., Kubota, H., Blancq, F.L., Lee, T.-C., Lorrey, A., Luterbacher, J., Maugeri, M., Mock, C.J., Moore, G.W.K., Przybylak, R., Pudmenzky, C., Reason, C., Slonosky, V.C., Smith, C.A., Tinz, B., Trewin, B., Valente, M.A., Wang, X.L., Wilkinson, C., Wood, K., Wyszyński, P., 2019. Towards a more reliable historical reanalysis: Improvements for version 3 of the Twentieth Century Reanalysis system. Q. J. R. Meteorol. Soc. n/a. https://doi.org/10.1002/qj.3598

Smerdon, J.E., 2012. Climate models as a test bed for climate reconstruction methods: pseudoproxy experiments. WIREs Clim. Change 3, 63–77. https://doi.org/10.1002/wcc.149

Smith, A.C., Wynn, P.M., Barker, P.A., Leng, M.J., Noble, S.R., Tych, W., 2016. North Atlantic forcing of moisture delivery to Europe throughout the Holocene. Sci. Rep. 6, 24745. https://doi.org/10.1038/srep24745

Smith, D.M., Booth, B.B.B., Dunstone, N.J., Eade, R., Hermanson, L., Jones, G.S., Scaife, A.A., Sheen, K.L., Thompson, V., 2016. Role of volcanic and anthropogenic aerosols in the recent global surface warming slowdown. Nat. Clim. Change 6, 936–940. https://doi.org/10.1038/nclimate3058

Smith, D.M., Eade, R., Scaife, A.A., Caron, L.-P., Danabasoglu, G., DelSole, T.M., Delworth, T., Doblas-Reyes, F.J., Dunstone, N.J., Hermanson, L., Kharin, V., Kimoto, M., Merryfield, W.J., Mochizuki, T., Müller, W.A., Pohlmann, H., Yeager, S., Yang, X., 2019. Robust skill of decadal climate predictions. Npj Clim. Atmospheric Sci. 2, 1–10. https://doi.org/10.1038/s41612-019-0071-y

Snowball, I., Muscheler, R., Zillén, L., Sandgren, P., Stanton, T., Ljung, K., 2010. Radiocarbon wiggle matching of Swedish lake varves reveals asynchronous climate changes around the 8.2 kyr cold event. Boreas 39, 720–733. https://doi.org/10.1111/j.1502-3885.2010.00167.x

Spahni, R., Chappellaz, J., Stocker, T.F., Loulergue, L., Hausammann, G., Kawamura, K., Flückiger, J., Schwander, J., Raynaud, D., Masson-Delmotte, V., Jouzel, J., 2005. Atmospheric Methane and Nitrous Oxide of the Late Pleistocene from Antarctic Ice Cores. Science 310, 1317–1321. https://doi.org/10.1126/science.1120132

Stahle, D.W., D'Arrigo, R.D., Krusic, P.J., Cleaveland, M.K., Cook, E.R., Allan, R.J., Cole, J.E., Dunbar, R.B., Therrell, M.D., Gay, D.A., Moore, M.D., Stokes, M.A., Burns, B.T., Villanueva-Diaz, J., Thompson, L.G., 1998. Experimental Dendroclimatic Reconstruction of the Southern Oscillation. Bull. Am. Meteorol. Soc. 79, 2137–2152. https://doi.org/10.1175/1520-0477(1998)079<2137:EDROTS>2.0.CO;2

Stansell, N.D., Steinman, B.A., Abbott, M.B., Rubinov, M., Roman-Lacayo, M., 2013. Lacustrine stable isotope record of precipitation changes in Nicaragua during the Little Ice Age and Medieval Climate Anomaly. Geology 41, 151–154. https://doi.org/10.1130/G33736.1

Steiger, N.J., Steig, E.J., Dee, S.G., Roe, G.H., Hakim, G.J., 2017. Climate reconstruction using data assimilation of water isotope ratios from ice cores. J. Geophys. Res. Atmospheres 122, 1545–1568. https://doi.org/10.1002/2016JD026011

Steinhilber, F., Beer, J., Fröhlich, C., 2009. Total solar irradiance during the Holocene. Geophys. Res. Lett. 36. https://doi.org/10.1029/2009GL040142

Stephenson, D., Pavan, V., participating CMIP1 modelling groups, 2003. The North Atlantic Oscillation in coupled climate models: a CMIP1 evaluation. Clim. Dyn. 20, 381–399. https://doi.org/10.1007/s00382-002-0281-5

Stephenson, D.B., Hannachi, A., O'Neill, A., 2004. On the existence of multiple climate regimes. Q. J. R. Meteorol. Soc. 130, 583–605. https://doi.org/10.1256/qj.02.146

Stevenson, S., Fasullo, J.T., Otto-Bliesner, B.L., Tomas, R.A., Gao, C., 2017. Role of eruption season in reconciling model and proxy responses to tropical volcanism. Proc. Natl. Acad. Sci. 114, 1822–1826. https://doi.org/10.1073/pnas.1612505114

Stocker, T. (Ed.), 2014. Climate change 2013: the physical science basis: Working Group I contribution to the Fifth assessment report of the Intergovernmental Panel on Climate Change. Cambridge University Press, New York.

Stoffel, M., Khodri, M., Corona, C., Guillet, S., Poulain, V., Bekki, S., Guiot, J., Luckman, B.H., Oppenheimer, C., Lebas, N., Beniston, M., Masson-Delmotte, V., 2015. Estimates of volcanic-induced cooling in the Northern Hemisphere over the past 1,500 years. Nat. Geosci. 8, 784–788. https://doi.org/10.1038/ngeo2526

Stone, J.R., Fritz, S.C., 2006. Multidecadal drought and Holocene climate instability in the Rocky Mountains. Geology 34, 409–412. https://doi.org/10.1130/G22225.1

Stuiver, M., Braziunas, T.F., 1993. Modeling Atmospheric 14C Influences and 14C Ages of Marine Samples to 10,000 BC. Radiocarbon 35, 137–189. https://doi.org/10.1017/S0033822200013874

Stuiver, M., Pearson, G.W., Braziunas, T., 1986. Radiocarbon Age Calibration of Marine Samples Back to 9000 Cal Yr BP. Radiocarbon 28, 980–1021. https://doi.org/10.1017/S0033822200060264

Sutton, R.T., Hodson, D.L.R., 2005. Atlantic Ocean Forcing of North American and European Summer Climate. Science 309, 115–118. https://doi.org/10.1126/science.1109496

Svalgaard, L., Schatten, K.H., 2016. Reconstruction of the Sunspot Group Number: The Backbone Method. Sol. Phys. 291, 2653–2684. https://doi.org/10.1007/s11207-015-0815-8

Svendsen, L., Hetzinger, S., Keenlyside, N., Gao, Y., 2014. Marine-based multiproxy reconstruction of Atlantic multidecadal variability. Geophys. Res. Lett. 41, 1295–1300. https://doi.org/10.1002/2013GL059076

Svensmark, H., Bondo, T., Svensmark, J., 2009. Cosmic ray decreases affect atmospheric aerosols and clouds. Geophys. Res. Lett. 36. https://doi.org/10.1029/2009GL038429

Sweeney, J., Salter-Townshend, M., Edwards, T., Buck, C.E., Parnell, A.C., 2018. Statistical challenges in estimating past climate changes. Wiley Interdiscip. Rev. Comput. Stat. 10, e1437. https://doi.org/10.1002/wics.1437

Swingedouw, D., Colin, C., Eynaud, F., Ayache, M., Zaragosi, S., 2019. Impact of freshwater release in the Mediterranean Sea on the North Atlantic climate. Clim. Dyn. 53, 3893–3915. https://doi.org/10.1007/s00382-019-04758-5

Swingedouw, D., Mignot, J., Ortega, P., Khodri, M., Menegoz, M., Cassou, C., Hanquiez, V., 2017. Impact of explosive volcanic eruptions on the main climate variability modes. Glob. Planet. Change 150, 24–45. https://doi.org/10.1016/j.gloplacha.2017.01.006

Swingedouw, D., Ortega, P., Mignot, J., Guilyardi, E., Masson-Delmotte, V., Butler, P.G., Khodri, M., Séférian, R., 2015. Bidecadal North Atlantic ocean circulation variability controlled by timing of volcanic eruptions. Nat. Commun. 6, 1–12. https://doi.org/10.1038/ncomms7545

Swingedouw, D., Terray, L., Cassou, C., Voldoire, A., Salas-Mélia, D., Servonnat, J., 2011. Natural forcing of climate during the last millennium: fingerprint of solar variability. Clim. Dyn. 36, 1349–1364. https://doi.org/10.1007/s00382-010-0803-5

Tardif, R., Hakim, G.J., Perkins, W.A., Horlick, K.A., Erb, M.P., Emile-Geay, J., Anderson, D.M., Steig, E.J., Noone, D., 2019. Last Millennium Reanalysis with an expanded proxy database and seasonal proxy modeling. Clim. Past 15, 1251–1273. https://doi.org/10.5194/cp-15-1251-2019

Terray, L., 2012. Evidence for multiple drivers of North Atlantic multi-decadal climate variability. Geophys. Res. Lett. 39. https://doi.org/10.1029/2012GL053046

Thiéblemont, R., Matthes, K., Omrani, N.-E., Kodera, K., Hansen, F., 2015. Solar forcing synchronizes decadal North Atlantic climate variability. Nat. Commun. 6, 8268. https://doi.org/10.1038/ncomms9268

Thompson, D.W.J., Solomon, S., 2002. Interpretation of Recent Southern Hemisphere Climate Change. Science 296, 895–899. https://doi.org/10.1126/science.1069270

Thompson, D.W.J., Solomon, S., Kushner, P.J., England, M.H., Grise, K.M., Karoly, D.J., 2011. Signatures of the Antarctic ozone hole in Southern Hemisphere surface climate change. Nat. Geosci. 4, 741–749. https://doi.org/10.1038/ngeo1296

Thompson, D.W.J., Wallace, J.M., 2001. Regional Climate Impacts of the Northern Hemisphere Annular Mode. Science 293, 85–89. https://doi.org/10.1126/science.1058958

Thompson, D.W.J., Wallace, J.M., 2000. Annular Modes in the Extratropical Circulation. Part I: Month-to-Month Variability. J. Clim. 13, 1000–1016. https://doi.org/10.1175/1520-0442(2000)013<1000:AMITEC>2.0.CO;2

Thompson, V., Dunstone, N.J., Scaife, A.A., Smith, D.M., Slingo, J.M., Brown, S., Belcher, S.E., 2017. High risk of unprecedented UK rainfall in the current climate. Nat. Commun. 8, 1–6. https://doi.org/10.1038/s41467-017-00275-3

Thornalley, D.J.R., Blaschek, M., Davies, F.J., Praetorius, S., Oppo, D.W., McManus, J.F., Hall, I.R., Kleiven, H., Renssen, H., McCave, I.N., 2013. Long-term variations in Iceland–Scotland overflow strength during the Holocene. Clim. Past 9, 2073–2084. https://doi.org/10.5194/cp-9-2073-2013

Timm, O., Ruprecht, E., Kleppek, S., 2004. Scale-Dependent Reconstruction of the NAO Index. J. Clim. 17, 2157–2169. https://doi.org/10.1175/1520-0442(2004)017<2157:SROTNI>2.0.CO;2

Tingley, M.P., Huybers, P., 2009. A Bayesian Algorithm for Reconstructing Climate Anomalies in Space and Time. Part I: Development and Applications to Paleoclimate Reconstruction Problems. J. Clim. 23, 2759–2781. https://doi.org/10.1175/2009JCLI3015.1

Toohey, M., Krüger, K., Bittner, M., Timmreck, C., Schmidt, H., 2014. The impact of volcanic aerosol on the Northern Hemisphere stratospheric polar vortex: mechanisms and sensitivity to forcing structure. Atmospheric Chem. Phys. 14, 13063–13079. https://doi.org/10.5194/acp-14-13063-2014

Toohey, M., Sigl, M., 2017. Volcanic stratospheric sulfur injections and aerosol optical depth from 500 BCE to 1900 CE. Earth Syst. Sci. Data 9, 809–831. https://doi.org/10.5194/essd-9-809-2017

Tourpali, K., Schuurmans, C.J.E., Dorland, R. van, Steil, B., Brühl, C., Manzini, E., 2005. Solar cycle modulation of the Arctic Oscillation in a chemistry-climate model. Geophys. Res. Lett. 32. https://doi.org/10.1029/2005GL023509

Trenberth, K.E., Dai, A., van der Schrier, G., Jones, P.D., Barichivich, J., Briffa, K.R., Sheffield, J., 2014. Global warming and changes in drought. Nat. Clim. Change 4, 17–22. https://doi.org/10.1038/nclimate2067

Trenberth, K.E., Shea, D.J., 2006. Atlantic hurricanes and natural variability in 2005. Geophys. Res. Lett. 33. https://doi.org/10.1029/2006GL026894

Trigo, R.M., Valente, M.A., Trigo, I.F., Miranda, P.M.A., Ramos, A.M., Paredes, D., García-Herrera, R., 2008. The Impact of North Atlantic Wind and Cyclone Trends on European Precipitation and Significant Wave Height in the Atlantic. Ann. N. Y. Acad. Sci. 1146, 212–234. https://doi.org/10.1196/annals.1446.014

Trouet, V., Esper, J., Graham, N.E., Baker, A., Scourse, J.D., Frank, D.C., 2009. Persistent Positive North Atlantic Oscillation Mode Dominated the Medieval Climate Anomaly. Science 324, 78–80. https://doi.org/10.1126/science.1166349

Tudhope, A.W., Chilcott, C.P., McCulloch, M.T., Cook, E.R., Chappell, J., Ellam, R.M., Lea, D.W., Lough, J.M., Shimmield, G.B., 2001. Variability in the El Niño-Southern Oscillation Through a Glacial-Interglacial Cycle. Science 291, 1511–1517. https://doi.org/10.1126/science.1057969

Turney, C.S.M., Wilmshurst, J.M., Jones, R.T., Wood, J.R., Palmer, J.G., Hogg, A.G., Fenwick, P., Crowley, S.F., Privat, K., Thomas, Z., 2017. Reconstructing atmospheric circulation over southern New Zealand: Establishment of modern westerly airflow 5500 years ago and implications for Southern Hemisphere Holocene climate change. Quat. Sci. Rev. 159, 77–87. https://doi.org/10.1016/j.quascirev.2016.12.017

Ummenhofer, C.C., Biastoch, A., Böning, C.W., 2016. Multidecadal Indian Ocean Variability Linked to the Pacific and Implications for Preconditioning Indian Ocean Dipole Events. J. Clim. 30, 1739–1751. https://doi.org/10.1175/JCLI-D-16-0200.1

Urban, F.E., Cole, J.E., Overpeck, J.T., 2000. Influence of mean climate change on climate variability from a 155-year tropical Pacific coral record. Nature 407, 989–993. https://doi.org/10.1038/35039597

Vance, T.R., Roberts, J.L., Plummer, C.T., Kiem, A.S., van Ommen, T.D., 2015. Interdecadal Pacific variability and eastern Australian megadroughts over the last millennium. Geophys. Res. Lett. 42, 129–137. https://doi.org/10.1002/2014GL062447

Vásquez-Bedoya, L.F., Cohen, A.L., Oppo, D.W., Blanchon, P., 2012. Corals record persistent multidecadal SST variability in the Atlantic Warm Pool since 1775 AD. Paleoceanography 27. https://doi.org/10.1029/2012PA002313

Verdon, D.C., Franks, S.W., 2006. Long-term behaviour of ENSO: Interactions with the PDO over the past 400 years inferred from paleoclimate records. Geophys. Res. Lett. 33. https://doi.org/10.1029/2005GL025052

Villalba, R., Lara, A., Masiokas, M.H., Urrutia, R., Luckman, B.H., Marshall, G.J., Mundo, I.A., Christie, D.A., Cook, E.R., Neukom, R., Allen, K., Fenwick, P., Boninsegna, J.A., Srur, A.M., Morales, M.S., Araneo, D., Palmer, J.G., Cuq, E., Aravena, J.C., Holz, A., LeQuesne, C., 2012. Unusual Southern Hemisphere tree growth patterns induced by changes in the Southern Annular Mode. Nat. Geosci. 5, 793–798. https://doi.org/10.1038/ngeo1613

Vinther, B.M., Andersen, K.K., Hansen, A.W., Schmith, T., Jones, P.D., 2003a. Improving the Gibraltar/Reykjavik NAO index. Geophys. Res. Lett. 30. https://doi.org/10.1029/2003GL018220

Vinther, B.M., Johnsen, S.J., Andersen, K.K., Clausen, H.B., Hansen, A.W., 2003b. NAO signal recorded in the stable isotopes of Greenland ice cores. Geophys. Res. Lett. 30. https://doi.org/10.1029/2002GL016193

Vinther, B.M., Jones, P.D., Briffa, K.R., Clausen, H.B., Andersen, K.K., Dahl-Jensen, D., Johnsen, S.J., 2010. Climatic signals in multiple highly resolved stable isotope records from Greenland. Quat. Sci. Rev. 29, 522–538. https://doi.org/10.1016/j.quascirev.2009.11.002

Visbeck, M., 2009. A Station-Based Southern Annular Mode Index from 1884 to 2005. J. Clim. 22, 940–950. https://doi.org/10.1175/2008JCLI2260.1

Voigt, I., Chiessi, C.M., Prange, M., Mulitza, S., Groeneveld, J., Varma, V., Henrich, R., 2015. Holocene shifts of the southern westerlies across the South Atlantic. Paleoceanography 30, 39–51. https://doi.org/10.1002/2014PA002677

Wang, B., Luo, X., Yang, Y.-M., Sun, W., Cane, M.A., Cai, W., Yeh, S.-W., Liu, J., 2019. Historical change of El Niño properties sheds light on future changes of extreme El Niño. Proc. Natl. Acad. Sci. 116, 22512–22517. https://doi.org/10.1073/pnas.1911130116

Wang, G., Hendon, H.H., Arblaster, J.M., Lim, E.-P., Abhik, S., van Rensch, P., 2019. Compounding tropical and stratospheric forcing of the record low Antarctic sea-ice in 2016. Nat. Commun. 10, 1–9. https://doi.org/10.1038/s41467-018-07689-7

Wang, J., Yang, B., Ljungqvist, F.C., Luterbacher, J., Osborn, T.J., Briffa, K.R., Zorita, E., 2017. Internal and external forcing of multidecadal Atlantic climate variability over the past 1,200 years. Nat. Geosci. 10, 512–517. https://doi.org/10.1038/ngeo2962

Wang, L., Chen, W., Huang, R., 2008. Interdecadal modulation of PDO on the impact of ENSO on the east Asian winter monsoon. Geophys. Res. Lett. 35. https://doi.org/10.1029/2008GL035287

Wang, Y., Cheng, H., Edwards, R.L., He, Y., Kong, X., An, Z., Wu, J., Kelly, M.J., Dykoski, C.A., Li, X., 2005. The Holocene Asian Monsoon: Links to Solar Changes and North Atlantic Climate. Science 308, 854–857. https://doi.org/10.1126/science.1106296

Wanner, H., Brönnimann, S., Casty, C., Gyalistras, D., Lutherbacher, J., Schmutz, C.J., Stephenson, D.B., Xoplaki, E., 2001. North Atlantic Oscillation - Concepts and studies. Surv. Geophys. 22, 321–382. https://doi.org/10.1023/A:1014217317898

Wanner, H., Solomina, O., Grosjean, M., Ritz, S.P., Jetel, M., 2011. Structure and origin of Holocene cold events. Quat. Sci. Rev. 30, 3109–3123. https://doi.org/10.1016/j.quascirev.2011.07.010

Wassenburg, J.A., Dietrich, S., Fietzke, J., Fohlmeister, J., Jochum, K.P., Scholz, D., Richter, D.K., Sabaoui, A., Spötl, C., Lohmann, G., Andreae, M.O., Immenhauser, A., 2016. Reorganization of the North Atlantic Oscillation during early Holocene deglaciation. Nat. Geosci. 9, 602–605. https://doi.org/10.1038/ngeo2767

Watanabe, T.K., Watanabe, T., Yamazaki, A., Pfeiffer, M., Claereboudt, M.R., 2019. Oman coral δ 18 O seawater record suggests that Western Indian Ocean upwelling uncouples from the Indian Ocean Dipole during the global-warming hiatus. Sci. Rep. 9, 1–9. https://doi.org/10.1038/s41598-018-38429-y

Wei, M., Qiao, F., Guo, Y., Deng, J., Song, Z., Shu, Q., Yang, X., 2019. Quantifying the importance of interannual, interdecadal and multidecadal climate natural variabilities in the modulation of global warming rates. Clim. Dyn. 53, 6715–6727. https://doi.org/10.1007/s00382-019-04955-2

White, S.M., Ravelo, A.C., Polissar, P.J., 2018. Dampened El Niño in the Early and Mid-Holocene Due To Insolation-Forced Warming/Deepening of the Thermocline. Geophys. Res. Lett. 45, 316–326. https://doi.org/10.1002/2017GL075433

Wilson, R., Cook, E., D'Arrigo, R., Riedwyl, N., Evans, M.N., Tudhope, A., Allan, R., 2010. Reconstructing ENSO: the influence of method, proxy data, climate forcing and teleconnections. J. Quat. Sci. 25, 62–78. https://doi.org/10.1002/jqs.1297

Wise, E.K., 2015. Tropical Pacific and Northern Hemisphere influences on the coherence of Pacific Decadal Oscillation reconstructions. Int. J. Climatol. 35, 154–160. https://doi.org/10.1002/joc.3966

Wittenberg, A.T., 2009. Are historical records sufficient to constrain ENSO simulations? Geophys. Res. Lett. 36. https://doi.org/10.1029/2009GL038710

Woollings, T., Blackburn, M., 2011. The North Atlantic Jet Stream under Climate Change and Its Relation to the NAO and EA Patterns. J. Clim. 25, 886–902. https://doi.org/10.1175/JCLI-D-11-00087.1

Wu, T., Hu, A., Gao, F., Zhang, J., Meehl, G.A., 2019. New insights into natural variability and anthropogenic forcing of global/regional climate evolution. Npj Clim. Atmospheric Sci. 2, 1–13. https://doi.org/10.1038/s41612-019-0075-7

Wulf, S., Dräger, N., Ott, F., Serb, J., Appelt, O., Guðmundsdóttir, E., van den Bogaard, C., Słowiński, M., Błaszkiewicz, M., Brauer, A., 2016. Holocene tephrostratigraphy of varved sediment records from Lakes Tiefer See (NE Germany) and Czechowskie (N Poland). Quat. Sci. Rev. 132, 1–14. https://doi.org/10.1016/j.quascirev.2015.11.007

Wulf, S., Ott, F., Słowiński, M., Noryśkiewicz, A.M., Dräger, N., Martin-Puertas, C., Czymzik, M., Neugebauer, I., Dulski, P., Bourne, A.J., Błaszkiewicz, M., Brauer, A., 2013. Tracing the Laacher See Tephra in the varved sediment record of the Trzechowskie palaeolake in central Northern Poland. Quat. Sci. Rev. 76, 129–139. https://doi.org/10.1016/j.quascirev.2013.07.010

Xoplaki, E., González-Rouco, J.F., Luterbacher, J., Wanner, H., 2004. Wet season Mediterranean precipitation variability: influence of large-scale dynamics and trends. Clim. Dyn. 23, 63–78. https://doi.org/10.1007/s00382-004-0422-0

Xoplaki, E., Luterbacher, J., Paeth, H., Dietrich, D., Steiner, N., Grosjean, M., Wanner, H., 2005. European spring and autumn temperature variability and change of extremes over the last half millennium. Geophys. Res. Lett. 32. https://doi.org/10.1029/2005GL023424

Xoplaki, E., Luterbacher, J., Wagner, S., Zorita, E., Fleitmann, D., Preiser-Kapeller, J., Sargent, A.M., White, S., Toreti, A., Haldon, J.F., Mordechai, L., Bozkurt, D., Akçer-Ön, S., Izdebski, A., 2018. Modelling Climate and Societal Resilience in the Eastern Mediterranean in the Last Millennium. Hum. Ecol. 46, 363–379. https://doi.org/10.1007/s10745-018-9995-9

Yan, H., Sun, L., Wang, Y., Huang, W., Qiu, S., Yang, C., 2011. A record of the Southern Oscillation Index for the past 2,000 years from precipitation proxies. Nat. Geosci. 4, 611–614. https://doi.org/10.1038/ngeo1231

Yao, J., Xiao, L., Gou, M., Li, C., Lian, E., Yang, S., 2018. Pacific decadal oscillation impact on East China precipitation and its imprint in new geological documents. Sci. China Earth Sci. 61, 473–482. https://doi.org/10.1007/s11430-016-9146-2

Yiou, P., Servonnat, J., Yoshimori, M., Swingedouw, D., Khodri, M., Abe-Ouchi, A., 2012. Stability of weather regimes during the last millennium from climate simulations. Geophys. Res. Lett. 39. https://doi.org/10.1029/2012GL051310

Zanchettin, D., Bothe, O., Graf, H.F., Lorenz, S.J., Luterbacher, J., Timmreck, C., Jungclaus, J.H., 2013. Background conditions influence the decadal climate response to strong volcanic eruptions. J. Geophys. Res. Atmospheres 118, 4090–4106. https://doi.org/10.1002/jgrd.50229

Zhang, R., Delworth, T.L., 2006. Impact of Atlantic multidecadal oscillations on India/Sahel rainfall and Atlantic hurricanes. Geophys. Res. Lett. 33. https://doi.org/10.1029/2006GL026267

Zhang, R., Sutton, R., Danabasoglu, G., Kwon, Y.-O., Marsh, R., Yeager, S.G., Amrhein, D.E., Little, C.M., 2019. A Review of the Role of the Atlantic Meridional Overturning Circulation in Atlantic Multidecadal Variability and Associated Climate Impacts. Rev. Geophys. 57, 316–375. https://doi.org/10.1029/2019RG000644

Zhang, T., Sun, D.-Z., 2014. ENSO Asymmetry in CMIP5 Models. J. Clim. 27, 4070–4093. https://doi.org/10.1175/JCLI-D-13-00454.1

Zhang, Z.-Y., Gong, D.-Y., He, X.-Z., Lei, Y.-N., Feng, S.-H., 2010. Statistical Reconstruction of the Antarctic Oscillation Index Based on Multiple Proxies. Atmospheric Ocean. Sci. Lett. 3, 283–287. https://doi.org/10.1080/16742834.2010.11446883

Zielhofer, C., Fletcher, W.J., Mischke, S., De Batist, M., Campbell, J.F.E., Joannin, S., Tjallingii, R., El Hamouti, N., Junginger, A., Stele, A., Bussmann, J., Schneider, B., Lauer, T., Spitzer, K., Strupler, M., Brachert, T., Mikdad, A., 2017. Atlantic forcing of Western Mediterranean winter rain minima during the last 12,000 years. Quat. Sci. Rev. 157, 29–51. https://doi.org/10.1016/j.quascirev.2016.11.037

Zielinski, G.A., Mayewski, P.A., Meeker, L.D., Whitlow, S., Twickler, M.S., Morrison, M., Meese, D.A., Gow, A.J., Alley, R.B., 1994. Record of Volcanism Since 7000 B.C. from the GISP2 Greenland Ice Core and Implications for the Volcano-Climate System. Science 264, 948–952. https://doi.org/10.1126/science.264.5161.948

Zolitschka, B., Francus, P., Ojala, A.E.K., Schimmelmann, A., 2015. Varves in lake sediments – a review. Quat. Sci. Rev. 117, 1–41. https://doi.org/10.1016/j.quascirev.2015.03.019

Zou, H., Hastie, T., 2005. Regularization and variable selection via the elastic net. J. R. Stat. Soc. Ser. B Stat. Methodol. 67, 301–320. https://doi.org/10.1111/j.1467-9868.2005.00503.x

Zubiate, L., McDermott, F., Sweeney, C., O'Malley, M., 2017. Spatial variability in winter NAO–wind speed relationships in western Europe linked to concomitant states of the East Atlantic and Scandinavian patterns. Q. J. R. Meteorol. Soc. 143, 552–562. https://doi.org/10.1002/qj.2943

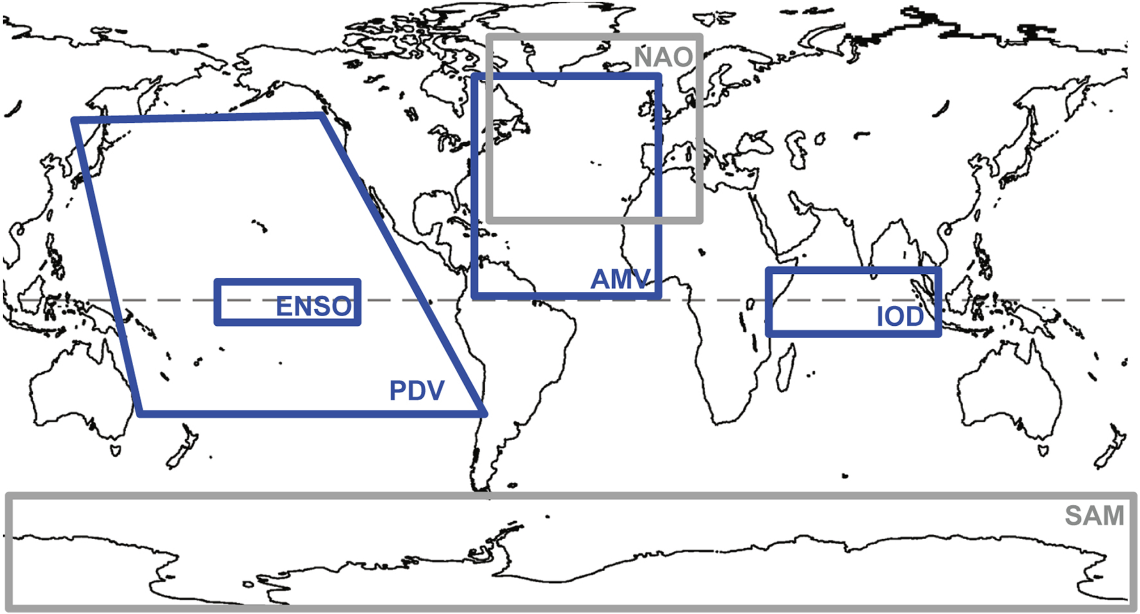

Figure 1

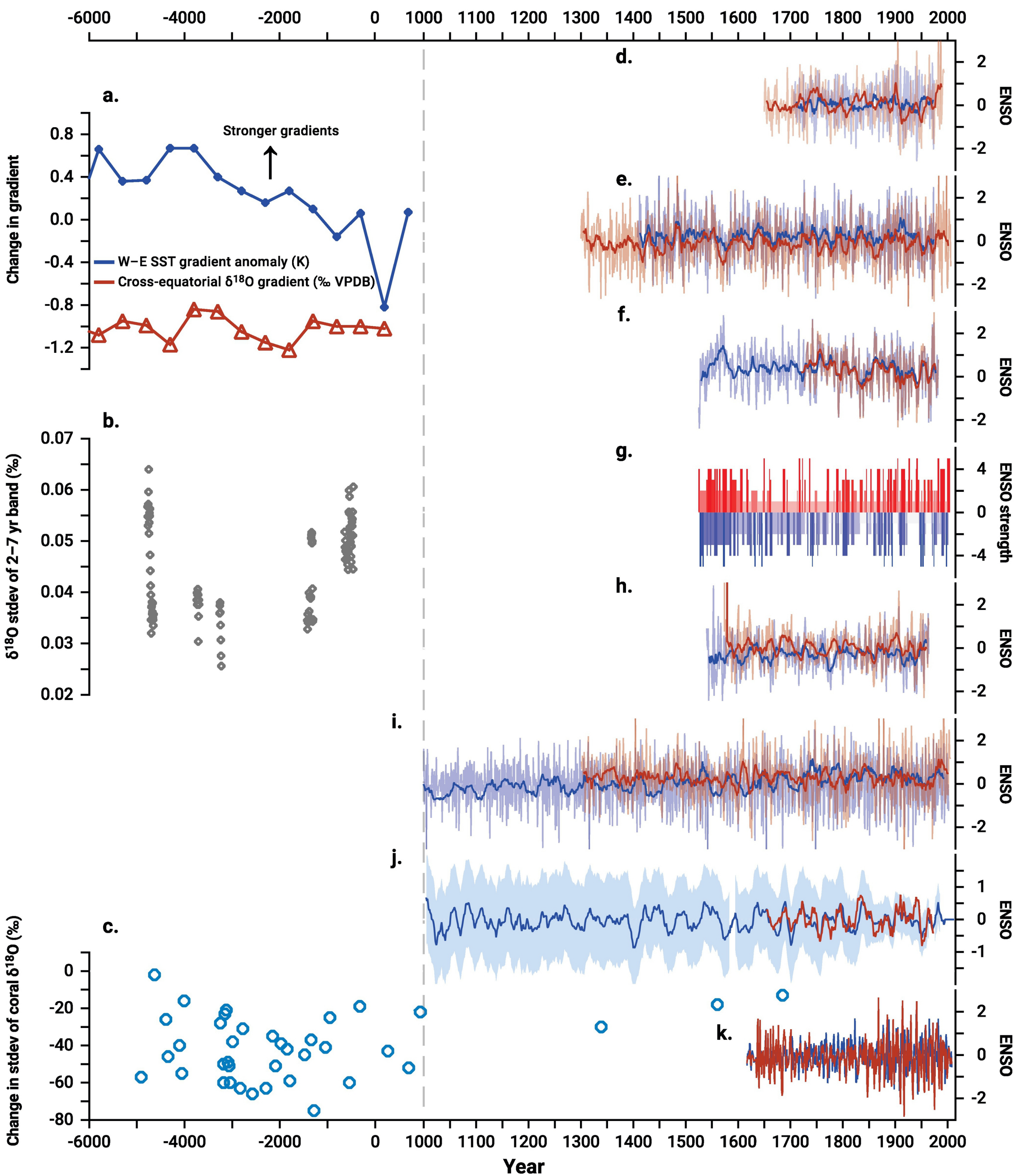

a.
Stronger gradients
Change in gradient
W–E SST gradient anomaly (K)
Cross-equatorial δ18O gradient (‰ VPDB)
b.
δ18O stdev of 2–7 yr band (‰)
c.
Change in stdev of coral δ18O (%)
d.
e.
f.
g.
h.
i.
j.
k.
ENSO
ENSO strength
Year

Figure 2

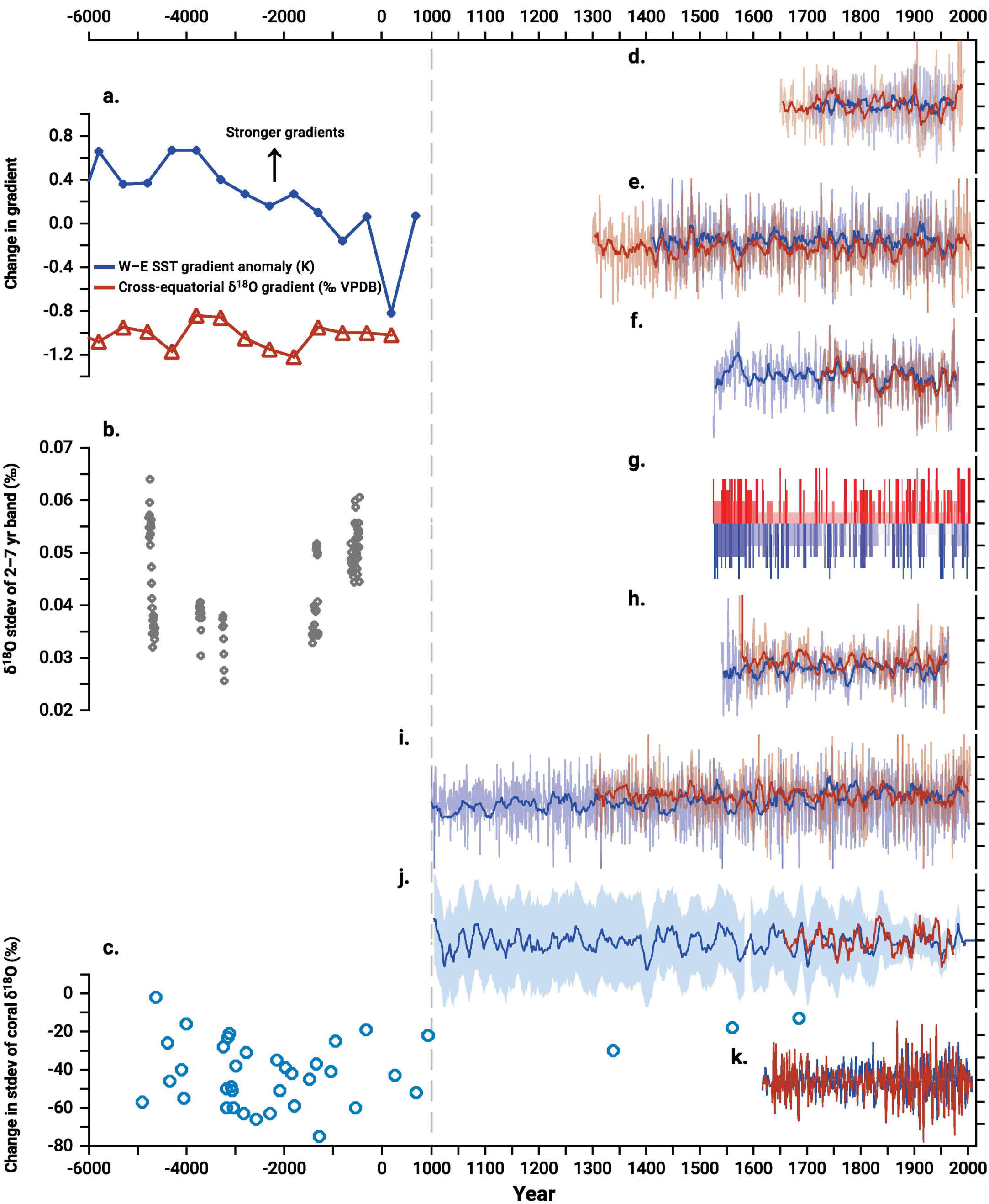

a.
Stronger gradients
Change in gradient
W–E SST gradient anomaly (K)
Cross-equatorial δ18O gradient (‰ VPDB)
b.
δ18O stdev of 2–7 yr band (‰)
c.
Change in stdev of coral δ18O (%)
d.
e.
f.
g.
h.
i.
j.
k.
ENSO
ENSO strength
Year

Figure 3

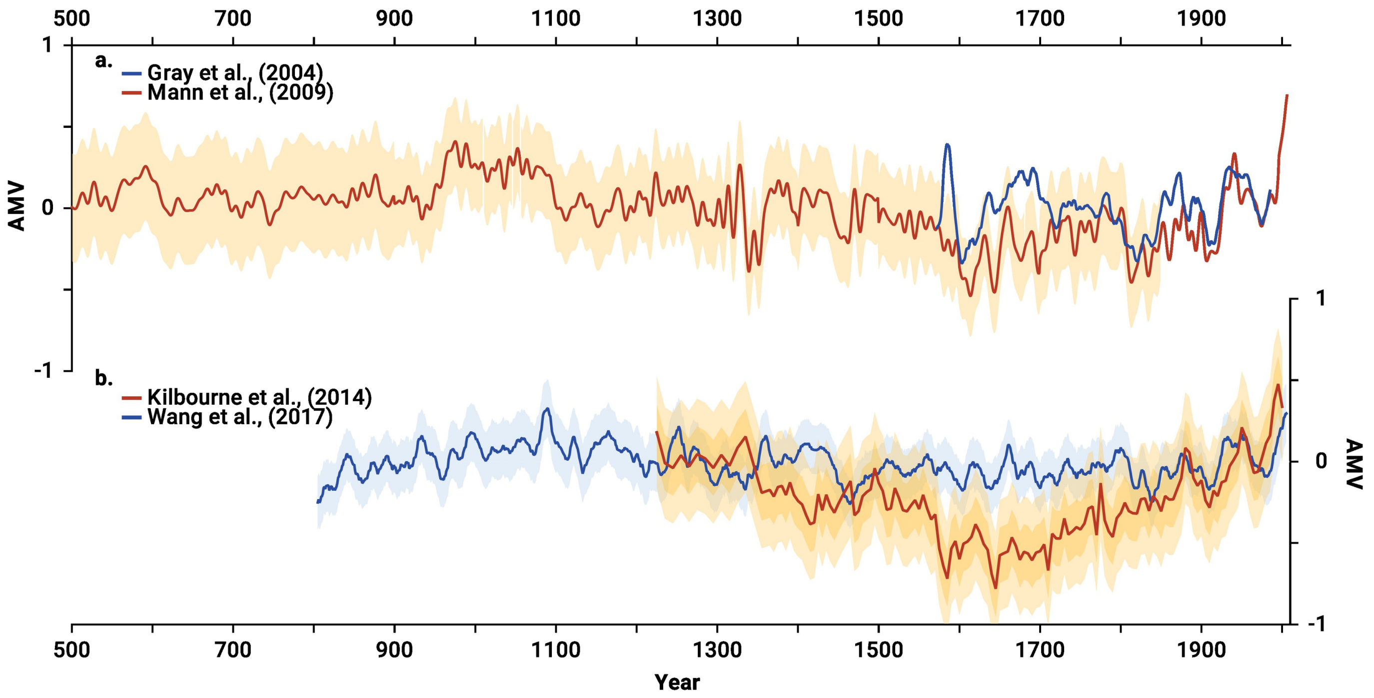

a.
Gray et al., (2004)
Mann et al., (2009)
b.
Kilbourne et al., (2014)
Wang et al., (2017)
AMV
AMV
Year
500
700
900
1100
1300
1500
1700
1900
1
0
-1

Figure 4

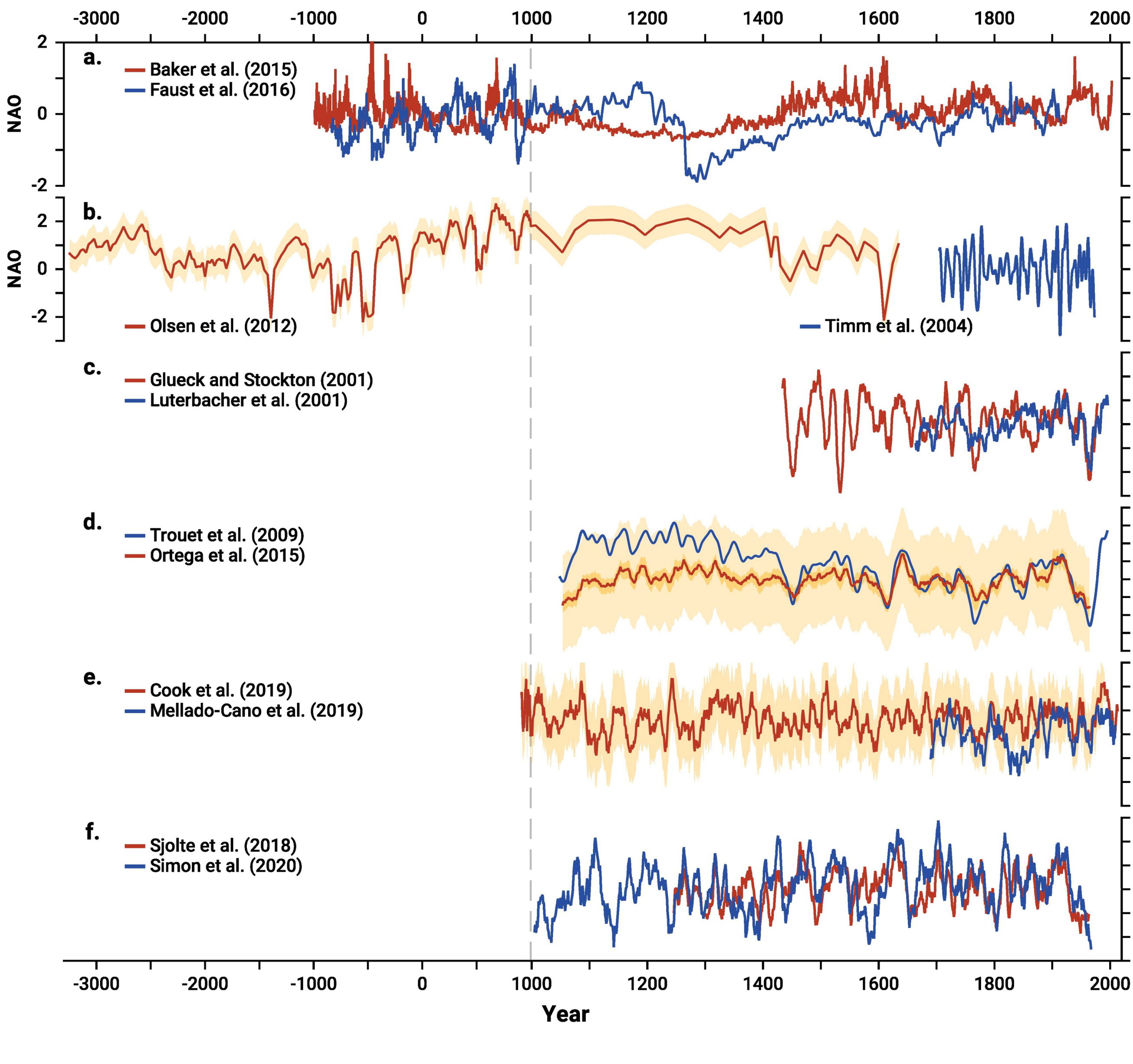
a.
Baker et al. (2015)
Faust et al. (2016)
b.
Olsen et al. (2012)
Timm et al. (2004)
c.
Glueck and Stockton (2001)
Luterbacher et al. (2001)
d.
Trouet et al. (2009)
Ortega et al. (2015)
e.
Cook et al. (2019)
Mellado-Cano et al. (2019)
f.
Sjolte et al. (2018)
Simon et al. (2020)
NAO
Year
-3000
-2000
-1000
0
1000
1200
1400
1600
1800
2000

Figure 5

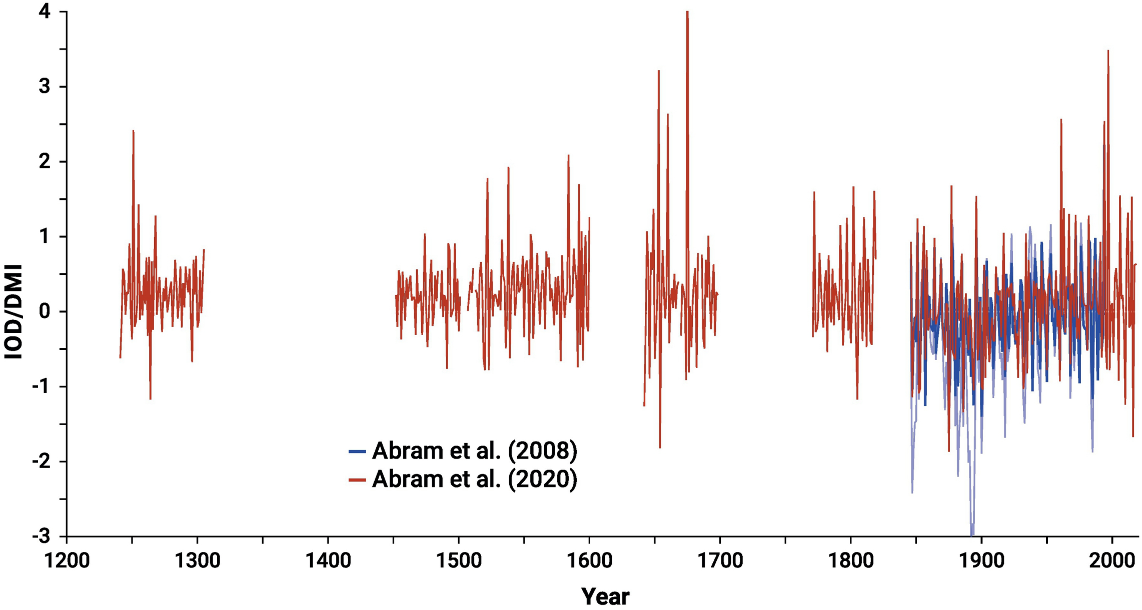

IOD/DMI
4
3
2
1
0
-1
-2
-3
1200
1300
1400
1500
1600
1700
1800
1900
2000
Year
Abram et al. (2008)
Abram et al. (2020)

Figure 6

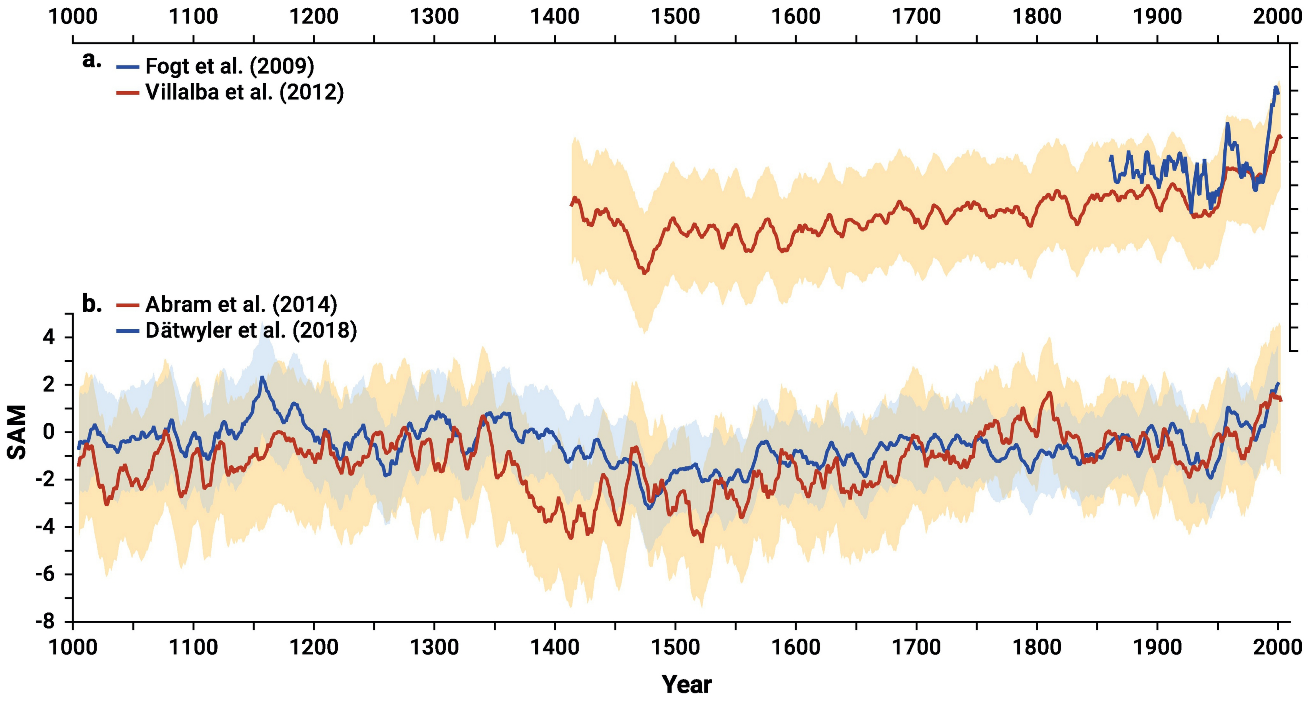
a.
Fogt et al. (2009)
Villalba et al. (2012)
b.
Abram et al. (2014)
Dätwyler et al. (2018)
SAM
SAM
Year
1000
1100
1200
1300
1400
1500
1600
1700
1800
1900
2000
4
2
0
-2
-4
-6
-8

Figure 7

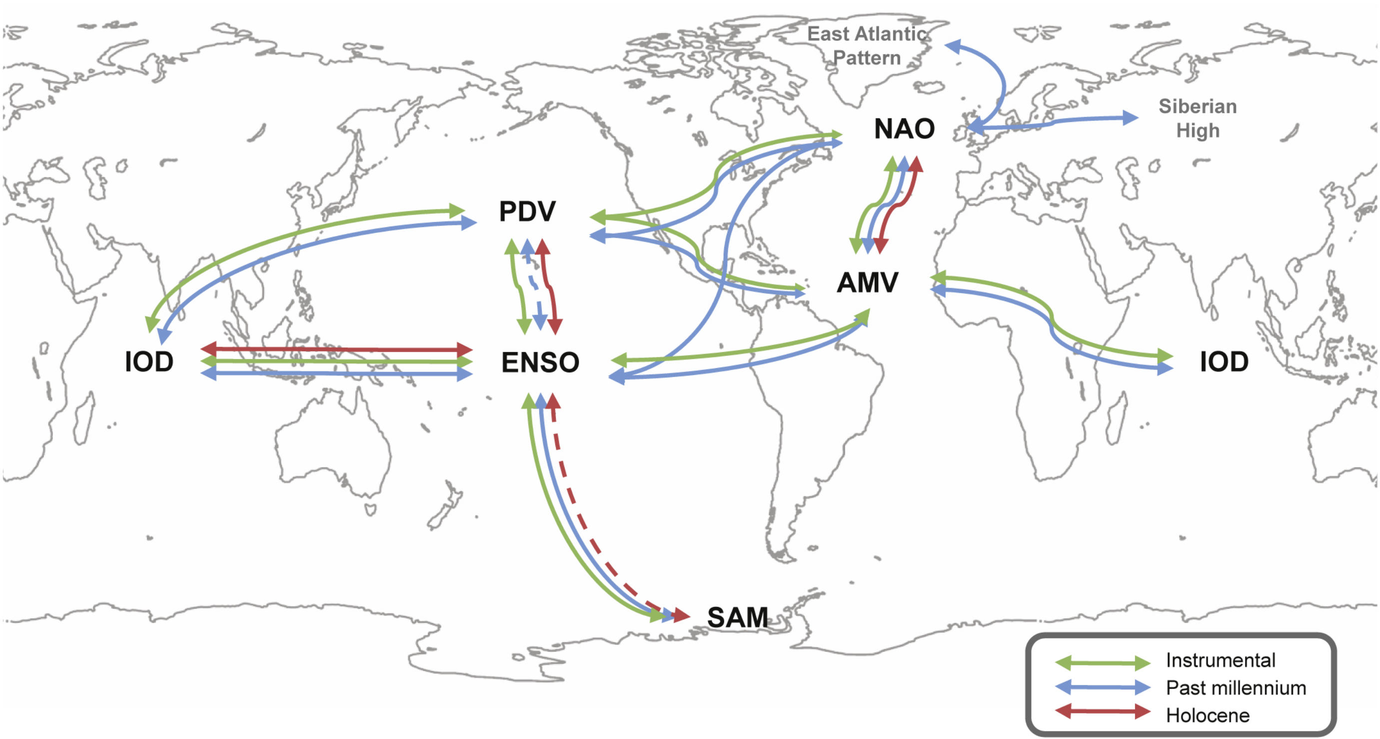
East Atlantic Pattern
Siberian High
NAO
PDV
AMV
IOD
ENSO
IOD
SAM
Instrumental
Past millennium
Holocene

Figure 8

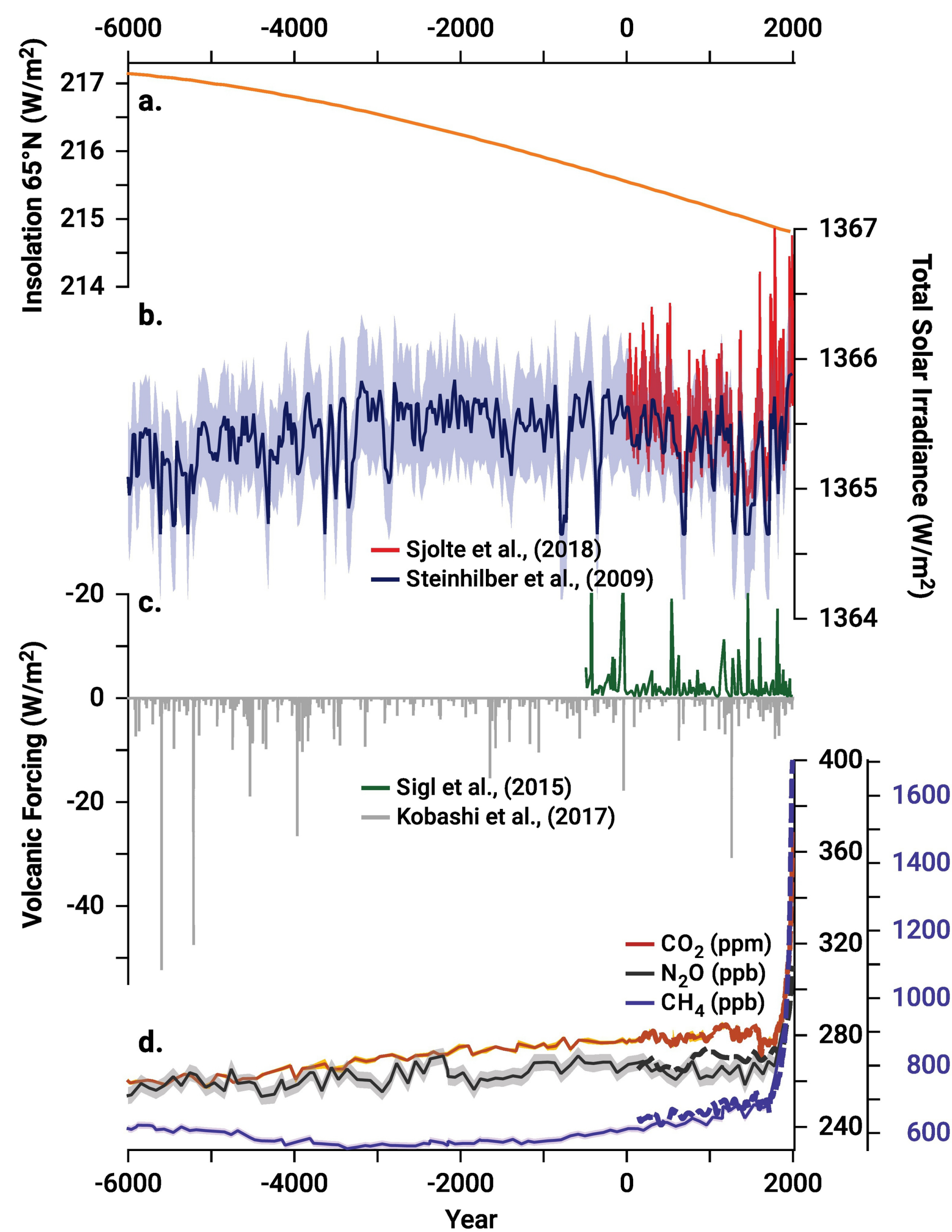

-6000
-4000
-2000
0
2000
Insolation 65°N (W/m2)
217
216
215
214
a.
1367
1366
1365
1364
Total Solar Irradiance (W/m2)
b.
Sjolte et al., (2018)
Steinhilber et al., (2009)
c.
-20
0
-20
-40
Volcanic Forcing (W/m2)
Sigl et al., (2015)
Kobashi et al., (2017)
CO2 (ppm)
N2O (ppb)
CH4 (ppb)
d.
400
360
320
280
240
1600
1400
1200
1000
800
600
Year

Figure 9